Humboldt-Universität zu Berlin – Geographisches Institut

Dissertation

Investigating the potential of hyperspectral remote sensing data for the analysis of urban imperviousness – a Berlin case study

zur Erlangung des akademischen Grades
doctor rerum naturalium

eingereicht von
Sebastian van der Linden

an der Mathematisch-Naturwissenschafltiche Fakultät II
Dekan: Prof. Dr. Wolfgang Coy

Gutachter:
Prof. Dr. Patrick Hostert
Prof. Dr. Hermann Kaufmann
Dr. Christopher Small

eingereicht: 1. November 2007
Datum der Promotion: 29. Januar 2008

Preface

Being a young researcher in environmental sciences I had to face two inevitable truths: at first, my data – enormously large data sets of uncountable dimensions, acquired on an odd-shaped ellipsoid and somehow projected onto 2-D. At second, my colleagues – interesting people who are lots of fun to work with. Let me extend on the second a little.

Patrick Hostert, head of the Geomatics Lab at Humboldt-Universität zu Berlin and advisor of this work, accompanied me during most of my remote sensing career. His feedback to my work was always valuable and honest, the outcome of discussions fruitful, and his advice was an important guideline. These were essential drivers for me to take up and – more important – to finish this dissertation.

For the past two years I was fortunate to work in two research groups. At the Geomatics Lab in Berlin it was always interesting, exciting, and enjoyable to work with my colleagues Ellen Diermayer, Frank Ebermann, Oliver Grübner, Simone Hofmann, Katja Janson, Jan Knorn, Tobias Kümmerle, Tobia Lakes, Magdalena Main, Ruth Sonnenschein and Magdalena Zwijacz-Kozica, or with students such as Patrick Griffiths, Mirjam Langhans and Thomas Scheuschner – the group has grown so big that it's a problem to write more than this simple list of names. Nevertheless I want to point out Alexander Damm for the many hours we jointly spent on processing HyMap data and on measuring in the field. Many times it was his endurance and cooperative way that kept me going. Andreas Janz introduced me to support vector machines and much of this work would not have been possible without his skills and great effort.

At the same time, I'd like to thank Matthias Braun, Gunter Menz and Walter Kühbauch for giving me the opportunity to join the team at the Center for Remote Sensing of Land Surfaces in Bonn. I've spent so many good times in- and outside the office with Vanessa Heinzel, Jonas Franke, Ellen Götz, Jan Jacobi, Roma Petravicute, Nora Schneevoigt,

Torsten Welle, my former office mates Roland Goetzke, Albert Moll and Christof Weissteiner, and all others involved in remote sensing at Bonn University.

There are many nice people I met during my ten-year career in remote sensing and I particularly want to thank

Björn Waske and Benjamin Kötz – once fellow undergrad students, now colleagues, co-authors, proof-readers and two of my very best and most important friends. I hope that one day we will learn to talk a little less about remote sensing while having time off.

Achim Röder, Thomas Udelhoven, Joachim Hill and others in Trier for introducing me to remote sensing during my times as an undergraduate and the good cooperation ever since.

Chris Small for giving me the opportunity to spend time at Columbia University and for being external advisor of this work. Field work in the East New York neighborhood is far more exciting than on the streets of Berlin-Mitte.

Hermann Kaufmann for taking over as external advisor of this work and being member of the scientific committee, Gunnar Nützmann for being head of the committee, and

Uwe Rascher and Michael Eiden for the good cooperation and hopefully for more joint field campaigns in the Bordeaux region.

I am especially grateful to the *German Federal Environmental Foundation (DBU)* that funded me during my time as a PhD student. It was always fun to spend time at seminars with my fellow stipends and the people from the Osnabrück office. I would also like to thank the *German Academic Exchange Service (DAAD)* for covering the cost of my stay at Columbia University, New York.

This work was co-funded by Berlin friends and colleagues such as Henrike Grundmann, Carl Jan Keuck, Jan Kürschner or Michael Schwarz who hosted me during my many visits.

Fortunately, there are also people who do not talk about science all day and night long and I really appreciate the effort of all the good friends and nice neighbors in Bonn and Berlin to make the past years so joyful.

This leads me to the few even more important people. I will always be thankful to my dear parents Karin and Wilhelm Schiefer, to my sister Susanne and brother Philipp with their families, and – most of all – my wife Anna and son Johann for their trust, the everlasting support, and simply being there. I am sure they are just as happy that I am done.

Abstract

Urbanization is one of the most powerful and irreversible processes by which humans modify the Earth's surface. Optical remote sensing is a main source of Earth observation products which help to better understand this dynamic process and its consequences. This work investigates the potential of airborne hyperspectral data to provide information on urban imperviousness that is needed for an integrated analysis of the coupled natural and human systems therein. For this purpose the complete processing workflow from preprocessing of the raw image to the generation of geocoded maps on land cover and impervious surface coverage is performed using Hyperspectral Mapper data acquired over Berlin, Germany. The traditional workflow for hyperspectral data is extended or modified at several points: a normalization of brightness gradients that are caused by directional reflectance properties of urban surfaces is included into radiometric preprocessing; support vector machines are used to classify five spectrally complex land cover classes without previous feature extraction or the definition of sub-classes. A detailed assessment of such maps is performed based on various reference products. Results show that the accuracy of derived maps depends on several steps within the processing workflow. For example, the support vector machine classification of hyperspectral data itself is accurate but geocoding without detailed terrain information introduces critical errors; impervious surface estimates correlate well with ground data but trees covering impervious surface below generally causes offsets; image segmentation does not enhance spectral classification accuracy of the spatially heterogeneous area but offers an interesting way of data compression and more time effective processing. Findings from this work help judging the reliability of data products and in doing so advance a possible extension of urban remote sensing approaches to areas where only little additional data exists.

Zusammenfassung

Durch den Prozess der Urbanisierung verändert die Menschheit die Erdoberfläche in großem Ausmaß und auf unwiederbringliche Weise. Die optische Fernerkundung ist eine Art der Erdbeobachtung, die das Verständnis dieses dynamischen Prozesses und seiner Auswirkungen erweitern kann. Die vorliegende Arbeit untersucht, inwiefern hyperspektrale Daten Informationen über Versiegelung liefern können, die der integrierten Analyse urbaner Mensch-Umwelt-Beziehungen dienen. Hierzu wird die Verarbeitungskette von Vorverarbeitung der Rohdaten bis zur Erstellung referenzierter Karten zu Landbedeckung und Versiegelung am Beispiel von Hyperspectral Mapper Daten von Berlin ganzheitlich untersucht. Die traditionelle Verarbeitungskette wird mehrmals erweitert bzw. abgewandelt. So wird die radiometrische Vorverarbeitung um die Normalisierung von Helligkeitsgradienten erweitert, welche durch die direktionellen Reflexionseigenschaften urbaner Oberflächen entstehen. Die Klassifikation in fünf spektral komplexe Landnutzungsklassen wird mit Support Vector Maschinen ohne zusätzliche Merkmalsextraktion oder Differenzierung von Subklassen durchgeführt. Eine detaillierte Ergebnisvalidierung erfolgt mittels vielfältiger Referenzdaten. Es wird gezeigt, dass die Kartengenauigkeit von allen Verarbeitungsschritten abhängt: Support Vector Maschinen klassifizieren Hyperspektraldaten akkurat aber die Kartengenauigkeit wird durch die Georeferenzierung deutlich gemindert; die Versiegelungskartierung stellt die Situation am Boden gut dar, aber die Überdeckung versiegelter Flächen durch Bäume bedingt systematische Fehlschätzungen; eine Bildsegmentierung führt zu keiner Verbesserung der Klassifikationsergebnisse, bietet jedoch eine sinnvolle Möglichkeit zur effektiveren Prozessierung durch Datenkomprimierung. Auf diesem Weg ermöglicht die vorliegende Arbeit Rückschlüsse zur Verlässlichkeit von Datenprodukten, die eine Ausweitung fernerkundlicher Analysen in weniger gut dokumentierte urbane Räume voranbringt.

Contents

List of Figures

List of Tables

Chapter I:
Introduction

1 The first urban century

The dynamic modification of the Earth's surface by humans has been identified to have relevant impact on future climate, the pollution of surface waters, biodiversity, and public health (e.g. Carpenter et al. 1998; Sala et al. 2000; DeFries et al. 2002; Patz et al. 2004; Foley et al. 2005). Despite all organisms modifying the environment they live in, the modification by humans is unique in a sense that no ecosystem on the Earth's surface is free of pervasive human influence (Vitousek 1997). Over the past 50 years, anthropogenic ecosystem changes were more rapid and extensive than in any comparable period of time in history (MEA 2005).

The concentration of humans in urban regions reflects the endpoint of landscape domestication. In cities every element of the environment has been consciously or unconsciously selected to accord with human desires and the flora and fauna are thus often quite different from those in rural settings (Kareiva et al. 2007). The process of urbanization – both as a social phenomenon and a physical transformation of landscapes – is one of the most powerful, irreversible, and visible anthropogenic forces on Earth (Sánchez-Rodríguez et al. 2005).

By the time this thesis was written, urban dwellers quite exactly made up one half of the world's population according to the United Nations' 2005 Revision of World Urbanization Prospects. 20 megacities, i.e. cities with a population greater 10 million, existed around the world. In 1950, for comparison, 29% of the world's population lived in cities and two megacities existed (UN 2006). Against the background of the rapid increase of urban population, it is of no surprise that the 21st century is more and more referred to as "the first urban century" (e.g. Park 1997; Dembrowski 2004; Cadenasso et al. 2007a).

Besides the pure quantity of people, it is the quality of the urbanization process that makes cities a good place to start, when considering broader implications of domesticated ecosystems (Kareiva et al. 2007): urbanization increases the per capita demand for energy, goods and services (Meyerson et al. 2007), and land conversions introduced by urban consumption patterns have regional consequences for the biophysical system that may lead to global consequences (Sánchez-Rodríguez et al. 2005). Thus, the total land area required to supply those resources can be used to quantify the cumulative demand of urban areas, a concept referred to as "ecological footprint" (Wackernagel and Rees 1997). The increasing attention received by such concepts underpins the need to understand the impacts of cities

as drivers of ecosystem change (e.g. York et al. 2003; Imhoff et al. 2004). With regards to population prospects, this need becomes even more important: by 2030, 60% of the world's population are expected to live in cities, a value that corresponds to 4.9 billion people; the number of megacities is predicted to grow to 22 until 2015 (UN 2006).

Relevant differences in terms of urbanization exist between developed regions and less developed regions. In 2005, 74% of the population of developed regions lived in urban areas, compared to 43% in the less developed regions. Despite the lower level of urbanization, the absolute number of urban dwellers in less developed regions is two and a half times higher (UN 2006). This disparity is of great importance. Firstly, urban planning often does not exist in less developed regions. Cities experience uncontrolled growth, which leads to problems with sanitation or fresh water supply and this way critical health conditions. Secondly, in these regions many people are concentrated in few places that are often subject to natural hazards (Sánchez-Rodríguez et al. 2005). Thus, feasible concepts for assessing and monitoring the structures and spatial patterns of urbanization are needed. Again, the expected population development underlines the importance of such concepts: until 2030, the urbanization rate in less developed regions will increase to 56% and the number of urban dwellers will be four times higher than in developed regions (UN 2006).

In the context of global environmental change and urbanization, two broad categories of impact exist (Sánchez-Rodríguez et al. 2005): those originating in urban areas that have a negative effect on global environmental change and those caused by global environmental changes that negatively affect urban areas. With respect to the first category, the uncoordinated growth of cities contributes to most of the human-induced negative impacts on regional and global environment, e.g. the emission of pollutants or green-house gases (EPA 2001; Marcotullio and Boyle 2003; Svirejeva-Hopkins et al. 2004). Climate-related natural disasters such as floods and droughts or sea-level rise, on the other hand, affect cities and migration patterns as part of the second category. Changes in average and extreme temperatures influence economic life, the comfort of living, and public health (Sánchez-Rodríguez et al. 2005).

With regard to the global dimension of urbanization and its consequences, the need for spatially explicit information on the state of the Earth's surface is evident. Earth observation (EO) can provide information to better understand the drivers of processes and to more accurately quantify their consequences. It is thus critical for an ever-increasing number of applications related to the health and well-being of society (NRC 2007).

2 Earth observation and urban areas

"Natural and human-induced changes in Earth's interior, land surface, biosphere, atmosphere and oceans affect all aspects of life. Understanding these changes and their implications requires a foundation of integrated observation – taken from land-, sea-, air-, and space-based platforms – on which to build credible information products, forecast models, and other tools for making informed decisions (NRC 2007)." With these lines the National Research Council's Committee on Earth Science and Applications from Space preludes its imperatives for future decades and this way emphasizes the emerging need for EO in the context of monitoring and assessing coupled natural and human systems.

Optical remote sensing is one main source of EO products. It delivers information on the impact of urbanization and global environmental change, for example by quantifying urban growth and its influences on the environment (Soegaard and Moller-Jensen 2003; Seto and Fragkias 2005) or by providing input for models on environmental quality and ecological performance of urban areas (Whitford et al. 2001; Nichol and Wong 2005). Miller and Small (2003) mention the increased availability of high resolution imagery from EO satellites in combination with global connectivity and information technology as a means to identify, monitor, and apprehend a number of urban environmental problems.

Municipal administrative infrastructure in less developed regions of the world is often not capable of supporting the sustained and publicly available record keeping and data collection for urban environmental analysis and planning. The analysis and monitoring of urban areas is therefore especially important and challenging in those regions of the world with rapid and uncontrolled urbanization (Miller and Small 2003; UN 2006). Remotely sensed observations can provide spatially explicit information over very large areas, which would be very expensive or impossible to be directly measured in the field. For example, the issue of informal settlements that are often highly susceptible to natural hazards requires special attention in urban planning (Alder 1995). Remote sensing offers means to provide spatially explicit information on such otherwise poorly documented and dynamically evolving phenomena (Weber and Puissant 2003).

In the developed regions of the world, a need for detailed spatial information has been identified, for example in the context of urban environmental analysis, ecology, and planning, (e.g. Svensson and Eliasson 2002; Alberti 2005). Remote sensing has been used to monitor urban growth for several years (e.g. Ward et al. 2000; Stefanov et al. 2001). Since the advent of spaceborne sensors with high spatial resolution, the value of urban

remote sensing is becoming more and more accepted (e.g. Mathieu et al. 2007; Thanapura et al. 2007). However, remote sensing of urban areas alone is often limited and cannot effectively compete with regulatory governmental and commercial sources or with census data (Miller and Small 2003). In regions where additional data sources are available, remotely sensed information is often combined with such data, e.g. digital surface models (Nichol and Wong 2005), census data (Mesev 1998) or cadastre information (Lu et al. 2006). By combining the different data sources before, during or after analysis a surplus of information can be generated (Mesev 1998). Nevertheless, spatial and spectral variation and compositional heterogeneity traditionally complicate the analysis of urban areas by EO (Mesev 1998; Herold et al. 2003).

Collier (2006) concludes a study on the impact of urban areas on weather by saying that the use of remote sensing must play a major role in providing the required observations but care has to be taken to understand the true nature of what is actually measured. This understanding is needed to make sensible use of products from EO for detailed and accurate analysis and for its combination with additional data sources. The derivation of reliable and consistent end-user products must therefore be one of the main goals for application development in remote sensing (Schläpfer et al. 2007). New applications should take advantage of the characteristics of remote sensing data with regard to routine updating or the description, classification, and measurement of the desired surface properties (Miller and Small 2003). Following these recommendations will help to better connect the so far only loosely connected three key elements of (1) information produced by raw observations, (2) analyses, forecasts, and models that provide timely and coherent syntheses of otherwise disparate information, and (3) the decision processes that produce actions with direct social benefits (NRC 2007).

A better connection of these key elements is of great interest when regions with little or no additional data are observed and only single source EO data is available. It is then important to know what source best provides which information and how reliable and accurate this information is. Tests that are required to answer these questions are ideally performed in well known areas where plenty of documentation and additional data exists. Based on findings from such tests, the step into the less known and poorly documented regions of the world is possible and information urgently needed for planning and decision making can be derived with a good estimate of possible inaccuracies.

3 Urban remote sensing with airborne hyperspectral data

3.1 Resolution requirements for urban remote sensing

Undoubtly, urban areas are one of the most challenging environments for EO (Mesev 1998). For the mapping of large areas or when only moderately resolved data is available, urban remote sensing makes use of metaindicators such as the distribution of nightlights (e.g. Small et al. 2005) or impervious surface coverage (e.g. Carlson and Arthur 2000) in order to estimate urban extent or density. Impervious surface coverage has been identified a key environmental indicator for urbanization (Arnold and Gibbons 1996). However, in most applications, impervious land cover is not directly mapped or not further differentiated into built-up and non built-up impervious areas. Instead, an aggregated degree of imperviousness is indirectly derived from vegetation cover as estimated by unmixing models (e.g. Wu 2004; Yuan and Bauer 2007) or vegetation indices (e.g. Morawitz et al. 2006). This is explained by the fact that impervious surface cannot be directly described by spectral properties in moderate resolution multispectral imagery (Small and Lu 2006). For directly mapping the degree of imperviousness and patterns of impervious surfaces, EO data have to meet certain requirements, such as very high spatial resolution and spectral information that goes beyond that of multispectral systems (Jensen and Cowen 1999; Herold et al. 2003; Gamba and Dell'Acqua 2007).

Welch (1982) identifies varying *spatial resolution* requirements for different regions in the world, that range from 5 m in the case of China to up to 80 m in the case of the United States. Small (2003) assesses the characteristic spatial scale of urban reflectance for 14 cities around the world based on spatial autocorrelation in multispectral data at 4 m resolution. The values he derives are consistently between 10 and 20 m. Recent multispectral spaceborne imagery, as acquired by Quickbird or Ikonos, capture the spatial requirements for the detailed analysis of urban environments to a great extent (Ehlers 2007). Still many mixed pixels can be expected at the 4 m resolution provided by Ikonos (Small 2003). Traditional moderate resolution EO satellite data, e.g. from Landsat Thematic Mapper, lack the spatial resolution for detailed monitoring in cities but provide the area coverage to image entire urban agglomerations (Miller and Small 2003). Most recent multispectral airborne line scanners yield even better spatial resolutions at 0.2 m and below (Ehlers et al. 2006). Thus, a trend in data resolution towards the *H*-resolution case according to Strahler et al. (1986) can be observed, which allows for resolving urban

objects, and an increasing number of infrastructure elements and socio-economic attributes can be remotely sensed (Jensen and Cowen 1999).

Jensen and Cowen (1999) state that "most image analysts would agree that, when extracting urban/suburban information from remotely sensed data, it is more important to have high spatial resolution than high *spectral resolution*." Gamba and Dell'Acqua (2007) compare the spatial and spectral very high resolution situation in a case study and conclude that spectral information is more important, once sufficient spatial resolution is achieved. Apparently, different opinions exist on the importance of spatial and spectral resolution. However, the importance of, for example, the information from the short-wave infrared (SWIR) region for detailed analysis has been stressed by several authors (e.g. Ridd 1995; Jensen and Cowen 1999). In a detailed study on the spectral resolution requirements of urban land cover mapping, Herold et al. (2003) discover drawbacks of multispectral sensors such as Quickbird and Ikonos to delineate urban surface types by statistical measures. This can be explained by the spectral ambiguity of materials from different land cover types. Spectral similarity is also identified by Gamba and Dell'Acqua (2007) who report increased differentiation capabilities by spectrally higher resolved data.

Airborne hyperspectral remote sensing data, also referred to as imaging spectrometry data, from sensors such as the Advanced Visible Near Infrared Imaging Spectrometer (AVIRIS) (Green et al. 1998) or the Hyperspectral Mapper (HyMap) (Cocks et al. 1998) provides very highly resolved spectral information. This quasi continuous spectral information covers spectral wavelengths that are not covered by the broader spectral bands of high spatial resolution multispectral instruments (Fig. I-1). Absorption features and the shape of spectral curves from imaging spectrometry data are frequently used for environmental and ecological applications (e.g. Johnson et al. 1994; McMorrow et al. 2004; Ustin et al. 2004) and have been shown to help differentiating urban surfaces (e.g. Ben-Dor et al. 2001; Segl et al. 2003; Herold et al. 2004; Heiden et al. 2007).

The spatial resolution of airborne hyperspectral data of as high as 4 m is similar to that of Ikonos (4 m multispectral) and Quickbird (2.5 m multispectral), while the spectral detail goes far beyond that of multispectral instruments (Fig. I-1). Thus, airborne hyperspectral data appears well suited to provide the information needed for detailed urban applications such as the direct mapping of impervious surface types.

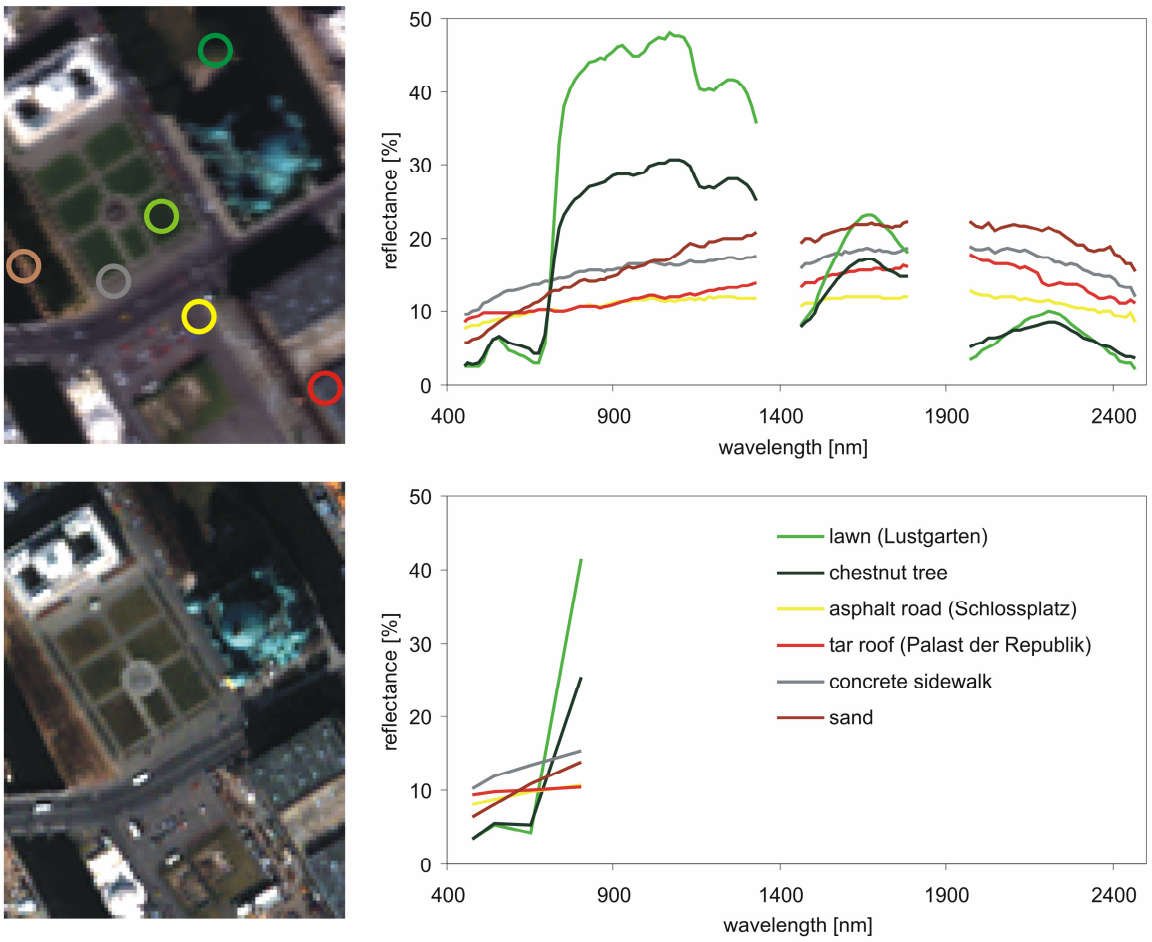

Figure I-1: Image data from Museumsinsel in Berlin-Mitte and spectral curves for six surface materials. The colored circles indicate the position of the sample spectra. The Quickbird data (bottom) has a slightly higher spatial resolution and shows more detail. The spectral resolution and wavelength coverage of the HyMap data (top) go far beyond that of Quickbird. Note: for matters of comparison the Quickbird spectra were resampled based on the HyMap spectra, since different acquisition dates, illumination conditions, and radiometric preprocessing do not allow direct comparison.

3.2 Processing airborne hyperspectral data from urban areas

Despite the very high spectral and spatial resolution of airborne hyperspectral data, image processing and analysis with methods developed for traditional, moderate resolution remote sensing data are not optimal. Instead, new approaches and workflows that make best use of the high information content are needed (e.g. Kuo and Landgrebe 2004; Richards 2005; Schläpfer et al. 2007). When this is given, information can be provided at a level of accuracy and detail that allows for a better understanding of the coupled natural and human system within the heterogeneous urban environment.

The challenges faced by urban remote sensing with airborne hyperspectral data affect several data processing steps. The *radiometric preprocessing* of airborne hyperspectral data differs from that of multispectral data, especially due to the influence of water vapor

absorption. By incorporating physically based approaches that model the radiative transfer of the atmosphere and perform a spatially explicit estimation of water vapor, such influences are sufficiently eliminated (Richter and Schläpfer 2002). Nevertheless, directional reflectance properties of the Earth's surface can lead to brightness gradients in the measured signal of instruments such as HyMap which acquire data at wide field-of-view (FOV) in order to cover large areas at low operating altitudes. Unlike the correction of atmospheric influences, the normalization of this effect requires further investigation (Beisl 2001; Richter and Schläpfer 2002; Schiefer et al. 2005a). Various approaches have been suggested that include the use of semi-empirical BRDF models (Beisl 2001) or the use of spectral libraries (Feingersh et al. 2005). Neither of these approaches appears feasible in heterogeneous urban environments, however. Directional reflectance properties of urban surface materials have been shown in the field (Meister et al. 2000) and their influence on spectral measurements at view-angles similar to those of the HyMap sensor has been demonstrated by the author of this thesis in Herold et al. (2006). During hyperspectral image analysis, directional reflectance increases intra-class variability (Lacherade et al. 2005) and negatively impacts results from frequently applied linear spectral unmixing or spectral angle mapper classifications (Langhans et al. 2007).

The complex geometric composition of the urban environment requires special attention during *geometric preprocessing* of airborne remote sensing data. Buildings are displaced as a function of sensor view-angle and their height – a phenomenon of great relevance in wide FOV data (Schläpfer and Richter 2002; Schiefer et al. 2005a). In the case of the Berliner Dom (Fig. I-1), for example, the high metal dome appears at different locations when viewed from different positions in HyMap and Quickbird data. In general, roofs appear further away from nadir than they actually are and also occlude lower objects. The orthorectification of displaced objects requires detailed information on their spatial position and vertical extent; additional image data from different viewing positions is needed to reconstruct occluded surfaces (Zhou et al. 2005). However, such information is not commonly available and the mentioned effects can often not be corrected. In general, insufficient digital elevation models (DEM) bear the greatest source of inaccuracy during parametric approaches for geometric correction of airborne hyperspectral data (Schläpfer and Richter 2002). For urban areas, such inaccuracies will negatively impact to a great extent mapping accuracy of hyperspectral analyses.

For many applications in urban areas it is required to delineate the three major elements of urban heterogeneity – vegetation, built structures and surface materials (Cadenasso et al.

2007b). Advanced *image classifications* are needed to produce accurate land cover maps of urban areas for two reasons. Firstly, urban land cover classes exhibit high intra-class variability. This is caused by the abundance of well-illuminated and shaded surfaces or reflectance anisotropy (e.g. Lacherade et al. 2005) as well as a great variety of spectrally different artificial surfaces materials, e.g. roofing tiles and metal roofs made from different materials or with various coatings and paint covers (Herold et al. 2004). Secondly, the separability of classes is low. Different land cover classes might include spectrally similar or identical materials such as tar roofs and asphalt roads (Herold et al. 2003). In addition, even at 4 m spatial resolution a high number of spectrally mixed pixels can be expected (Small 2003). These are made up of two or more different surface materials and will be located in between clusters of purer pixels in the spectral feature space.

Thus, land cover and spectral reflectance do not describe a one-to-one relationship. Traditional parametric classifiers like the Gaussian maximum likelihood classifier cannot handle such many-to-one relationships (Seto and Liu 2003). At the same time, mixed pixels cause problems during the discretization of the originally continuous spectral feature space inherent to image classification. Spectral mixture analysis (SMA) constitutes an alternative concept that avoids this discretization (Smith et al. 1990; Ridd 1995; Small 2001). It can provide a physically based framework for spectral characterization of urban reflectance, e.g. by representing urban surfaces as a linear combination of the three endmembers substrate, vegetation and dark surface (Small 2004). However, the further differentiation of urban surfaces such as built-up and non built-up impervious area in a spectral mixing space is problematic: due to the spectral heterogeneity of the urban environment an enormous number of potential endmembers exists and endmembers that represent different surface types will be spectrally similar. Multi-step approaches that first identify pure seed pixels and then perform a locally optimized unmixing are promising (Roessner et al. 2001; Segl et al. 2003). Nevertheless, delineating different impervious surfaces types requires some way of classification.

The assessment of HyMap spectra from four land cover classes underlines the complexity of land cover classification in urban areas (Fig. I-2). In the feature space of the first four principal components (PC), no single clusters can be identified for all classes. Classes like built-up areas or soil show more than one cluster. All four classes exhibit great illumination differences that result in generally high variances for the first PC. Built-up and non built-up impervious areas are characterized by spectral similarity and therefore overlapping class distributions in PC feature space.

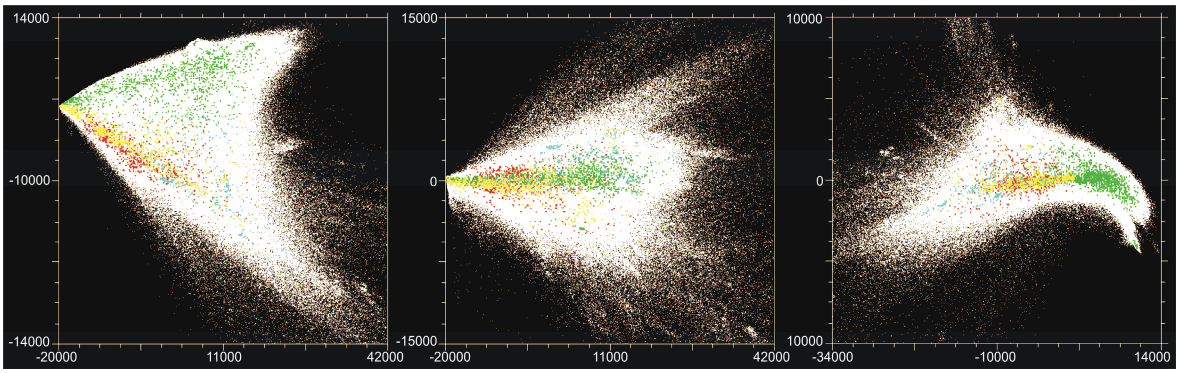

Figure I-2: Distribution of sample spectra from four urban land cover classes in 2-dimensional representations of the PC feature space. HyMap spectra from vegetation (green), built-up (red) and non built-up impervious areas (yellow), and soil (cyan) are shown as scatter plots for PC 1 vs. PC 2 (left), PC 1 vs. PC 3 (center), and PC 2 vs. PC 4 (right). The white background shows the distribution of all pixels from a 512 by 7277 pixel HyMap image from a heterogeneous urban environment.

Several authors try to overcome this spectral complexity by combining spectral information with additional sources of information before classification, e.g. texture (Baraldi and Parmiggiani 1995; Benediktsson et al. 2005), segment features (Shackelford and Davis 2003) or terrain elevation (Hodgson et al. 2003). In most of these approaches, the overall quality of results is increased. However, the need for additional data sources or the required additional processing steps make such approaches more complicated, harder to transfer, and sometimes infeasible. In the case of segment-based approaches, the definition of transferable aggregation levels for the image data is very time consuming (Schöpfer and Moeller 2006). It is thus desirable to develop easy-to-perform single source land cover classifications that are based solely on spectral information. For the mentioned combined approaches it is also useful to make best use of the available spectral information.

According to Richards (2005) *support vector machines* (SVM) are perhaps the most interesting development in data classification. They were introduced in the remote sensing context almost 10 years ago (Gualtieri and Cromp 1998) and are receiving increasing attention. In terms of accuracy, they outperformed other approaches under varying conditions in the very most cases or performed at least equally well (Huang et al. 2002; Foody and Mathur 2004; Melgani and Bruzzone 2004; Pal and Mather 2006). In particular, SVM have been shown to be robust in terms of small training sample sizes (Melgani and Bruzzone 2004; Pal and Mather 2006). By exploiting a margin-based "geometrical" criterion rather than a purely "statistical" criterion, SVM are not affected by the so-called curse of dimensionality originally described in Hughes (1968) and they are capable of delineating linearly not separable classes directly in the hyperdimensional feature space (Melgani and Bruzzone 2004).

Before the introduction of SVM, the progress in remote sensing image classification was characterized by the refinement of methods originally developed for multispectral imagery. In order to make statistical classifiers like the Gaussian maximum likelihood classifier applicable to hyperspectral imagery, feature extraction and selection techniques have been developed and integrated into the workflow (Fig. I-3) (e.g. Kuo and Landgrebe 2004). Such approaches always lead to an unavoidable loss of information and processing times are often infeasible (Melgani and Bruzzone 2004). In addition, spectral sub-classes have to be defined to avoid multi-modal class distributions – a very time intensive and almost infeasible task in urban areas. In order to simplify the classification process and make best use of the characteristics of airborne hyperspectral data, SVM-based approaches appear promising even for delineating spectrally complex urban classes.

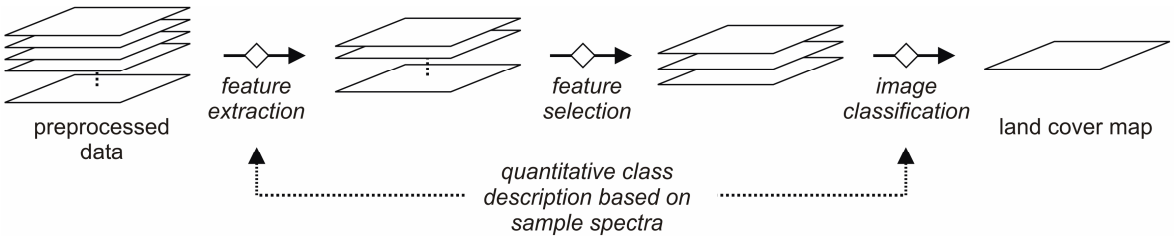

Figure I-3: Workflow for the use of parametric classifiers with hyperspectral data. Traditional classifiers that assume certain class distributions and rely on statistical parameters require the hyperspectral feature space to be modified and reduced. (Kuo and Landgrebe 2004, modified)

4 The Berlin case study

4.1 Motivation

According to Miller and Han (2001) geography has changed from a data-poor and computation-poor to a data-rich and computation-rich environment, wherein traditional spatial methods cannot be used to discover hidden information from huge amounts of spatially related data sets. The development of Earth observation data products in optical remote sensing over the past three decades mirrors this development: data resolution in all information dimensions has increased and the user can choose from a great variety of image products depending on the scope of investigation; methods for the processing and analysis of these products exhibit constant improvement and extension (Richards 2005). Nowadays, the decision on the appropriate data and the selection of the best suited methods for its processing pose one of the greatest challenges in application. For the optimal generation of different end-user products from hyperspectral data the full

processing workflow requires harmonization, e.g. to reduce processing times or to avoid unnecessary resampling (Schläpfer et al. 2007).

The ongoing urbanization and its consequences, on the one hand, and the high EO data requirements due to the complex spatial and spectral situation of urban areas, on the other, create a special situation for application development. At the moment, the preprocessing of hyperspectral data from urban areas does not result in reliable and consistent products; this is a result of the inaccuracy introduced into geometric correction by the complex surface composition and the existence of brightness gradients caused by directional reflectance. In the context of hyperspectral image classification, sequential processing with feature extraction/selection and the definition of a multitude of sub-classes increases processing times while decreasing the amount of information actually used (Melgani and Bruzzone 2004). In addition, feature extraction or classification approaches that assume certain class distributions are still very common although they are often not suited for urban areas. This can probably be explained by the complexity of more sophisticated, recent developments that deters many users from their application.

With regard to processing times and the amount of data to process for regular updating or large area application, airborne hyperspectral data require special attention. High spatial and spectral resolution lead to very large physical file sizes and data compression appears useful to make advanced processing techniques feasible. To maintain the high spectral information content, i.e. the main characteristic and advantage of hyperspectral data, a spatial generalization should be performed that conserves a sufficient degree of spatial detail. The issue of data compression is one so far neglected side effect of segment-based image processing that reduces the spectral information of groups of adjacent pixels to single mean values (Schiefer et al. 2005b). However, especially in heterogeneous urban environments the decision for well suited levels of aggregation inherent to segment-based approaches constitutes another challenge as well as additional error source.

In terms of reliability and quality, a separate assessment of potential error sources is desirable to better understand results. Besides processing related and data specific errors, general drawbacks of remote sensing based analysis, e.g. the impact of surfaces obscured by tree crowns, still require detailed investigation and quantification. Such assessments are important against the background of data availability: so far, hyperspectral remote sensing data with sufficient radiometric quality is only available from airborne sensors. It is therefore limited to episodic campaigns, covers relatively small areas and comprises high

acquisition costs. Thus, applications in less developed regions are for the moment not likely. Nevertheless, the number of airborne hyperspectral sensors is steadily increasing (e.g. Müller et al. 2005; Nieke et al. 2006); results from first experimental spaceborne sensors are promising (Guanter et al. 2005) and operational satellite missions are in advanced planning phases (Kaufmann et al. 2005). Advanced processing techniques and optimized workflows can help to achieve reliable end-user products and will this way also increase the acceptance of future hyperspectral data products. Therefore, comprehensive case studies are needed. In addition to the use for future missions, findings from case studies on the reliability of results are useful for the work with data from existing sensors, particularly when the increasing data availability might lead to more studies in so far poorly documented areas. Moreover, further knowledge on the processing of airborne hyperspectral data might be of value for other airborne sensors with similar characteristics (e.g. a wide FOV) or for the spectro-radiometric design of new sensors with fewer bands.

4.2 Study area

HyMap data acquired over the metropolitan area of Berlin, Germany, in 2003 and 2005 is used for experiments in this work. The history and structure of the city make it an ideal study area for the addressed research questions. The rise of the Prussian empire and the era of industrialization dominate the original structure of the city. After heavy destruction during World War II, a period of separation and parallel development under opposite political systems led to diverse new urban structures. Following the fall of the Berlin Wall and the closing down of industrial complexes from socialist times, many derelict sites exist and Berlin has recently been experiencing large scale development in very central areas. (Sukopp 1990; SenStadt 2007)

This situation is probably unique for a metropolitan area in the western hemisphere. Thus, a great variety of urban structure types exists within an area that can be covered by a single airborne hyperspectral data set. At the same time, the abundance of additional data sources in Berlin helps to evaluate the quality of results and sources of inaccuracy (SenStadt 2007). This way, main findings from this case study are expected to be of value for applications in other urban areas as well as for airborne and/or hyperspectral analyses in general.

4.3 Objectives

This work investigates the potential of airborne hyperspectral remote sensing data for the analysis of urban imperviousness. This analysis of imperviousness includes the estimation

of the areal degree of impervious surface coverage and the attempt to delineate built-up and non built-up impervious surfaces. In doing so, a challenging application is performed in a complex environment and new insights on hyperspectral image processing are expected that might be important for a variety of other applications. The overarching goal is to optimize data processing with regard to the accuracy and reliability of results while assessing possible error sources. In previous sections, existing problems and remaining challenges of hyperspectral image processing and urban remote sensing have been identified. These include not only data preprocessing and the classification process but at the same time more general issues like the limits of airborne remote sensing or workflow optimization. Thus, individual processing steps as well as the entire workflow have to be considered for a comprehensive case study. In this work, a focus is put on processing steps that appear to require further improvement to make best use of the hyperspectral information. Concurrently, the entire workflow, i.e. the selection and sequence of processing steps, is assessed in consideration of efficient processing of large data sets.

The central part of this work is a land cover classification with SVM which includes the delineation of built-up and non built-up impervious surfaces. Based on this land cover information a map on impervious surface coverage is derived. Prior to the classification, the issue of across-track brightness gradients is looked at and a normalization procedure is suggested. The land cover map and the map on impervious surface coverage are evaluated for accuracy and potential error sources with a focus on the needs of potential end-users such as urban planners, ecologist or environmental modelers. In addition to the classification of the original image data, segmented data sets are classified and the potential of image segmentation to function as a mean of data compression is assessed against the background of the complete processing workflow.

In detail, the following four research questions will be addressed:

(1) Can brightness gradients in airborne hyperspectral data from urban areas be eliminated using an empirical normalization approach that requires no additional field measurements?

(2) Do support vector machines bear the potential to directly use the full hyperspectral information for the successful delineation of urban land cover classes such as built-up and non built-up impervious surfaces without separate feature extraction or the previous definition of spectral sub-classes?

(3) How accurate can land cover and impervious surface coverage be mapped from hyperspectral images and what are the main sources of inaccuracy?

(4) To what extent is the efficiency of the processing workflow in terms of processing times and accuracy influenced by alternative processing sequences and the introduction of data compression by image segmentation?

At several points an emphasis is put on the detailed accuracy assessment of results. This way, the potential of airborne hyperspectral data and remote sensing in general shall be evaluated for detailed analyses in the urban environment.

4.4 Structure

The four research questions and more specific objectives are addressed in Chapters II-V of this work. Chapter VI is a synthesis of the outcomes of the individual chapters. It draws more general conclusions with regard to the applicability of suggested approaches or expected data availability, and provides directions for future research. Chapters II, III, and V are stand alone manuscripts to be published in international peer-reviewed journals.

Chapter II, *Correcting brightness gradients in hyperspectral data from urban areas*, introduces an empirical approach for the class-wise correction of across-track brightness gradients. The approach adapts existing procedures that are solely based on the image data to the special needs of urban areas with high frequent changes of spectrally different surface materials.

Chapter III, *Classifying segmented hyperspectral data from a heterogeneous urban environment using support vector machines*, examines the quality of a purely spectral classification of urban land cover classes. An additional focus is put on the influence of image segmentation on classification accuracy in different urban structure types.

Chapter IV, *Processing large hyperspectral data sets from urban area mapping*, provides the foundation for Chapter V and assesses the role of geometric correction and image segmentation for an efficient data processing workflow.

Chapter V, *Mapping urban areas using airborne hyperspectral remote sensing data*, evaluates the sources of inaccuracy in the maps on land cover and impervious surface coverage after geometric correction. The impact of different inaccuracies is quantified in consideration of the needs of different end-users.

Chapter II:
Correcting brightness gradients in hyperspectral data from urban areas

Remote Sensing of Environment 101 (2006) 25-37

Sebastian Schiefer, Patrick Hostert and Alexander Damm

doi: 10.1016./j.rse.2005.12.003
Received 24 August 2005; revised 29 November 2005;
accepted 1 December 2005.

Abstract

The analysis of airborne hyperspectral data is often affected by brightness gradients that are caused by directional surface reflectance. For line scanners these gradients occur in across-track direction and depend on the sensor's view-angle. They are greatest whenever the flight path is perpendicular to the sun-target-observer plane. A common way to correct these gradients is to normalize the reflectance factors to nadir view. This is especially complicated for data from spatially and spectrally heterogeneous urban areas and requires surface type specific models. This paper presents a class-wise empirical approach that is adapted to meet the needs of such images.

Within this class-wise approach, empirical models are fit to the brightness gradients of spectrally pure pixels from classes after a spectral angle mapping (SAM). Compensation factors resulting from these models are then assigned to all pixels of the image, both in a discrete manner according the SAM and in a weighted manner based on information from the SAM rule images. The latter scheme is designed in consideration of the great number of mixed pixels.

The method is tested on data from the Hyperspectral Mapper (HyMap) that was acquired over Berlin, Germany. It proves superior to a common global approach based on a thorough assessment using a second HyMap image as reference. The weighted assignment of compensation factors is adequate for the correction of areas that are characterized by mixed pixels.

A remainder of the original brightness gradient cannot be found in the corrected image, which can then be used for any subsequent qualitative and quantitative analyses. Thus, the proposed method enables the comparison and composition of airborne data sets with similar recording conditions and does not require additional field or laboratory measurements.

1 Introduction

In the field of imaging spectrometry, the number of urban applications has increased over the past five years (e.g. Ben-Dor et al. 2001; Herold et al. 2003; Benediktsson et al. 2005). Before that time, imaging spectrometry data was almost exclusively used in studies on vegetation or minerals in land cover applications. This can be explained to some extent by the great challenge posed by the complex structure of urban surfaces, an insufficient spatial resolution, and deficiencies in signal-to-noise ratio (SNR) and sensor calibration of early imaging spectrometers. Due to technical sensor development and increasing availability, hyperspectral data may be utilized for numerous urban remote sensing applications in the future. Especially those approaches that already proved successful with data of medium spatial and spectral resolution will further improve by including hyperspectral information, e.g. the modeling of urban sprawl (Wilson et al. 2003) or mapping of impervious surfaces (Wu and Murray 2003).

In general, a spatial resolution of 5 m or finer is suggested for urban applications (Welch 1982; Small 2003). Airborne imaging spectrometers like the Hyperspectral Mapper (HyMap) can be flown at altitudes as low as 1900 m resulting in a spatial resolution of 4 m for the 128 spectral bands. The very high spectral resolution of such instruments allows for analyses that cannot be conducted with spaceborne, multispectral instruments of similar spatial resolution like IKONOS; most classification schemes in urban applications require spectral information beyond the bandwidths of multispectral sensors (Herold et al. 2003).

However, a low operating altitude requires a wide field-of-view (FOV) to cover an appropriate area; in the case of HyMap the FOV is 61.3°. Especially in urban areas, this wide FOV leads to severe image distortions like object displacement and obscured surfaces. In addition, brightness artifacts exist, which are exacerbated by large view-angles. They result from anisotropic, bidirectional reflectance and are greatest when the flight path is perpendicular to the sun-target-observer plane (e.g. Beisl 2001). Generally speaking, the reflectance signal is higher in backscattering direction, i.e. when view and illumination direction are similar and shaded proportions of the viewed scene are hidden by sunlit proportions. This effect leads to an across-track brightness gradient that depends on the view-angle of the sensor and the illumination conditions during the over-flight. The brightness gradient “prevents precise intra- and intercomparison of images, affects spectral ratios and is adverse to proper mosaicking” (Beisl and Woodhouse 2004) and it hinders the

integration of information from spectral libraries that include laboratory and field measurements. For example, Ben-Dor et al. (2001) perform a Mixture Tuned Matched Filtering on urban imaging spectrometer data that was acquired perpendicular to the sun-target-observer plane and has not been corrected for bidirectional effects. They describe problems at large view-angles along the edges of the image using this quantitative method.

Thus, a complete preprocessing chain of imaging spectrometer data should include the correction of a possible across-track brightness gradient. This way, field and laboratory measurements can better be integrated for the design and training of subsequent classifications, quantitative models can be applied, and images that were acquired at different times or under varying conditions are easier to compare.

Existing approaches do not meet the requirements of data from urban areas. Approaches to model bidirectional effects and to assign derived compensation factors to individual pixels are not capable of describing the heterogeneous spectral and spatial structure of data from this environment. This paper extends and modifies an existing empirical approach and presents a simple, yet effective method for the removal of an across-track brightness gradient in HyMap data from urban areas.

2 Background

2.1 Bidirectional reflectance

The characteristics of bidirectional reflectance are determined by structural and optical properties of the viewed land surface (Lucht et al. 2000) and depend on illumination geometry, the sensor's view-angle and -direction, as well as the wavelength. They are completely described by the bidirectional reflectance-distribution function (BRDF)

$$f_r(\theta_i, \varphi_i, \theta_r, \varphi_r, \lambda) = \frac{dL_r(\theta_i, \varphi_i, \theta_r, \varphi_r, \lambda)}{L_i(\theta_i, \varphi_i, \lambda)\cos\theta_i d\omega_i} \quad (1)$$

according to Nicodemus et al. (1977), where f_r is the BRDF, L_i and L_r are the incident and reflected radiance, θ_i and θ_r are the zenith angles that describe the directions of incident and reflected flux, φ_i and φ_r are the respective azimuth angles, ω_i is the solid angle element of irradiance in the given direction. In Eq. (1), the original, purely geometric BRDF was extended by a wavelength dependency that is indicated by λ (compare Sandmeier et al. 1998).

Actually, the BRDF is a useful concept, but it can never be measured directly, since infinitesimal elements of solid angles do not include measurable amounts of radiant flux (Nicodemus et al. 1977). In practice, reflectance is measured over finite solid angles, i.e. biconical or hemispherical-conical. However, the term bidirectional reflectance factor (BRF) is most often used to describe the measured reflectance and the term bidirectional reflectance is rather loosely used for BRF(s) measured over targets from one or more nadir and off-nadir viewing angles. (Deering 1989)

Lucht et al. (2000) mention several reasons for anisotropic bidirectional reflectance, e.g. mirror BRDF caused by specular reflectors, by sunglint or forward scattering leaves and soil elements; volume scattering BRDF of scatterers like leaves in closed canopies; and gap-driven BRDF in the case of geometric-optical surface scattering, e.g. in sparse forests, driven by shadow casting and mutual obscuration of 3-dimensional surface elements. Pinty et al. (2002) visualize and discuss how the distribution of vegetation within single pixels can influence the gap-driven BRF at different view-angles.

2.2 BRDF models

BRDF models have been developed for different purposes and are not necessarily exclusive to the correction of brightness gradients. Actually, the bidirectional properties of certain surfaces are often used to derive information that is difficult to be deduced solely from the spectral signal. Several physical, semi-empirical and empirical BRDF models have been described and successfully applied over the past 25 years, especially for vegetation canopy reflectance, e.g. Goel (1988). A good overview on the different models in the context of the present paper is given by Beisl (2001).

Physical models are not suited for the correction of unwanted brightness gradients, but rather adapted for the interpretation of the BRDF information content. They are based on radiative transfer theory (Ross 1981; Verhoef 1984) or ray tracing methods (Li and Strahler 1986; North 1996) and describe the actual interactions between electro-magnetic radiation and surface materials. They can, for example, be used for the retrieval of the biophysical parameters that are closely linked to the measured signal, like leaf area index and canopy water content (e.g. Kötz et al. 2004) or canopy architectural properties (e.g. White et al. 2002). Kimes et al. (2000) give an overview on physical models and their possible applications.

The most common semi-empirical models are so-called kernel-driven models, which already have been used for a correction of brightness gradients (e.g. Leroy and Roujean

1994; Beisl 2001). Kernel-driven models describe the BRDF as a linear superposition of a set of kernels, e.g. an isotropic, a volume and a geometric scattering kernel, all of which model basic BRDF shapes and are derived from approximations of more detailed physical models (Wanner et al. 1995). This way, they are simple and fast to invert (Hu et al. 1997; Chopping 2000). The most common models have been developed for data from sensors like the Advanced Very High Resolution Radiometer (AVHRR) or the Moderate Resolution Imaging Spectroradiometer (MODIS). They are applied to derive various parameters at a global scale, e.g. the MODIS BRDF and Albedo Product (Lucht et al. 2000) but also for an improved differentiation between land cover classes using multi-angular data (Chopping et al. 2002).

In purely empirical approaches, mathematical functions are chosen to model the actually observed BRF without a physical basis, solely because of their shape. It is thus impossible to directly derive biophysical parameters from theses models. Early empirical models for a description of the bidirectional reflectance from vegetated surfaces (e.g. Royer et al. 1985; Walthall et al. 1985) are frequently used for the correction of brightness gradients in airborne line scanner imagery. Based on the mentioned models Kennedy et al. (1997) use a second degree polynomial to describe and remove brightness gradients in airborne data as a function of the view-angle only. They conclude that an intelligent use of these fairly simple methods can be an efficient preprocessing tool. This approach is implemented as the so-called “Cross Track Illumination Correction” in the Environment for Visualizing Images (ENVI) software package (RSI 2004). The neglect of the azimuth dependence is feasible in this context, because the illumination geometry does not change between pixels from different scan lines that are viewed at the same angle. Thus, all differences induced by directional reflectance occur in across-track direction, i.e. within the scan lines, and are sufficiently modeled as a function of view-angle (Kennedy et al. 1997).

Beisl (2001) compares various kernel-driven approaches and the mentioned empirical model for the correction of HyMap data from South-east Spain. He concludes that some kernel-driven models definitely perform better than the empirical approach for low solar zenith angles, especially due to their ability to model the so-called hotspot effect on vegetated surfaces. For medium solar zenith angles their performance is slightly better, for high solar zenith angles it is similar. He cannot identify one kernel-driven model that performs best for all situations.

However, image data from urban environments is very complex. Besides vegetation canopies in park areas, urban areas are to a great extent characterized by man-made surface materials with geometric structures that can hardly be described by physical approaches, i.e. roofs of various inclinations or facades at large view-angles. Against this background and given the following reasons, an empirical model was chosen to compensate for brightness gradients in the HyMap data in this study: (1) it takes into account the influence of surface geometry at small scales; (2) according to Beisl (2001) the chosen empirical approach is robust and performs equally for all illumination situations. He explicitly recommends it for “stiff problems”; (3) an empirical approach is completely independent of the viewed surface types and spatial resolution of the image, whereas most semi-empirical kernels have been developed to model structures of vegetated surfaces at moderate resolution scales; (4) the main drawback of this approach is a lacking term to model the hotspot effect, a phenomenon that does not exist in the data of this work; (5) the approach is very simple, computationally fast, and requires no ground measurements.

2.3 Correction of surface type dependent brightness gradients

Several authors mention variations in the bidirectional properties of different surface types: Richter and Schläpfer (2002) notice the need of a class-wise correction of bidirectional effects and implement an index-based pre-classification in their software for the atmospheric correction of airborne scanner data. They do not suggest a certain method for the correction of possible brightness gradients, though. Schlerf et al. (2005) eliminate the brightness gradient in a coniferous forest by masking all other pixels prior to the fit of an empirical model. Kennedy et al. (1997) classify an airborne image prior to the correction and fit individual models to those classes. They describe great differences in the bidirectional properties of soil and vegetation and recommend a class-wise approach. Beisl (2001) describes the significant differences between classes like *bright sand/soil*, *bright vegetation* and *dry vegetation* and tests a class-wise correction. Feingersh et al. (2005) suggest empirical models for different surfaces based on laboratory measurements with a goniometer for the correction of BRDF effects.

The spatial and spectral heterogeneity of urban areas exceeds that of other environments by far and a high number of mixed pixels exist. Great differences in the bidirectional reflectance of urban surfaces in HyMap data have previously been described by the authors (Schiefer et al. 2005a). In consideration of all mentioned aspects, the compensation of the brightness gradient will be conducted in a class-wise empirical approach with a focus on

the two questions of (1) how to best fit an empirical model to the brightness gradient in data from urban areas, and (2) how to correct all pixels from an image of such a spectral and spatial heterogeneity.

3 Data

3.1 HyMap imagery

The HyMap sensor acquires data in the visible (VIS), the near-infrared (NIR) and short-wave infrared (SWIR) between 0.4 and 2.5 µm. The data are stored in 128 spectral bands with an average sampling interval of approximately 15 nm. 512 pixels are recorded for each scan line with an instantaneous field of view (IFOV) of 2.0 and 2.5 mrad in across and along-track direction, respectively. Given the FOV of 61.3°, the maximum view-angle is slightly greater than 30° (in this paper, negative view-angles are used to indicate a view-direction towards the sun). Limited by the operating altitude and minimum speed of the aircraft, HyMap is typically flown between 1900 and 5000 m above ground and the spatial resolution is thus between 3.9 and 10 m, the swath width between 2 and 5 km.

The HyMap imagery for this study was acquired over Berlin, Germany, during the HyEurope 2003 campaign of the German Aerospace Centre (DLR), on July 30, 2003, around 12 am local time. Sun elevation was 56° (θ_i = 34°) and its azimuth φ_i 148°.

One of four flight lines of Berlin is corrected for its across-track brightness gradient in the present work. The flight direction was at 78° leading to a sun-target-observer geometry that causes a severe brightness gradient (Fig. II-1). The scene is located around E 397397 and N 5821900 in UTM zone 33 and covers a great variety of urban structures in an area of 16 by 2.59 kilometers at a ground instantaneous field of view (GIFOV) of 4.6 m. It extends from the central governmental district eastwards to suburban areas and includes densely built-up areas with orthogonal street patterns in the city center, park areas and allotments, industrial grounds, and railway areas. In addition, structures are viewed that are characteristic for Berlin, e.g. trees along most of the streets, or – typical for formerly socialist cities – wide boulevards in the center and large apartment complexes in suburban areas. The across-track brightness gradient is present on all surfaces but most obvious for vegetation.

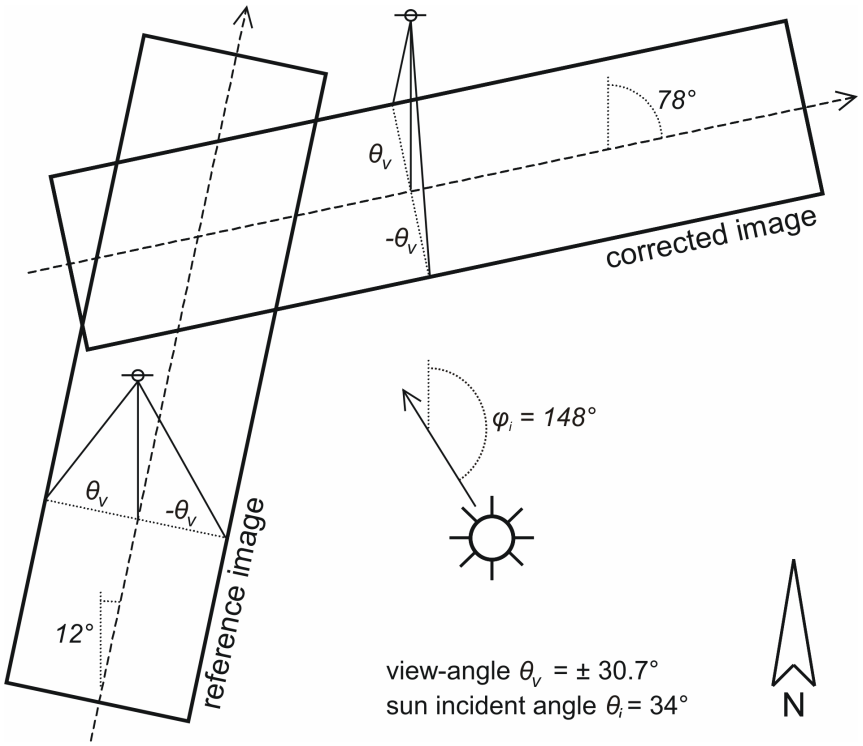

Figure II-1: Illumination and viewing geometry of the corrected image and the reference image.

A second flight line was acquired from South to North with a heading of 12° and a spatial resolution of 3.9 m, overlapping the first image in the city center (Fig. II-1). The brightness gradient in this flight line is negligible due to its sun-target-observer geometry and it is used for validation of the correction results.

3.2 Preprocessing

Prior to the removal of the brightness gradient, the data sets were corrected for atmospheric influences and transformed to reflectance values (ρ). One of the most prominent atmospheric effects is the so-called path radiance, which is also view-angle dependent and might cause an additional brightness gradient (Beisl and Woodhouse, 2004). The atmospheric correction was performed using the Fast Line-of-sight Atmospheric Analysis of Spectral Hypercubes (FLAASH) algorithm version 1.7 as implemented in ENVI 4.0 (RSI 2004). The approach removes the path radiance and was carried out first. Otherwise the path radiance might be modeled by both the empirical correction of the bidirectional effects and the subsequent parametric atmospheric correction, and this way be overcorrected. FLAASH incorporates the MODTRAN-4 radiation transfer code (Matthew et al. 2000). The amount of water vapor is calculated for each pixel individually from the 1.135 µm water feature and adjacency effects are considered. In the present case, images were corrected using the mid-latitude summer atmosphere. The ISAACS method was used

to model multiple scattering of solar irradiance. Since there is no significant industry in Berlin, a rural aerosol model without soot-like aerosols was chosen. Best results were achieved with an initial visibility of 30 km for a retrieval of the aerosol optical thickness. Finally, FLAASH's spectral polishing – a linear renormalization similar to the method introduced by Boardman (1998) – was applied to smooth the spectra.

Following this correction, the signal-to-noise ratio was estimated for the very homogenous area of an artificial soccer field and bands with insufficient SNR-values were deleted. The remaining 116 bands are used in the present work.

4 Methods

A class-wise correction requires a preliminary classification of the data, an empirical modeling of the brightness gradients for all bands of the individual classes, the calculation of compensation factors that result from these models, and their application to the entire image. The individual steps will be explained in the following with a focus on the classification as well as the class-wise application of the models to the data.

4.1 Preliminary classification

Brightness gradients are removed in order to guarantee better results for subsequent analyses -including classifications. It thus seems paradoxical to classify an image for the removal of brightness gradients. In this context the preliminary classification must not be seen as a classification into land use classes; areas are rather delineated by BRF characteristics. A combination of band ratios and results from a spectral angle mapping (Kruse et al. 1993a), which minimizes the influence of a brightness gradient, are used for this purpose. Being a supervised classification, the spectral angle mapping (SAM) requires training spectra. Therefore, training areas were manually selected for each surface type that appears relevant for the urban environment.

The results of the classification are actually needed for two objectives: (1) to identify pure pixels from specific surfaces to fit representative empirical models to present brightness gradients and (2) to assign class membership values to all pixels in order to apply the surface-type specific compensation factors to the entire image.

In a first approach the classes *water*, *cast shadow*, and *specular reflector* are masked based on thresholds in single bands or band ratios; these classes are often either very bright or dark and hinder the work with empirical models. Afterwards spectrally pure classes are

determined using SAM with restrictive angular thresholds. In this case, a large number of unclassified pixels is accepted in favor of a high user accuracy. These classes are expected to avoid pixels in transition zones to different surface types and statistically robust models are fit to the brightness gradients of the spectrally pure classes. The fit requires a sufficient representation of each class for all view-angles to compensate the influence of bright or dark outliers. This condition is important for the decision on the final number of classes to be used.

In a second classification the SAM is conducted without prior masking and with less restrictive thresholds for the angular values in order to classify the entire image into the previously defined classes.

4.2 The empirical correction of brightness gradients

The empirical correction is based upon approaches by Kennedy et al. (1997) and Walthall et al. (1985). It comprises a normalization of bidirectional reflectance factors to nadir view: Existing brightness gradients are modeled by calculating the mean reflectance for each view-angle and fitting a quadratic curve to these values. This is done for each spectral band individually. The modeled reflectance ρ^* is described by the view-angle θ_v, which is equivalent to θ_r, the quadratic and linear coefficients q and l, and the constant c:

$$\rho^*(\theta_v) = q\theta_v^2 + l\theta_v + c \tag{2}$$

Assuming bidirectional effects to be zero at nadir position, brightness gradients can be removed via the multiplicative or additive compensation factors k_m and k_a,

$$k_m(\theta_v) = \rho^*(\theta_v) / \rho^*(\theta_{nadir}) \tag{3}$$

$$k_a(\theta_v) = \rho^*(\theta_v) - \rho^*(\theta_{nadir}), \tag{4}$$

respectively. The application of Eq. (3) or (4) to all pixels from the image results in a compensation layer for each spectral band. Using this compensation layer, the normalized reflectance values ρ' of all pixels are calculated as

$$\rho'_m(\theta_v, r) = \rho(\theta_v, r) / k_m(\theta_v, r) \tag{5}$$

$$\rho'_a(\theta_v, r) = \rho(\theta_v, r) - k_a(\theta_v, r), \tag{6}$$

where ρ is the atmospherically corrected BRF, and r the pixel's position in along-track direction, i.e. row.

4.3 Class-wise correction

As in many analyses of remotely sensed data, the mixed pixel phenomenon and false classifications play a crucial role in the present approach and interfere with the correction in two ways:

At first, potentially included mixed or falsely classified pixels would render the models less representative. Mixed pixels are avoided in a classification with restrictive thresholds as outlined in Section 4.1. The pixels of the resulting pure classes are used to fit the surface specific models (Eq. (2)).

At second, the entire image needs to be corrected, including pixels of rare materials or mixed composition. This requires a useful way to assign the compensation layers of the pure classes that result from Eq. (3) or (4) to every pixel of the image, including those pixels that were not classified during the first restrictive classification. Two different approaches are tested for this processing step with a focus on the correction of mixed pixels and compared to a global approach. Thus, three different corrections are discussed in this paper:

a) a *global* correction, using one compensation layer for all pixels that was generated with an empirical model fit to the entire image,
b) a *class-wise* correction, that applies surface specific models based on classes from the restrictive SAM to all pixels according to classification results using non-restrictive angular thresholds (Fig. II-2),
c) a *weighted class-wise* correction, applying a mixture of the compensation layers in (b) to all pixels, according to class membership values of the individual pixels, that are derived from the SAM rule images (Fig. II-2).

This last approach is the attempt to take into account the mixed bidirectional properties of spectrally mixed pixels. It requires information on the abundance of the previously modeled surface types for every pixel. A spectral mixture analysis is not appropriate in this context due to several reasons: its results are influenced by the brightness gradient, a complete set of spectral endmembers is required to produce reliable results and the effort needed is contradictory to the idea of a simple empirical approach.

Instead, the existing rule images of the SAM and their inherent information on class membership are utilized to describe possible mixed pixels. These rule images contain the pixel-wise angles between the vector that describes a reference spectrum in data space, i.e. the average spectrum from a previously selected training area, and the vector of the

respective pixel. This way, one rule image exists for every reference spectrum. Within these, small angles indicate great similarity. Histograms from these rule images typically show two peaks (Fig. II-3). At small angles, to the left, a narrow peak relates to pixels that are spectrally very similar to the reference spectrum, i.e. belong to the same class. A second peak further to the right represents the pixels of all other classes at once, since the angular difference is independent from a direction in spectral space. The slopes to the sides of this second peak are less steep and sometimes contain relative maxima.

During a regular SAM classification, thresholds for the angular values are defined to generate discrete classes. To describe the abundance of surface types in mixed pixels in terms of class membership values, a transition zone between pure and mixed pixels is derived interactively for the rule image of every final class (Fig. II-3). The values of the corresponding angular intervals are inverse linearly normalized between 1 and 0 for each pixel; values left and right of the transition zone are set to 1 and 0, respectively. In a second step, the transformed values of all rule images are pixel-wise divided by their sum in order to guarantee unity. During the weighted class-wise correction, the surface specific compensation layers will be combined for every pixel individually according to these transformed rule images, i.e. class weights.

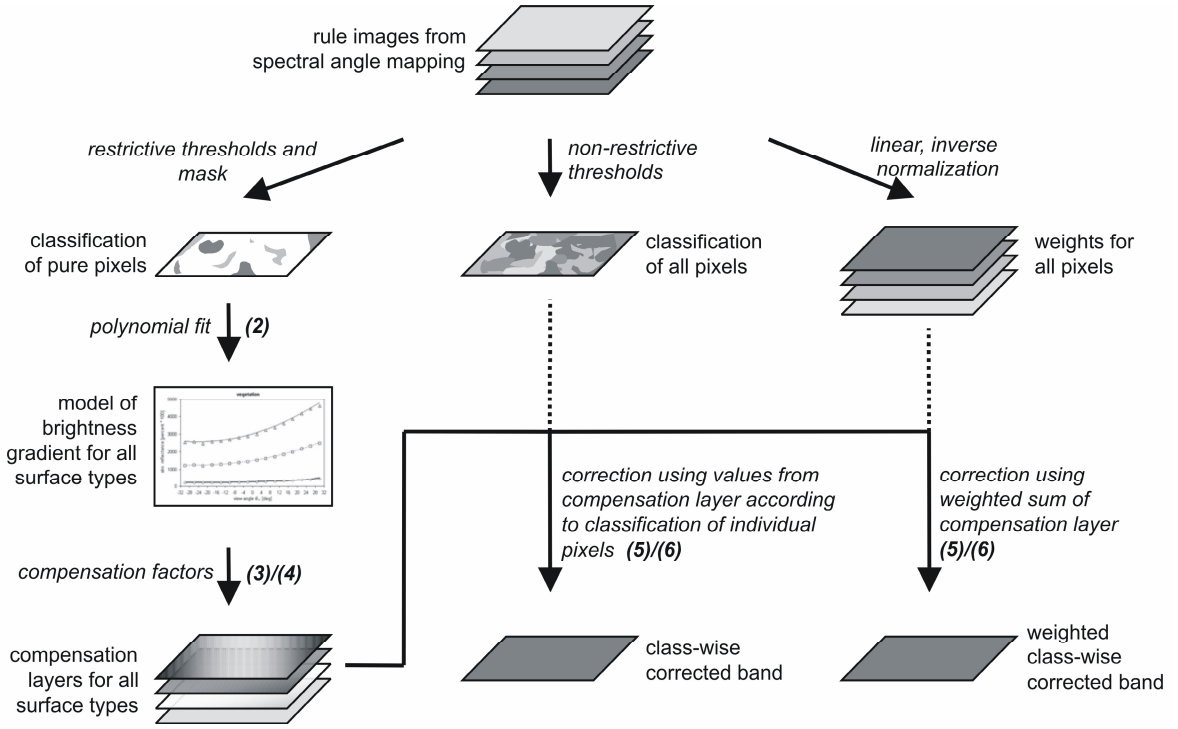

Figure II-2: *Class-wise* and *weighted class-wise* correction of brightness gradients in individual bands of HyMap data. Results from a SAM with restrictive angular thresholds are used to model the brightness gradients and to generate the compensation layers of classified surface types. Rule images are then used to assign these compensation layers to individual pixels in a discrete and weighted manner. The numbers in brackets indicate the corresponding equations in the text.

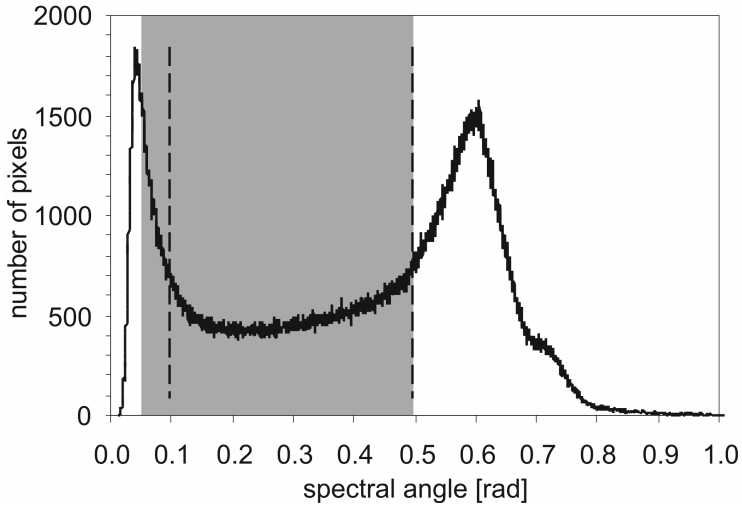

Figure II-3: Histogram of a rule image from the class vegetation during SAM classification. The vertical lines indicate angular thresholds of the restrictive (left) and non-restrictive (right) classifications. The grey area shows the transition zone as used to transform the rule image for the weighted class-wise correction.

All three correction approaches are performed twice, using multiplicative and additive compensation factors. Within the *class-wise* and *weighted class-wise* approach the fit of the empirical models is based upon all pixels of the corresponding pure classes, not upon angular means as in the global approach. This way, unequal distributions are better taken into account and the influence of outliers at angles with only few pixels is reduced.

5 Results and discussion

5.1 Preliminary classification

A thorough analysis of the SAM results leads to four spectral classes that are used for the class-wise correction of the brightness gradient. The class *vegetation* is actually a combination of five sub-classes with reference spectra from different tree stands and well irrigated photosynthetically active grass surfaces. For this purpose a minimum image was produced from the five original rule images to receive the maximum class membership values for *vegetation*. Besides for classification, this combined minimum image was also used for the transformation into class-weights as described in Section 4.3. A differentiated treatment of these surface types would certainly be useful, but the number of well irrigated grass surfaces in the image is too small for the reliable fit of an empirical model, due to the very dry and hot summer of 2003 in central Europe. By combining different types of vegetation a statistically robust model can be fit and the spectral heterogeneity of vegetation is represented. Given the dry weather conditions, the class dry vegetation

Table II-1: Results from the restrictive and non-restrictive classification. The size of the four classes *vegetation*, *dry vegetation*, *dark roof* and *street* enables the fit of empirical correction models to the brightness gradients of the respective surface types. Specular reflectors, water and cast shadows are masked prior to the classification.

	Restrictive classification		Non-restrictive classification	
	No. pixels	% pixel	No. pixels	% pixel
Unclassified	1,003,039	64.3	19,312	1.2
Vegetation	279,237	17.9	615,091	39.4
Dry vegetation	81,044	5.2	311,213	20.0
Dark roof	46,951	3.0	90,922	5.8
Street	83,285	5.3	523,526	33.6
Mask	66,508	4.3	-	-

turns out to be appropriate and sufficiently large. This class includes non-irrigated surfaces with dry grass and varying fractions of background soil signal. The transition between the classes *vegetation* and *dry vegetation* is smooth and the number of pixels that are a mixture of the two is high. *Dark roof* represents a great part of the various roof types. All other roof types, i.e. red or metal roofs, lead to very small classes that are spectrally too different to be combined with the dark roofs. The class *street* includes non-built up impervious surfaces. Attempts to add more classes, e.g. open soil of construction areas, result in unsatisfactory results. The classes are too small or not present in all angular intervals, making a good model fit impossible.

Whereas only 31.4% of the pixels are assigned to one of the four spectral classes in the first classification with restrictive thresholds, 98.8% are classified in the second (Table II-1). The remaining 1.2% are spectrally extreme pixels like specular reflecting roofs or water bodies that differ extremely from the four spectral classes. The high number of pixels being classified as *vegetation* or *dry vegetation* is explained by several park areas in the city and more rural areas in the eastern part of the image.

The decision on these four final classes and on the angular thresholds for the restrictive classification was driven by the class size and the quality of the model fit. Obviously, not every urban surface type is represented by one of the four classes.

During the second classification, previously unclassified or masked pixels were assigned to one of the four final classes. This way the entire image can be corrected with the class-wise approach using the compensation layers that base on the pure classes. However, the areal increase of the four classes is unequal. The class *street*, for example, increases significantly more than the class *dark roof*. This is in parts explained by the spectral heterogeneity of non built-up areas. At the same time, several pixels from different roof types were added to

the class street during the second classification. Misclassifications of materials from built up and non-built up areas in urban environments are a well known problem (e.g. Herold et al. 2004). Nevertheless, a more sophisticated and hence complex classification was not intended and a wrong assignment does not necessarily worsen the results of the brightness correction, i.e. roofs that are spectrally similar to ground materials might have similar bidirectional properties.

5.2 Empirical models

Empirical models are fit to the pixels from the four spectral classes in each spectral band based on the results of the restrictive classification (Fig. II-4). The distinct brightness gradients of the four classes can all be modeled well using a second degree polynomial. The different shapes of the models underline the need of a class-wise approach. The models appear to capture different phenomena and are reminiscent of the kernels used in semi-empirical models (e.g. Wanner et al. 1995).

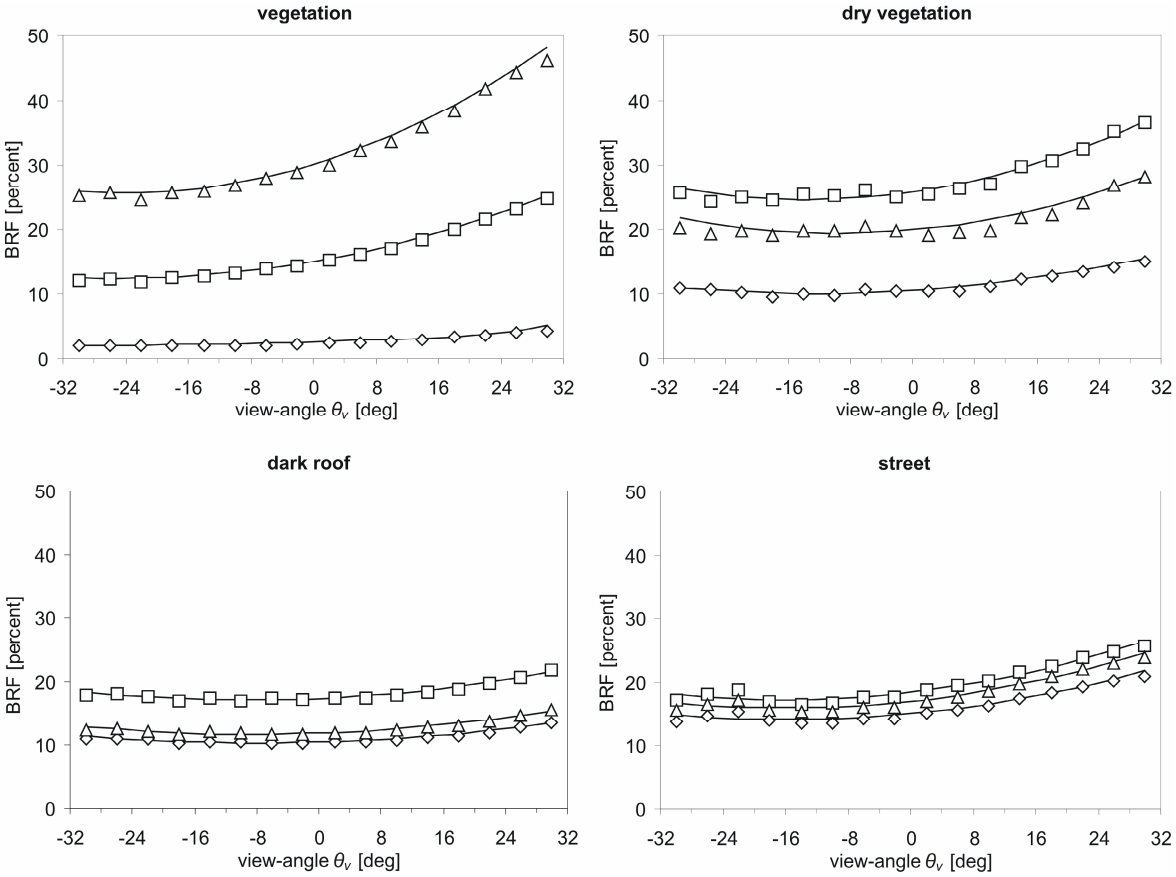

Figure II-4: Brightness gradients and empirical models of four spectral classes. Gradients are illustrated by average brightness of 4° view-angle intervals for three spectral bands at 661.6 (diamonds), 828.5 (triangles) and 1647.8 nm (squares); fitted models are displayed as solid lines. The sun incident angle θ_i is 34°.

Table II-2: Standard deviations of classes and unclassified pixels after restrictive classification for all view-angles (SD all) and mean standard deviation of 4° view-angle intervals (SD angles). Values are averaged over all bands.

	SD all	SD angles
Unclassified	857.18	798.24
Vegetation	569.75	432.51
Dry vegetation	546.45	472.72
Dark roof	318.66	294.34
Street	735.39	680.94

The brightness gradient of *vegetation* is dominated by a steady, concave increase towards backscatter direction, i.e. positive view-angles. This corresponds well with findings by Jacquemoud et al. (2000). They simulate the bidirectional reflectance factor of vegetation as a function of view-angle with four physical models. Their results agree with the gradients for vegetation in the present work for the HyMap view-angle interval. Kimes (1983) explains this shape by the sensor viewing forelit surfaces when looking with the sun and backlit surfaces when looking towards the sun.

The gradient for *dry vegetation* differs from this shape: it is almost constant in forwardscatter direction and then increases similar to the one of vegetation in backscatter direction. The dry grass surfaces are missing the 3-dimensional structure that causes a great part of the typical directional effects of vegetation mentioned above. The effects are thus weakened and the brightness gradient is also expected to be influenced by the bidirectional properties of the background soil signal.

The increase towards backscatter direction in the brightness gradient for *street* is less distinct. The abnormal feature around $\theta_v = -22°$ might be explained by the structure of alternating houses and streets; the sensor views differently illuminated surfaces depending on the width of streets and the height of houses. The influence of surface geometry is also very obvious in the gradient of *dark roofs*: The brightness is almost constant for all view-angles. This was expected, since the high frequent changes in inclination of the roofs superpose the view-angles' influence on the target-observer-geometry.

The standard deviations of the classes are compared to their standard deviations of 4° view-angle intervals, following Beisl (2001). The mean standard deviations of the intervals are significantly lower than the overall standard deviation values for all four classes (Table II-2). This underlines the existence of the brightness gradients. The difference between the two values is most obvious for *vegetation* and *dry vegetation*, i.e. classes with very distinct gradients. The standard deviation's decrease is less obvious for *street* and small for *dark roof*.

5.3 Evaluation of the class-wise correction of brightness gradients

Assessing a correction of brightness gradients is complicated, because reliable references often do not exist for all angles and surface types. Besides an inspection of the brightness gradient in the corrected image and a visual analysis of results, the aforementioned overlapping HyMap image is utilized as a reference. At first, the class-wise correction will be discussed based on the results from the multiplicative approach. Afterwards the additive approach will be examined in comparison.

The empirical models are based on the pixels classified during the restrictive classification, i.e. only 31.4% of all pixels. However, remaining pixels show a brightness gradient, too. This gradient is completely removed during the class-wise correction (Fig. II-5). It thus seems feasible to apply empirical models derived from pure classes to the entire image.

The visually observable brightness gradient is removed by all three approaches that are compared in this study (Fig. II-6b). Especially the most dominant gradients of areas with *vegetation* and *dry vegetation* cannot be observed in the corrected images.

The differences between the class-wise and weighted class-wise approach become obvious in areas with many mixed pixels, e.g. transition zones between the classes *vegetation* and *dry vegetation*: the class-wise approach is characterized by abrupt brightness differences caused by discrete class boundaries (Fig. II-6f). A similar phenomenon is described by Beisl (2001) for agricultural areas with varying vegetation cover. At this point the advantage of the weighted class-wise approach comes into play: differences between

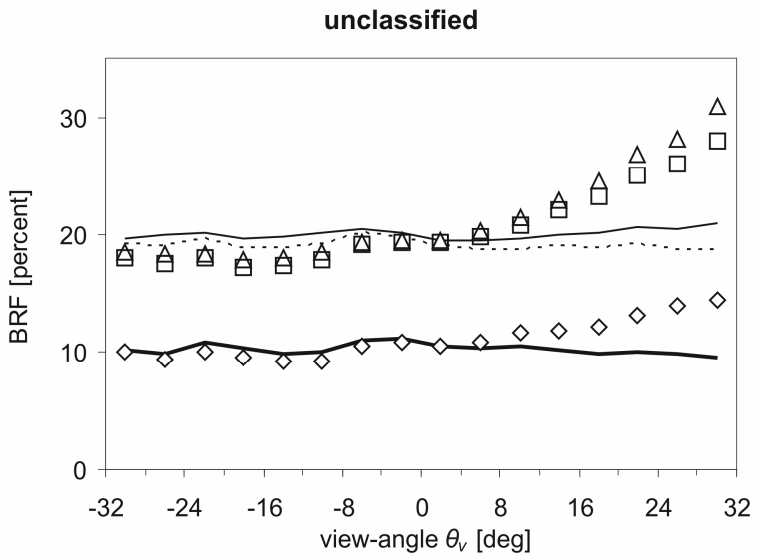

Figure II-5: Comparison of the brightness gradients before and after multiplicative class-wise correction of pixels that were not classified during the restrictive classification in spectral bands at 661.6 (diamonds/thick solid), 828.5 (triangles/solid) and 1647.8 nm (squares/dashed). The sun incident angle θ_i is 34°.

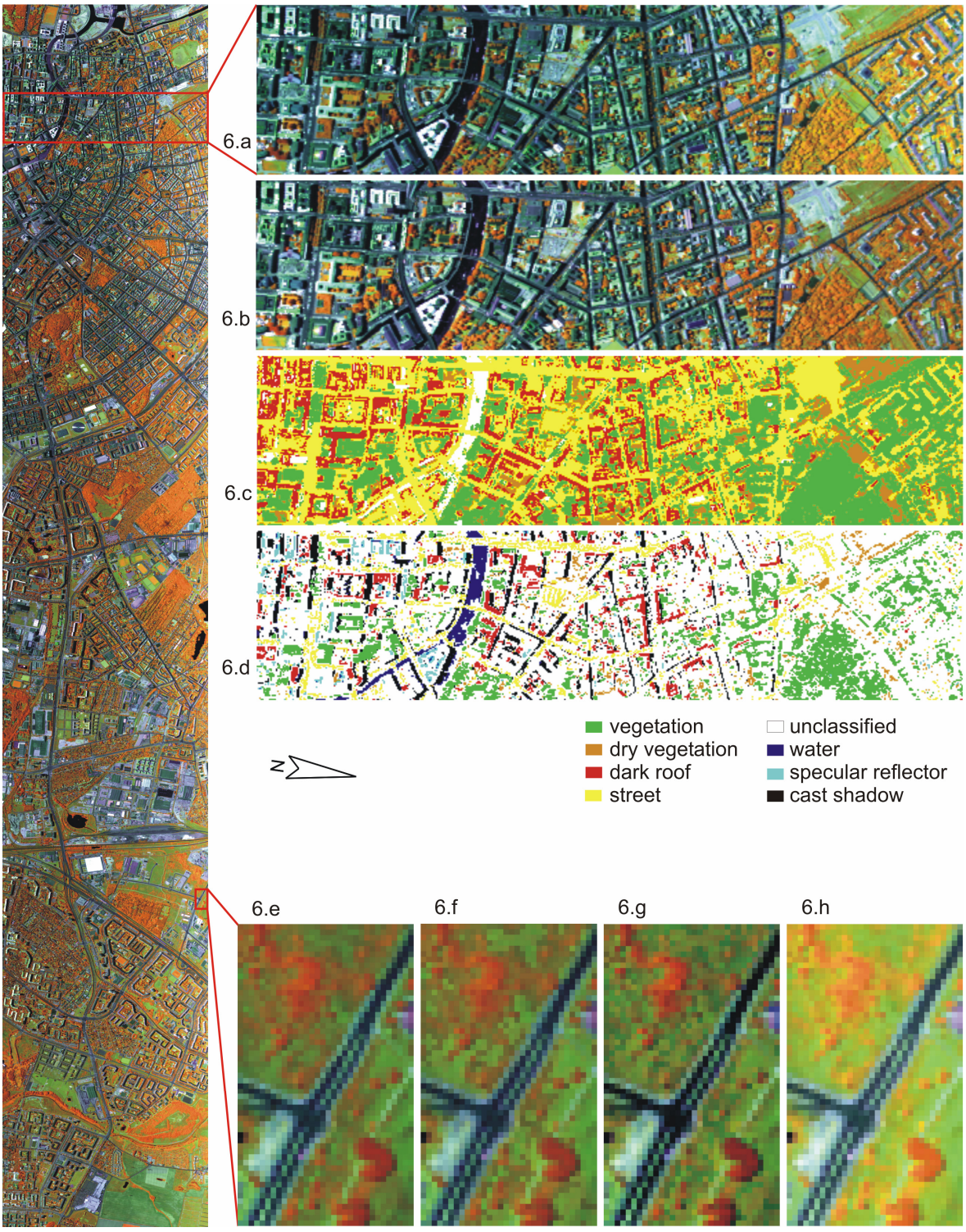

Figure II-6: Subsets of the corrected image before and after the class-wise correction (R = 828.5 nm; G = 1647.8 nm; B = 661.6 nm): In the uncorrected data (a), the bright surfaces to the right (backscatter direction) lead to obvious gradients over the entire FOV. These gradients do not exist after the multiplicative class-wise correction (b); the performance of other approaches appears similar at this scale. (c) illustrates the classification of the entire image; (d) shows the restrictive SAM classification (including previously masked areas) that was used to fit the empirical models. The advantages of the weighted class-wise approach (e) over the multiplicative (f) and additive (g) class-wise approaches are obvious in transition zones with mixed pixels; the original subset (h) is shown for comparison. The full image is displayed left. Note the rotated northing of all images.

neighboring mixed pixels are smoother (Fig. II-6e). This way, abrupt changes that might hamper subsequent quantitative analyses can be avoided. The overall quality and image statistics are almost identical. The idea to generate weights based on SAM rule images, thus, proved useful. Nevertheless, the authors do not consider the rule images a generally appropriate quantitative measure; especially the assumption of a linear relation between the spectral angle and surface abundance is critical.

Results from the different correction approaches are compared to data from the reference image. A direct areal comparison of the entire overlapping area is not possible, because of the view-angle dependent object-displacement and the different spatial resolutions of the two images. Instead, pixels from the same distinct surfaces were manually selected in both images and the average spectra are compared. All surfaces are located in the nadir area of the reference image and at large view-angles in the corrected image. This way, areas with high compensation factors are assessed. However, different proportions of sub-pixel scale objects might be compared, due to the respective nadir and off-nadir view. This might be a source of uncertainty during the assessment, e.g. for 3-dimensional structures like tree crowns, which is difficult to quantify.

Spectra from the image before and after the different corrections are compared to spectra from the reference image (Fig. II-7). The class-wise correction leads to better results in all cases except for irrigated lawn, which is overcorrected by all multiplicative approaches. In the case of non-irrigated vegetation, a roof and a school yard, the class-wise approach performs exceptionally better. Results from the weighted class-wise method are almost identical to the class-wise approach and differences cannot be displayed.

The class-wise correction of the soil surface is only slightly better than the global correction. However, its advantage over the global correction is shown by an interesting feature: Between 700 and 800 nm a decrease in the reflectance of the spectrum after global correction exists that cannot be found in the other three spectra. This is an overcorrection, caused by the influence of vegetated surfaces and their spectral characteristics in the red and NIR region on the compensation factors of the global approach. The same phenomenon was observed for a concrete surface and a second roof surface (not shown).

Vegetated surfaces are hardest to correct. The influence of bidirectional effects is high and brightness gradients are severe, especially in the NIR. The class-wise approach performs very well in the VIS and SWIR regions of a spectrum extracted from a tree group (Fig. II-7). In the NIR, reflectance is slightly overcorrected, but results are better than using

the global approach. Similar patterns can be observed for additional vegetated surfaces (not shown). Differences might to some extent be explained by the different view-angles of corrected and reference image.

The class *vegetation* combines vegetation canopies of different structures and thus different bidirectional effects. Park areas with trees dominate and the correction of an extremely

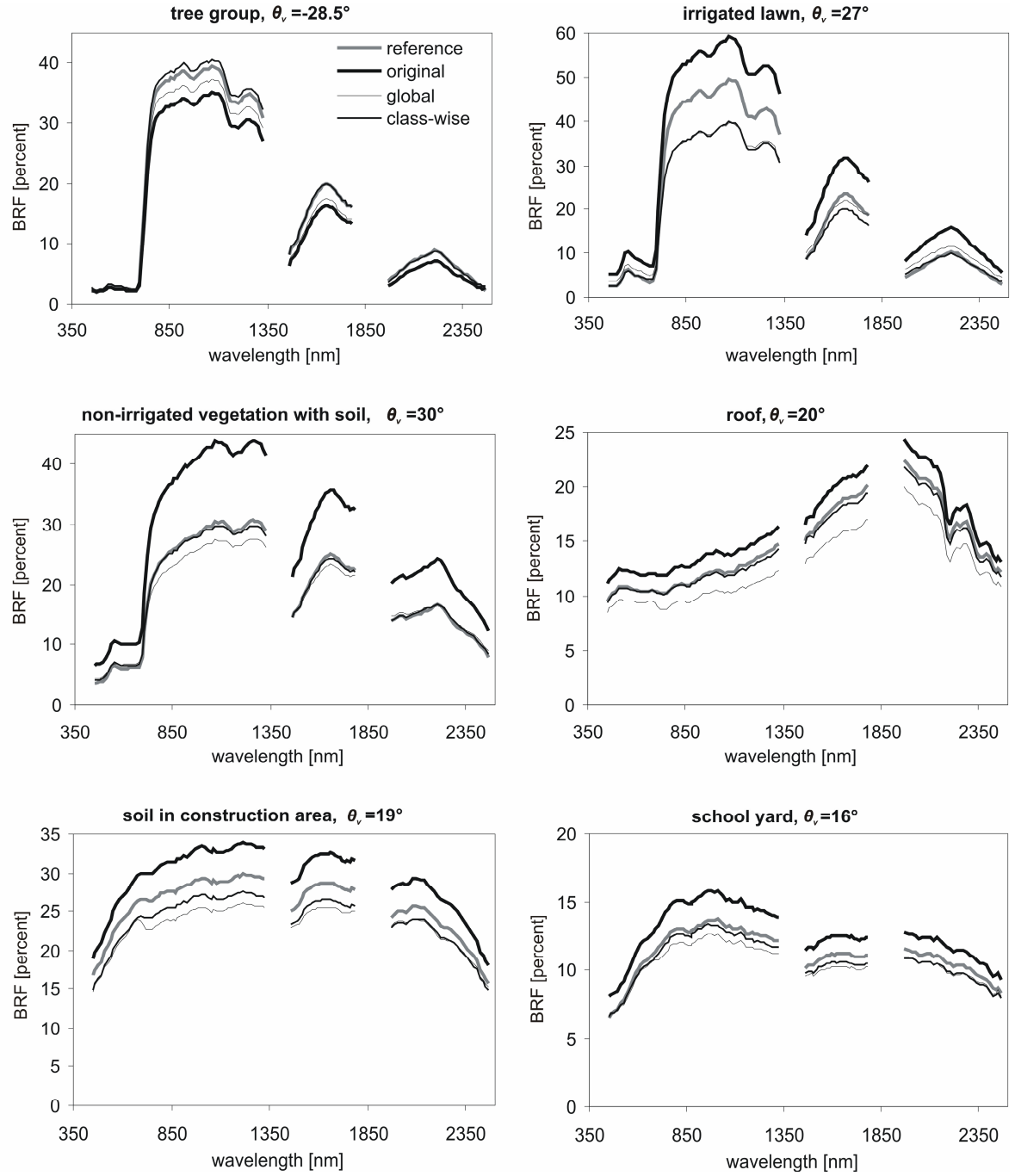

Figure II-7: Spectra from six selected surfaces at large view-angles in HyMap data before and after correction with multiplicative global and class-wise approach. Spectra from the same surfaces in the nadir area of the reference image are shown for comparison.

bright irrigated lawn surface (Fig. II-7) does not perform adequately with either method. The empirical model is not well suited for this surface type.

At this point a general problem needs to be mentioned: in a single image, surfaces are always classified by spectral values, not by bidirectional properties. This drawback has to be considered, when applying a class-wise approach. Classes like *vegetation* that are spectrally heterogeneous might require several models. Especially for non-urban environments more than one class for vegetated surfaces is recommendable.

However, the four correction functions and possible combinations of these prove capable of correcting most bidirectional behaviors. An increase in the number of classes – if statistically possible – should only be considered, when an additional bidirectional effect is observed and can be modeled.

Overall, results from the additive approaches are not as good as results from the multiplicative corrections. Constant compensation factors cause very low and often negative values for dark surfaces, like streets (Fig. II-6g). They appear overcorrected. The original standard deviation is maintained even when average brightness is clearly reduced. Hence, images exhibit artificial noise in low albedo areas. This phenomenon is reduced by the class-wise approaches, but still exists in all classes.

As for the multiplicative approach, spectra from additively corrected images were compared to spectra from the reference image (not shown). Again, the class-wise approach performed better than the global. In two cases, the class-wise additive correction actually performed better than the multiplicative: the irrigated lawn was less overcorrected in the NIR and the very bright soil surface is corrected even better. In both cases, surface brightness differs significantly from the modeled gradient. The constant compensation factors of the additive approach thus generate smaller errors for extremely bright areas than the relative compensation factors of the multiplicative method.

6 Conclusions

The suggested class-wise and weighted class-wise empirical approaches are capable of correcting the brightness gradient in HyMap data from an urban area. They always perform better than a global approach and are not limited to certain surface types, like most semi-empirical models that are designed to model vegetation canopies. This is especially advantageous for the correction of urban data. At the same time, the approach taken does

not require any directional field measurement with a goniometer or additional images at different viewing conditions. This makes it superior to other approaches described in the literature and applicable independent from the provision of additional information.

The multiplicative normalization performs better than the additive for the present data set. Its advantages are expected to be generally valid.

The correction of brightness gradients from vegetated surfaces might be further enhanced by a differentiation between vegetation types. In case the focus of subsequent analyses is put on vegetation issues, working with more than one vegetation class is useful. This should be tested using images that represent different vegetation types equally well.

The weighted class-wise approach overcomes problems of the discrete transitions in the class-wise approach. It is probably close to the ideal correction of brightness gradients in complex environments: one correction model is determined for each relevant surface type and individual pixels are corrected with a weighted term according to the abundance of the basic surface types.

The concept of the spectral angle mapper proved appropriate. It requires one interactive step and it would be desirable to extract spectral classes for all environments during preprocessing in an automated way.

A brightness gradient cannot be observed for the corrected image, not even for the pixels that were discarded when fitting the brightness models. Spectra from the corrected image fit those from a reference image, even at large view-angles. Thus, the entire area of the processed image and its full hyperspectral information can be used in both qualitative and quantitative analyses, including the work with spectral libraries or in multi-temporal studies. The suggested class-wise approach can easily be transferred to other hyperspectral data sets that show similar brightness gradients.

Acknowledgments

The authors would like to thank the German Aerospace Center (DLR) for the HyMap data. Sebastian Schiefer is funded by the scholarship programme of the German Federal Environmental Foundation (DBU), Alexander Damm by the Young Scientists Programme of the State Berlin. This research is partly funded by the German Research Council (DFG) under project no. HO 2568/2-1 and 2-2. The authors are also thankful and the three anonymous reviewers who provided helpful comments to improve this manuscript.

Chapter III:
Classifying segmented hyperspectral data from a heterogeneous urban environment

Journal of Applied Remote Sensing 1 (2007) 013543

Sebastian van der Linden, Andreas Janz, Björn Waske, Michael Eiden and Patrick Hostert

doi: 10.1117/1.2813466
received 28 March 2007; revised 15 October 2007;
accepted 16 October 2007.

Abstract

Classifying remotely sensed images from urban environments is challenging. Urban land cover classes are spectrally heterogeneous and materials from different classes have similar spectral properties. Image segmentation has become a common preprocessing step that helped to overcome such problems. However, little attention has been paid to impacts of segmentation on the data's spectral information content. Here, urban hyperspectral data is spectrally classified using support vector machines (SVM). By training a SVM on pixel information and applying it to the image before segmentation and after segmentation at different levels, the classification framework is maintained and the influence of the spectral generalization during image segmentation hence directly investigated. In addition, a straightforward multi-level approach was performed, which combines information from different levels into one final map. A stratified accuracy assessment by urban structure types is applied. The classification of the unsegmented data achieves an overall accuracy of 88.7%. Accuracy of the segment-based classification is lower and decreases with increasing segment size. Highest accuracies for the different urban structure types are achieved at varying segmentation levels. The accuracy of the multi-level approach is similar to that of unsegmented data but comprises the positive effects of more homogeneous segment-based classifications at different levels in one map.

1 Introduction

The number of remote sensing applications in urban areas has significantly increased over the past years (Roessner et al. 2001; Benediktsson et al. 2005; Small et al. 2005; Lu and Weng 2006). This development is mainly driven by two factors: at first, the rapid global urbanization process raises the demand for time and cost effective space- and airborne monitoring (UN 2006). At second, the spatial resolution of recently available remote sensing imagery allows an accurate representation of urban structures (Small 2003; Bruzzone and Carlin 2006). Despite the fine spatial resolution of new sensors, urban areas are still challenging to be studied with remotely sensed data. Spectral properties of the urban environment influence the performance of image analyses like the classification of land cover types. The number of surface materials and hence the spectral heterogeneity in urban imagery is very high and spectrally similar materials might occur on different surface types, e.g. tar roofs and asphalt roads (Herold et al. 2004). Common multispectral sensor configurations as used for IKONOS or Landsat Thematic Mapper are not sufficient to differentiate such urban categories. In addition, the high frequent spatial patterns of urban reflectance suggest a relatively high number of mixed pixels (Small 2003). A detailed classification of urban areas thus requires data of high spectral and spatial resolution, as for example provided by airborne imaging spectrometers like the Hyperspectral Mapper (HyMap).

Various authors improve urban classifications of spectrally ambiguous surfaces by using additional information like census data on population density (Lu and Weng 2006), LiDAR information on surface structure (Hodgson et al. 2003), or texture measures like extended morphological profiles (Benediktsson et al. 2005). In Shackelford and Davis (2003), results of a pixel-based spectral classification are combined with the classification of a segmented image that bases upon information on the segments' shapes and neighborhoods; in doing so, a higher accuracy for typical urban classes like buildings, roads and other impervious surfaces is achieved. The successful incorporation of segment properties into the classification of urban areas is described by various authors (Damm et al. 2005; Bruzzone and Carlin 2006; Diermayer et al. 2006; Schöpfer and Moeller 2006).

In the context of segmentation-based analysis, so far only little attention has been paid to its influence on spectral image information: during the segmentation process segments are assigned the mean spectral value of their constituent pixels as primary spectral

information. The effect of this spectral generalization can hardly be predicted. On the one hand noise or unwanted detail will be eliminated, but on the other hand important spectral information might be removed. To directly investigate the influence of the spectral generalization, an image needs to be classified with and without prior segmentation, while all other basic conditions are maintained, i.e. the same classifier with identical training must be used. Most studies, however, compare pixel- and segment-based classifications of optical images under varying conditions, either by using different classifiers (Wang et al. 2004) or by incorporating additional features into the segment-based classification (Song et al. 2005; Bruzzone and Carlin 2006).

The present work investigates the impacts of image segmentation on the purely spectral classification of a hyperspectral data set from a large heterogeneous urban environment. The influence of image segmentation is assessed at different scales and for different urban structure types. The conceptual framework for this investigation and the classification approach are described in Section 2. Section 3 explains the image and training data as well as the methods used for segmentation and classification. Results of the experiments are shown in Section 4 and discussed in Section 5. The paper ends with concluding remarks in Section 6.

2 Conceptual framework

2.1 Segment-based classification

From a spectral perspective, image segmentation, especially region-growing approaches, can be considered a locally optimized generalization procedure: adjacent pixels from presumably homogeneous areas are merged into image segments. The original spectral information is reduced to a mean value, which is then assigned to the corresponding image segment. Ideally, segment outlines follow boundaries of natural objects and possible spectral heterogeneity within this object is intentionally eliminated. This has an important impact on subsequent processing, e.g. the classification of the data: the spectral feature space is modified by averaging the spectral information from adjacent pixels, and classification results are different. If segment outlines match those of natural objects, the pixels' original spectral information is changed towards values that are more representative for the object as a whole and presumably its class. The confusion between overlapping classes will decrease, produced maps appear more homogeneous and are easier to perceive.

The positive effect is weakened when segments are smaller than natural objects, but – more important – it turns into a disadvantage when segments are too large and include pixels that belong to adjacent natural objects from different classes. In this case, spectral values from different classes are averaged, i.e. confusion increases. The following possible disadvantages of segment-based classification are summarized in (Song et al. 2005): an inaccurate segmentation will not improve classification, the classification error is accumulated due to errors in segmentation and classification, and the misclassification of a segment means a misclassification of all pixels of the object. Simultaneously to the generalization of the segments' spectral properties, segment specific features are generated, e.g. shape features, textural information, and relationships between segments. The availability of this additional information is an important advantage of many segment-based approaches over pixel-based classifications (Damm et al. 2005; Bruzzone and Carlin 2006). Regardless of this advantage, however, it is desirable to make best use of the spectral information in segment-based approaches. The airborne hyperspectral data from a heterogeneous urban environment as used in this work is ideal to investigate the spectral properties of segmented image data: the high spectral information content promises high classification accuracy, even for critical land cover classes like built-up and not built-up impervious surfaces. At a spatial resolution of 4 m the quality of the image segmentation is expected to be influenced by mixed pixels, especially in areas with small characteristic spatial scales and high local spectral variance (Woodcock and Strahler 1987; Small 2003). Spectral similarity between adjacent objects from different classes will additionally complicate the analysis. Moreover, the various urban structure types in the data show very different spatial properties and patterns, and they are not assumed to be well represented by a single segmentation level.

The segment-based classification in this work is set up to directly investigate the influence of spectral generalization. At first, the unsegmented image is classified using a SVM classifier (Fig. III-1, left). Then, segmented images with different levels of aggregation are individually classified using the SVM that was previously trained on the pixel information of the unsegmented image (Fig. III-1, center). This way, the differences between the two approaches are reduced to the data to be classified and the effects of image segmentation. Following this analysis of individual segmentation levels, a multi-level approach is performed to test whether positive impacts of segment-based classification at varying levels can be combined into one map by a multi-level classification (Fig. III-1, right). Intermediate results, i.e. rule images, of the previous SVM classifications are combined

and a single map is derived (for details see Section 2.2). This straightforward approach does not require a supervised training at different scales or the definition of relationships between different segmentation levels by the user.

2.2 Support vector machine classification

A spectral classification approach for heterogeneous urban environments should fulfill two requirements: (1) the chosen algorithm has to be capable of describing multi-modal classes, i.e. heterogeneous classes including more than one cluster in the feature space; (2) the classification of the smooth transition zones between classes is critical, due to the ambiguity of the classes' spectral information and the high number of mixed pixels. Over the past two decades, a variety of non-parametric classifiers has been introduced into remote sensing image analysis, e.g. artificial neural networks (Benediktsson et al. 1990), decision tree classifiers (Friedl and Brodley 1997), and support vector machines (SVM) (Huang et al. 2002; Foody and Mathur 2004). These do not assume specific class distributions and are thus well suited for complex environments or approaches using fused data sets. SVM are one of the more recent developments in the field of machine learning. They outperformed other approaches under varying conditions in the very most cases or performed at least equally well (Huang et al. 2002; Foody and Mathur 2004; Melgani and Bruzzone 2004; Pal and Mather 2006). In particular, SVM have been shown to be insensitive to high data dimensionality and robust in terms of small training sample sizes (Melgani and Bruzzone 2004; Pal and Mather 2006).

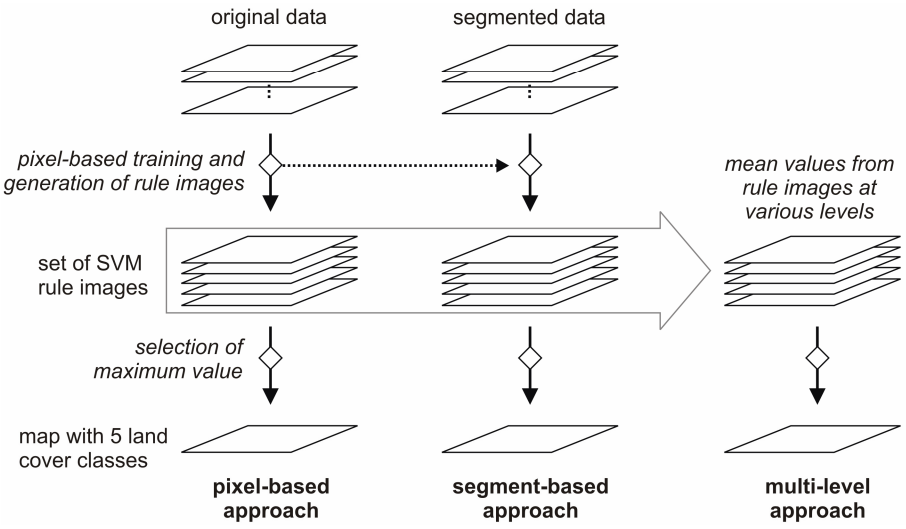

Figure III-1: Flowchart of the pixel-based (left), segment-based (center), and multi-level approach (right). The SVM for both the pixel- and segment-based approach were trained on pixel data. For details on SVM classification see Section 2.2.

SVM delineate two classes by fitting an optimal separating hyperplane to the training data in the *d*-dimensional feature space (Vapnik 1998). They are based on structural risk minimization: a hyperplane is optimal when it minimizes a cost function that expresses a combination of (1) maximizing the margin, i.e. the distance between the hyperplane and the closest training samples, and (2) minimizing the error on training samples that can not be separated (Bruzzone and Carlin 2006). The influence of the non separable samples is controlled by a regularization parameter *C*. For linearly not separable cases, the input data are implicitly mapped into a higher dimensional space by a kernel function, e.g. Gaussian radial basis function (RBF). Explicitly, the kernel function is integrated into the optimization of the cost function in a way that only dot products between sample vectors in the high dimensional space are computed. The parameters of the kernel function are chosen to allow the best possible fitting of the hyperplane. For the RBF kernel this is the parameter γ that controls the width of the Gaussian function. A detailed description on the concept of SVM and the formulation of the problem is given in Burges (1998), comprehensive introductions in a remote sensing context in Huang et al. (2002), Foody and Mathur (2004), and Melgani and Bruzzone (2004).

Two main strategies exist to solve multi-class problems with originally binary SVM: the one-against-one (OAO) and the one-against-all strategy (OAA) (Huang et al. 2002; Foody and Mathur 2004). Additional approaches are described in Melgani and Bruzzone (2004) and Hsu and Lin (2002). In this work the OAA approach was preferred, since first tests showed no significant differences to other approaches in terms of accuracy. In addition, the suggested multi-level classification could easily be performed on intermediate results of the OAA strategy: SVM produce an image that shows the distance of pixels to the separating hyperplanes for each binary problem. In the OAA approach, a set of such images, from now on referred to as rule images in analogy to other classifiers, is generated to individually separate each class from the remaining ones, e.g. *vegetation* from the rest. The final class label is then determined by comparing the values in the rule images and selecting the maximum value. For the multi-level approach, rule images from different segmentation levels that were generated during the segment-based classification were averaged for each binary case. The final map was derived by applying the maximum value decision to resulting mean values of each OAA case (Fig. III-1, right). The success of a combined use of SVM rule images for data fusion has previously been demonstrated for multi-sensoral data (Waske and Benediktsson 2007).

The classifications of this work target to map five typical urban land cover categories: *vegetation*, *built-up* areas, non built-up *impervious* areas, non-vegetated *pervious* areas and *water*. Especially *built-up* areas include all kinds of roof materials at different illumination conditions, in parts being specular reflectors, and hence show a multi-modal spectral distribution. Non built-up *impervious* surfaces comprise all other artificial surfaces like roads, sidewalks, other open spaces, plus cars, railroad tracks, or trains. By defining such spectrally heterogeneous classes the ability of SVM to delineate complex class distributions is tested.

2.3 Stratified accuracy assessment of the support vector machine classifications

The classification accuracy is expected to vary between different urban structure types due to the unequal distribution of phenomena like shadow, the portion of mixed pixels depending on the average size of spatial structures, or the abundance of the spectrally more distinct classes *vegetation* and *water*. For a thorough validation of the SVM classification in urban areas with heterogeneous structural composition, map accuracy has to be assessed following an adapted strategy. Thus, urban structure types like the central business district, industrial and commercial grounds, residential areas of different densities, and suburban areas will be stratified and individually validated.

When segmenting data that comprises different urban structure types, the quality of segmentation results can be expected to vary as a consequence of variations in the size of natural objects and the spectral contrast to adjacent surfaces. Possible positive or negative impacts will more than likely occur simultaneously. Thus, the stratified accuracy assessment of the segment-based classifications functions as an indirect measure of segmentation quality for the corresponding regions in the image. This way, general information on appropriate average segment sizes for the analysis of different urban areas shall be derived. By reducing the description of segmentation results to the value of overall average segment size, a flexible measure is used that is independent from the segmentation algorithm and that might also function as a guideline for the work with data sets from other urban areas.

3 Material and methods

3.1 HyMap imagery and data preprocessing

The airborne imaging spectrometer HyMap acquires data between 0.4 and 2.5 µm in 128 spectral bands. Its spatial resolution is 3.9 by 4.5 m at nadir, when operated at 1,930 m. The sensor's field-of-view (FOV) is at 61.3°. The HyMap flight line that is classified in the present work was acquired over Berlin, Germany on 20 June, 2005 around 10.46 am central European summer time. The flight direction was East-West at 256°; the center of the 512 by 7,277 pixel scene is located at E 392254 and N 5820441 in UTM zone 33. An area of 32.5 by 2.2 km is covered including a great variety of urban structure types: the governmental district, residential areas of different densities and ages, recreational areas, suburban areas towards the city's borders, industrial grounds, as well as large apartment complexes and wide boulevards from socialist time. In addition, agricultural areas, forest patches and water bodies are present.

The data set was corrected for atmospheric effects and transferred to reflectance values (Richter and Schläpfer 2002). The number of bands was reduced to 114 based on the signal-to-noise ratio. View-angle dependent brightness gradients that are caused by anisotropic surface reflectance were eliminated following an approach for urban hyperspectral data (Schiefer et al. 2006; Chapter II of this work). Geometric correction was not performed to avoid spatial resampling and the interpolation of spectral information.

3.2 Image segmentation

Image segmentation was performed using the region merging approach suggested in Baatz and Schaepe (Baatz and Schaepe 2000). Despite other region-growing approaches (Evans et al. 2002) or edge-delineation approaches (Rydberg and Borgefors 2001), this approach is most frequently used in remote sensing (e.g. Hodgson et al. 2003; Shackelford and Davis 2003). A detailed description of the underlying formulae can be found in Bruzzone and Carlin (2006). In general, the spectral variance within user-defined bands and compactness or smoothness of generated segments controls the termination of the segmentation process. In this work segment shape was not utilized and only spectral information was used. This is in accord with the focus of the analysis in this work. The segmentation was performed on the first 20 principal components, since segmentation of all 114 spectral bands was not

feasible. Segment outlines were then transferred onto the original spectral data. Ten segmented images with average segment sizes between 2.4 and 21.4 pixels were generated using increasing values for the termination criterion (Fig. III-2).

The spectral information from the segmented images was stored in a generic band sequential file format, where every pixel corresponds to a segment. The band values of each segment represent the average spectral information of its constituent pixels in the respective band. The segments are stored sequentially according to an index number they receive during the segmentation process. In order to re-localize the segments after image processing a separate file with the spatial positions of the indices is used. The generic format enables a software-independent processing of the spectral information derived from the segmentation process. At the same time, the physical data size is reduced during spectral generalization, i.e. spectrally compressed, and processing speed hence increased – an important, but so far neglected side effect of segment-based analysis, especially in the case of large data volumes.

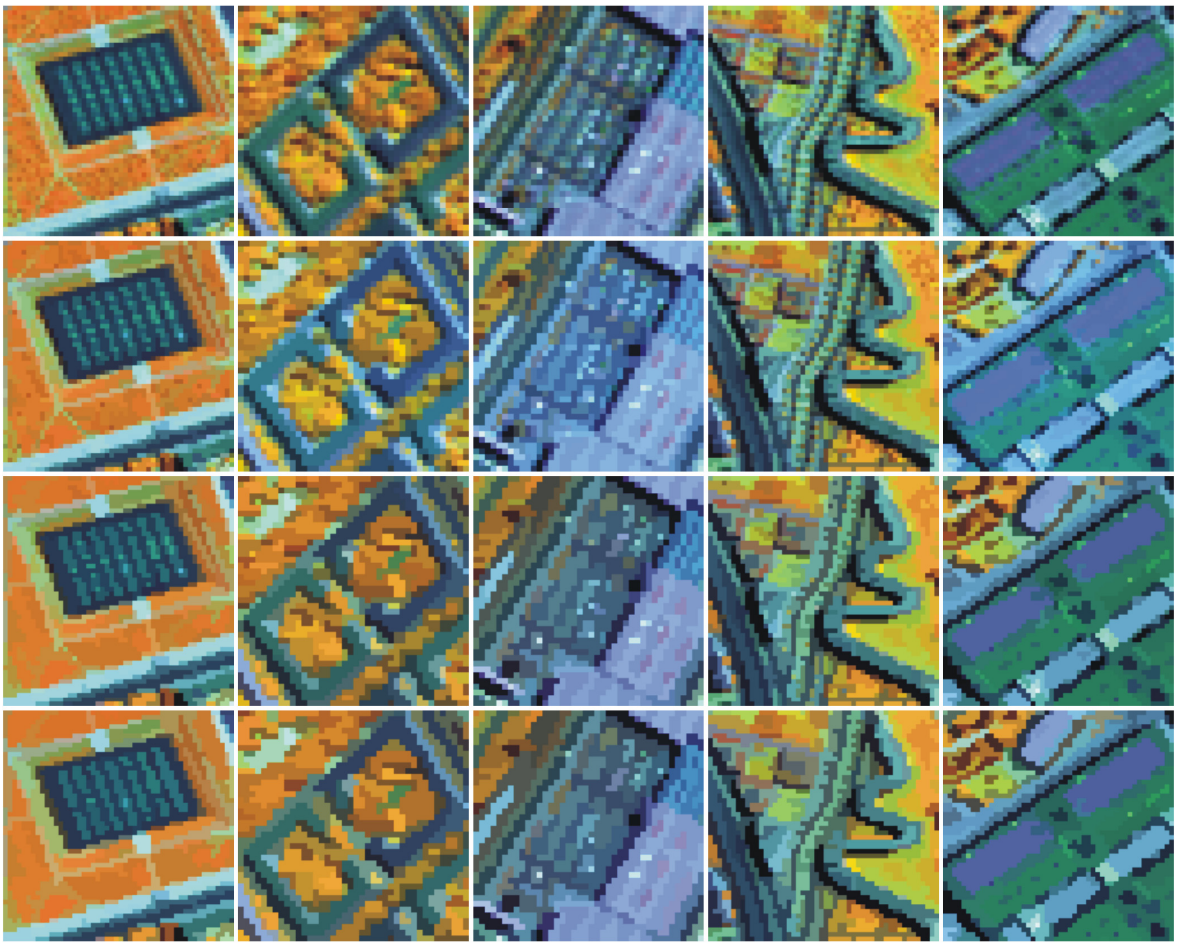

Figure III-2: Five subsets from the HyMap image before segmentation and data at average segment sizes of 3.4, 8.5, 13.1 (top to bottom; R = 829 nm; G = 1648 nm; B = 662 nm).

3.3 Support vector machines

The training of the SVM was performed using the *C*-SVM approach in LIBSVM (Chen and Lin 2001). An RBF kernel was used to transform the data (Vapnik 1998). An in-house implementation of LIBSVM for remote sensing data was used to train wide ranges of values for γ and C and evaluate the quality based on a 4-fold cross validation (Janz et al. 2007). This way, optimal parameters could be found for the binary OAA classifiers and an over-fitting to the training data was avoided.

3.4 Training and validation data

The sampling strategy of the present work rather focuses on the description of the transition zones between classes than on homogeneous areas. Since spectrally heterogeneous urban classes are too manifold to generate artificial mixtures as in Foody and Mathur (2006), a clustered sampling strategy was performed: at first, 64 seed pixels were randomly drawn from the full image. 29 pixels around each of these seeds (5 x 5 windows plus the four outer diagonal pixels) were then assigned to one of the five land cover classes. A smaller number of additional seed pixels were interactively placed on rare but characteristic surfaces, which were not present in the randomly selected data set. These included unweathered asphalt, very bright parking lots, impervious sports fields with artificial lawn or tartan, soil surfaces at both construction areas and on fallow land, plus rare roof materials. All pixels were labeled based on very high resolution aerial photographs. Most of the clusters contained at least one class boundary and thus mixed pixels of two or more classes. By sampling adjacent pixels, mixed pixels were usually sampled along with corresponding purer pixels. This way, the transition zones between two classes were represented by sets of pixels describing a gradient from pure over differently mixed to, again, pure pixels, and the position of the hyperplane was narrowed down at several positions in spectral feature space. The original number of pixels from vegetated areas – the most frequent surface type – was randomly reduced. This way, the proportion of the three main classes *vegetation*, *impervious* and *built-up* was more balanced and training times decreased, while the accuracy for *vegetation* was expected to remain good (Table III-1). The overall number of 2133 training pixels corresponds to 0.057% of all pixels.

For statistical validation 1253 independent reference pixels were selected from the HyMap image and assigned to one of the five land cover classes based on very high resolution aerial photographs. The sampling was not purely random to investigate the classification

Table III-1: Distribution of training pixels by classes.

Class	*vegetation*	*built-up*	*impervious*	*pervious*	*water*	Total
No. training pixels	631	564	556	266	116	2133

Table III-2: Reference pixels of the five land cover classes as distributed over the urban structure type.

Class	Reference pixels randomly selected from								Total
	center	dense	single	complexes	suburban	industrial	dark	rest	
vegetation	28	52	91	77	112	42	55	108	565
built-up	58	41	36	23	5	29	-	32	224
impervious	57	54	18	40	2	62	42	34	309
pervious	1	4	4	7	26	18	-	12	72
water	4	-	-	2	5	-	61	11	83
Total	148	151	149	149	150	151	158	197	1253

accuracy with regard to different urban structure types. Rectangular polygons of about 200 by 300 pixels were manually drawn in homogeneous areas of six typical urban structure types, including: the city centre with business areas and the governmental district (center); dense residential areas with attached buildings and narrow courtyards (dense); open residential areas with private gardens (single); pre-cast apartment complexes surrounded by recreational areas (complexes); individual houses surrounded by agricultural patches and forest along the urban-suburban fringe (suburban); industrial and commercial grounds (industrial). About 150 reference pixels were randomly drawn from each urban structure type. Each structure type is characterized by different class proportions (Table III-2). To better investigate the classification quality in dark areas, 158 extra points were randomly selected using a dark area mask (reflectance at 1.650 μm < 5%). In addition, 197 pixels were randomly selected from the rest of the image, to represent remaining areas.

4 Results

4.1 SVM classification of pixels

The SVM classification of the original image leads to an overall accuracy of 88.7% and a kappa coefficient (κ) of 0.84 using all 1,253 reference pixels. Slightly more than half of the area is classified as *vegetation* (52.7%). 22.3% of the area are *impervious* grounds, 16.2% *built-up* areas. *Pervious* and *water* are the smallest classes at 4.8% and 3.9%, respectively. The accuracy assessment shows different degrees of confusion between the classes (Table III-3).

Table III-3: Confusion matrix including producer's/user's accuracy [%] of pixel-based SVM classification.

Image pixels	Reference pixels					Total	User's accuracy
	vegetation	built-up	impervious	pervious	water		
vegetation	541	4	5	7	2	559	96.8
built-up	0	183	24	5	0	212	86.3
impervious	20	33	270	21	3	347	77.8
pervious	4	4	6	39	0	53	73.6
water	0	0	4	0	78	82	95.1
Total	565	224	309	72	83	1253	
Producer's acc.	95.8	81.7	87.4	54.2	94.0		

Table III-4: Producer's and user's accuracies [%] of vegetation, built-up, impervious, and pervious and the overall accuracy by urban structure types in the pixel-based approach. Values for n < 20 are not shown.

Class	Urban structure type					
	center	dense	single	complexes	suburban	industrial
vegetation	89.3/100	80.8/95.5	97.8/98.9	100/97.5	99.1/95.7	100/95.5
built-up	84.5/81.7	85.4/89.7	77.8/87.5	87.0/90.0	-	72.4/80.8
impervious	77.2/80.0	90.4/75.8	-	95.0/88.4	-	85.5/77.9
pervious	-	-	-	-	80.8/95.5	-
Overall	83.1	84.6	89.3	94	94.7	80.8

Based on the stratified set of reference pixels, the quality of the SVM classification was evaluated for different urban structure types (Table III-4). The accuracy of vegetation is lowest in dense residential areas, where many trees are located in dark courtyards or along streets in the shadow behind houses. The class *built-up* shows producer's accuracies of about 85% or higher for the city center, dense residential areas, and apartment complexes. The lowest value exists for industrial areas at 72.4%. The accuracies of *impervious* areas are nowhere below 75% and reach 95% for areas with apartment complexes. Looking at the overall values, accuracies of more than 80% are achieved for all structure types. The accuracies of single residential, apartment complexes and suburban, i.e. areas with great proportions of vegetated areas, are highest.

4.2 SVM classification of segments

At first, the results from the segment-based approach are assessed by a visual comparison of maps based on the pixel image and the segmented data (Fig. III-3). In general, segment-based maps appear more homogeneous, but misclassified segments result in an areal misclassification of a group of pixels and some necessary spatial detail is removed. A typical example of the effects of image segmentation can be seen in the case of a sports gym (Fig. III-3.a). The building is best represented at an average segment size of 8.5 or 13.1, whereas surrounding patterns of paved paths and vegetated as well as non-vegetated

patches result in large, mainly misclassified areas at these levels. Within residential areas, the fragmented patches of *built-up* and *impervious* pixels disappear in the segment-based maps (Fig. III-3.b). At the same time, the increasing segment size leads to the misclassification of groups of *built-up* pixels, especially next to shadowed areas and bright facades, which are visible at large view-angles. Cars are often classified *built-up* at pixel level, because of their similarity to metal roofs. This phenomenon can for example be observed on parking lots (Fig. III-3.c). At increasing segment sizes this heterogeneous area is spatially and hence spectrally generalized and the area is uniformly classified *impervious*. In the case of small trees on *impervious* areas a similar effect exists, which is not necessarily intended by the generalization (Fig. III-3.d).

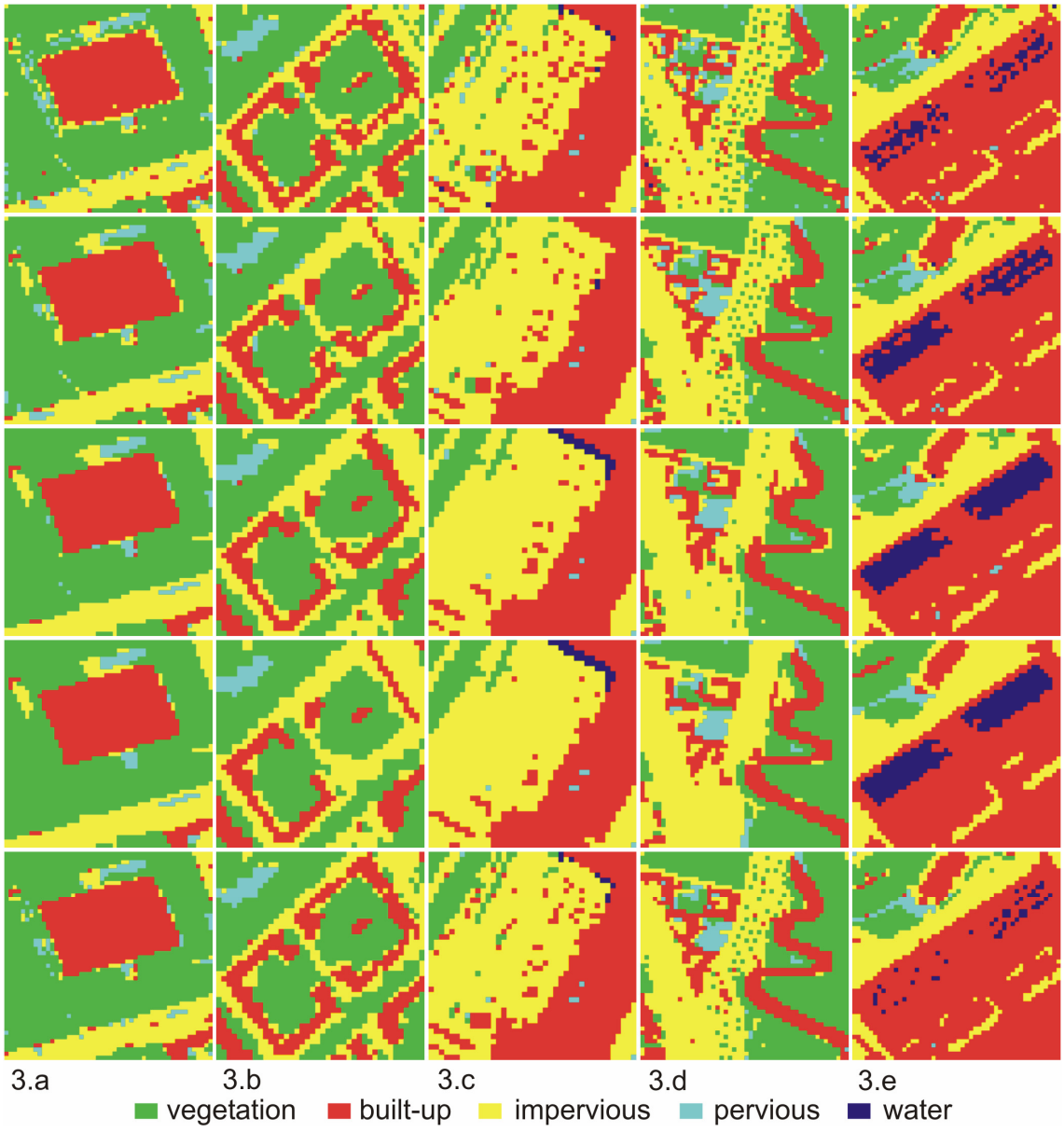

Figure III-3: Subsets from classified data at different levels. Pixel level, segment sizes of 3.4, 8.5, 13.1, and the multi-level classification are displayed (top to bottom).

Table III-5: Accuracies of segment-based classifications and multi-level approach by urban structure types. The highest accuracy of each region is indicated by bold numbers.

Avg. segment size	center	dense	single	complexes	suburban	industrial	Overall
pixel	83.1	**84.6**	**89.3**	**94.0**	94.7	**80.8**	**88.7**
2.4	85.1	82.0	88.6	91.2	96.0	78.2	87.6
3.4	85.1	82.0	87.9	91.2	**97.3**	76.8	87.6
4.8	83.1	78.7	85.2	89.9	94.7	76.2	85.4
6.5	83.1	77.3	82.6	87.3	94.0	75.5	84.1
8.5	83.1	76.8	82.6	84.6	94.0	75.5	83.3
10.7	83.8	74.8	83.9	85.2	95.3	74.8	83.4
13.1	84.5	75.5	85.2	85.2	94.7	71.5	83.2
15.7	84.5	74.2	83.2	84.6	95.3	72.2	83.1
18.5	83.1	74.2	82.6	83.2	94.7	72.8	82.4
21.5	82.4	73.5	81.2	83.2	94.7	71.5	81.8
multi-level	**85.8**	83.4	87.2	91.3	96.7	78.1	87.8

The positive impression from the more homogeneous segment-based maps is not confirmed by the statistical accuracy assessment. A decrease of 1.1% from pixels to smallest segments followed by constantly decreasing accuracy with increasing segment sizes can be observed (Table III-5). The best segment-based overall accuracy of 87.2% ($\kappa = 0.82$) is achieved at average segment sizes of 2.4 and 3.4 pixels. From segment size 4.8 onwards, the increasing difference to the pixel-based result becomes greater 5% and is significant at the 95% level of confidence (e.g. $Z = 3.79$ for size 4.8) based on a McNemar test (Foody 2004).

A detailed assessment of the overall accuracy at different aggregation levels shows different developments between the urban structure types, but also some similarities (Table III-5). Most areas experience a decrease between pixel level and the lowest aggregation level. The center and the suburban area are exceptions to this: accuracy increases by 2.0% and 2.6%, respectively, for the two smallest segment sizes. The accuracy for suburban areas remains about the value for pixel level at all segment levels, whereas the accuracy for the center decreases with a relative maximum at segment size 13.1. For the other four inner urban areas, the overall accuracy shows varying irregular patterns of decrease with one or two relative maxima, which are usually below those of the pixel level. The relative maxima of classification accuracy for the various urban structure types occur at different segment sizes.

For matters of comparison, a second segment-based approach was performed. In this approach segment-based training is performed, i.e. the spectral mean values of those segments that contain the original training pixels are used for the training. This way, an individual SVM is trained for each segmented image and then used for the classification of

this data set, as it is usually done in segment-based studies. The overall accuracies achieved by this approach at different aggregation levels are generally 2% or more below the ones of corresponding classifications with SVM trained on pixels. (Results not shown)

In addition, it was tested to integrate segment features like area or texture measures into a segment-based approach. Again, results were worse and more irregular than those presented. This might be explained by the low accuracy of spectral classification at segment sizes that lead to meaningful values for segment-specific features.

4.3 Multi-level classification of fused data

For the multi-level approach three sets of OAA rule images were combined into one set of mean values (pixel level; average segment sizes 3.4 and 13.1). The visual assessment shows that many positive effects of classifications at varying segment sizes are combined in this fused classification result (Fig. III-3, bottom). For example, some detail of the paths around the gym is preserved while the shape of the building's roof is well represented (Fig. III-3.a, bottom); individual trees are not generalized in the map, while the building complexes appear as homogenous areas with relatively accurate outlines (Fig. III-3.d, bottom). The case of a metal roof is especially interesting (Fig. III-3.e): several roof pixels are classified as water at pixel level, caused by the similarity of this rare roof material to specular reflecting water pixels in the training data. Entire patches of the roof are misclassified in the segment-based approach, whereas the fused classification achieves the overall best results.

The statistical assessment shows that results are not a simple average of the three individual maps derived from the comprised rule images (Table III-5). The overall accuracy is slightly, but not significantly higher than in the single layer segment-based approaches at 87.8% ($\kappa = 0.82$) and lower than the pixel-based results. The confusion matrix is similar to that of the pixel-based approach and overall accuracies for different urban structure types are similar to and in the case of the center and suburban areas better than those achieved by the pixel-based approach (Table III-5). So are the producer's and user's accuracies of the individual classes. (Results not shown)

5 Discussion

5.1 Performance of the pixel-based classification

At 88.7% the overall accuracy of the SVM classification of the urban HyMap data is high. To a certain extent, the accuracy owes to the high abundance of vegetated surfaces in Berlin. Still, the overall producer's accuracies of the critical classes impervious, pervious, and built-up are well balanced and all close to 75% or clearly above. This underlines the capability of SVM to differentiate spectrally similar, multi-modal classes. The assessment of dark areas, i.e. shaded impervious and vegetation pixels plus water, exhibits an overall accuracy of 89.2% based on 282 corresponding reference pixels. These high accuracies show that SVM can be recommended for mapping complex classes in urban areas. The classification problem can be tackled in a one-step approach, where thematic and spectral definitions are identical and accurate maps are produced in a simple yet more intuitive and time saving manner.

Despite this high accuracy, some confusion remains that is partially caused by the spectral similarity of materials from different land cover classes. Sometimes, complete roofs or impervious surfaces are misclassified. This underlines the limits of purely spectral classification and the ambiguity of urban surfaces even in hyperspectral data (Herold et al. 2003). The accuracy of the class pervious differs between low values for open soils on construction sites in the city and high accuracies for natural soils at the urban fringe. The distinction between non-vegetated pervious and impervious areas within the city appears critical even with hyperspectral data. This generally questions the suitability of approaches like the vegetation-impervious surface-soil model (Ridd 1995).

Besides the spectral ambiguity of materials, the occurrence of mixed pixels can be named as a source of error. In this context, the assessment of individual reference pixels shows problems for pixels from built-up, impervious, or pervious areas with little abundance of vegetation. They are often confused because the influence of the vegetation signal obscures the slight spectral changes among the three non-vegetated surfaces (Fig. III-3.a,c).

Considering the high overall accuracy and the remaining patterns of confusion, the strategy of performing a clustered sampling of the training data performs very well and significantly decreases the time needed for sample collection. A further assessment of ideal sampling approaches for urban areas is worthwhile but goes beyond the scope of this work.

The classification accuracy in the different urban structure types reflects the discussed causes of confusion against the background of spatial patterns: vegetation shows high accuracies for all areas, but in dense residential areas with many small vegetated patches, i.e. a high number of mixed vegetation pixels, the producer accuracy decreases to 80.8%. Due to the same phenomenon, values are low for built-up in single-house residential areas. The low accuracy of this class in industrial areas can often be explained by spectral similarity of tar roofs to impervious surfaces or by the manifold painted or coated roof materials that are not all represented in the training data. In the city center, dense residential areas and in areas with apartment complexes, materials are less diverse and the accuracy for built-up is hence higher. The relatively low accuracy of the class impervious in the city center owes in parts to the high number of cars on the wide boulevards, which are spectrally more similar to roof materials.

5.2 Effect of image segmentation on spectral classification

Maps based on segmented data (Fig. III-3) are more homogeneous than the pixel-based classification and thus better suited for many subsequent analyses. The spectral generalization definitely removes some disturbing effects, e.g. cars on impervious surfaces. While positive and negative influences can be observed simultaneously, no single segment level can be identified where positive effects seem to clearly dominate for all urban structure types. However, negative impacts become more frequent at average segment sizes greater 13.1. This is in accordance with Bruzzone and Carlin (2006), who also discover a shift towards negative effects when segments become larger than natural objects.

The size of natural objects and the contrast to surrounding areas turns out to be of great influence with increasing segment sizes. Natural object outlines correspond to the outlines of large segments in the case of great contrast between an object and its surrounding pixels (Fig. III-3.a,d). Within these large segments, mixed pixels along the edges are of little spectral influence and maps are more accurate than at small segment sizes. In densely populated residential areas, the thematic boundaries between buildings, roads and vegetated areas are often obscured by non-thematic phenomena like shadow, visible facades and illumination differences on roofs (Fig. III-3.b). In the case of shadowed areas, for example, dark vegetated and non-vegetated pixels exist next to another. Segment outlines heavily depend on the overall illumination and rather follow the outline of the shadowed area. In a similar way, large segments might comprise bright facades, adjacent sidewalks, and sometimes parts of the well illuminated southern side of a roof or they

include dark roofs and adjacent dark shadowed areas (Fig. III-3.b). A correct assignment of such two-class segments is not possible and phenomena like shadow pose severe problems to segment-based approaches. Segment-based results are thus very sensitive to slight changes to the setup and difference of large areal extent might occur from one segmentation level to the next (Fig. III-3.b).

In the same way as spectral generalization of very small natural objects is positive concerning cars on roads, it can be negative in the case of individual trees (Fig. III-3.d) or along linear objects represented by mixed pixels (Fig. III-3.a). In general, the large number of mixed pixels impacts results twice: at first, areas with many mixed pixels are always hard to classify. At second, segment outlines might be arbitrarily placed in such regions and as a consequence all pixels in the corresponding segments have a higher chance of misclassification.

The quality of classifications at increasing aggregation levels differs between the urban structure types, due to the differences of spatial structures and material composition. As expected, this can to some extent be related to dominating structures: the rather small structured residential areas should be classified at lowest aggregation levels (Table III-5). The city center and suburban areas perform well at medium levels, due to larger spatial structures. Accuracy for apartment complexes suffers from the shadow and facade phenomenon. The high accuracy for single house residential structures can be explained by the high fraction of vegetation. Results underline that no ideal average segment size exists for the work in heterogeneous urban environments. This drawback might be tackled by using additional information on the outlines of natural objects from external knowledge bases like cadastres or GIS layers.

Compared to visual impression from the segment-based maps, the decrease in statistical accuracy from pixel to segment level in inner-urban areas is not surprising. Increased homogeneity can not be considered more accurate, but rather more favorable for human perception. Two main reasons can be named for decreasing accuracy: (1) the spatial composition of urban areas is very heterogeneous, even within a single urban structure type (e.g. Fig. III-3.d), and the manifold natural objects can hardly be represented in one segmentation level; (2) the level of detail aimed for in the present classification, i.e. the distinction between buildings and other impervious areas, is at the limit of the 4 m spatial resolution of HyMap. This is underlined by the fact that only the two very small segment sizes of 2.4 and 3.4 pixels lead to results not significantly below those in the pixel-based

approach. To further test local heterogeneity, a 3x3 majority filter was applied to pixel-based results. Unlike in many other studies, the filtering leads to significantly lower results at 85.8% ($Z = 3.37$). This underlines the heterogeneity of the area, but at the same time shows that the adaptive region-growing during segmentation is superior to generalization with fixed window sizes.

The development of segment-based classification accuracy for different urban structure types with increasing segment sizes suggests the ratio between the average size of natural objects and the area represented by one pixel to be of great importance. It can thus be expected that a similar analysis on higher resolved data leads to a better description of the characteristic spatial scale and results with presumably higher accuracies for low or medium aggregation levels. However, there is no hyperspectral data with HyMap's spectral properties and better spatial resolution available.

5.3 Performance of the multi-level classification

Despite the slightly, i.e. not significant, lower overall accuracy of the multi-level classification, the corresponding map is preferred over the single level approaches. It combines positive effects of different segmentation levels into one single result and this way achieves good results for varying urban structure types.

Although information from three levels is fused by simply averaging the rule images, the result appears superior to a simple average: the overall accuracy is above an average value of the three original ones and positive effects seem to outweigh negative influences. This can to some extent be explained by the maximum value decision in the OAA approach: (1) in the case of mixed pixels or pixels from ambiguous materials, two or more classes might show positive values for their corresponding OAA decision value. At different aggregation levels, this pixel is then merged with different groups of neighboring pixels and hence information on the local situation at different scales included into the classification (Bruzzone and Carlin 2006). The average of the three decision values for this pixel in the rule images is expected to be more representative. The successful concept of classifier ensembles relies on a similar assumption (Kittler 1998). (2) If, for example, a single tree achieves a very high positive decision value for the class *vegetation* at pixel level, plus lower positive values for *vegetation* and a second class at segment levels, the class *vegetation* will win in the combined approach, although the tree might not be recognized in all segment-based classifications.

The multi-level approach is straightforward and fast to perform: only one SVM classifier is trained on pixel information and applied to unsegmented data and all segmented images. Results might be improved by giving different weights to classes at different levels or by incorporating hierarchical information. Such optimized multi-level approaches are often suggested in literature to deal with complex environments (Damm et al. 2005; Schöpfer and Moeller 2006). However, the development of transferable approaches that include information from different levels of aggregation is a time-consuming task (Schöpfer and Moeller 2006). Especially for very large heterogeneous data sets that comprise very different urban structure types as data in this work, more complex multi-level approaches appear not feasible.

In Bruzzone and Carlin (2006) two subsets of pan-sharpened Quickbird data from an urban area are used to test a similar multi-level SVM classification approach. They combine the spectral information at pixel level with spectral mean values and variances from segmented data sets and perform training and classification on this fused data set. In the present work, it was also tested to train SVM on combinations of several segmentation levels, with and without spectral variance values or texture measures. Results did not improve compared to pixel level and again training based on the spectral information from spectrally generalized segmented data appears not useful, as in the second segment-based approach (compare Section 4.2). This might be explained by the lower spatial resolution of HyMap compared to Quickbird.

Thus, the simple multi-level approach taken here with a pixel-based training and classification at multiple segmentation levels appears useful for the classification of heterogeneous data. It can be expected to be transferable to other spectral classification problems. For the work with very high spatial resolution data, the number of mixed pixels and hence their negative influence is significantly lower. Results are then expected to be more positively influenced by image segmentation, as shown in Bruzzone and Carlin (2006) and Shackelford and Davis (2003).

6 Conclusions

High overall accuracies are achieved using a purely spectral SVM classification approach on hyperspectral data from an urban area. SVM delineate broad thematic classes without the previous definition of spectrally homogeneous sub-classes or separate treatment of dark areas. This way, it was proven that SVM are capable of describing complex class distributions.

This study advances the understanding of segment-based image processing in heterogeneous environments by performing a segment-based approach with a narrow focus on spectral properties and in direct comparison to pixel-based results. The influence of the spectral generalization on the purely spectral, supervised classification was investigated. Different effects were identified with regard to average segment sizes. The findings can be a guideline in future remote sensing analyses of urban areas.

Results from the present work suggest that spectral information from data at this spatial resolution should best be included into segment-based analyses at low aggregation levels or at pixel level. More important, the training of a spectral classifier should be performed on original pixel values. When segment-specific features are used in the classification, a combined pixel- and object-based approach similar to the one performed in Shackelford and Davis (2003) appears useful, although no positive influence of segment specific features could be identified for the present data set.

The multi-level approach applied in this work can be recommended for its ability to incorporate positive effects of segment-based analyses at various levels into one single map. The quality of segment-based or multi-level approaches might be enhanced by incorporating more segment features and multi-level hierarchies. However, designing such multi-level segmentations and corresponding classifiers is time consuming and they are harder to be transferred to new environments. The simplicity and fast implementation are additional assets of the approach taken in this work.

Acknowledgments

The authors are thankful to A. Damm, P. Griffiths and M. Langhans (HU Berlin) for performing most of the atmospheric preprocessing. S. van der Linden was funded by the scholarship programme of the German Federal Environmental Foundation (DBU). This research was partly funded by the German Research Foundation (DFG) under project no. HO 2568/2-1. The two anonymous reviewers provided valuable input on the experimental setup and the manuscript.

Chapter IV:
Processing large hyperspectral data sets for urban area mapping

1 Introduction

The traditional workflow for airborne hyperspectral data includes the sequential processing steps of (1) system correction by the provider, (2) geometrical rectification, (3) radiometric correction, i.e. the removal of atmospheric influence and normalization of reflectance anisotropy, and (4) derivation of application products (e.g. Richter and Schläpfer 2002; Schläpfer and Richter 2002; Schläpfer et al. 2007). The radiometric correction of airborne hyperspectral data has been discussed in Chapter II of this work and a new empirical approach for normalizing reflectance anisotropy in urban imagery was introduced.

In the context of an optimized processing workflow the geometrical rectification, also referred to as geocoding or orthorectification, is of special interest: on the one hand, geocoding is an essential image processing step in remote sensing to provide consistent data sets (Goshtasby 1988; Toutin 2004). Geocoded imagery can be combined with other Earth observation data or additional spatial information. This way, results like land cover maps can be assimilated into environmental models (e.g. Wilson et al. 2003; Nichol and Wong 2005). Moreover, results from image analysis itself can be improved by using additional geocoded data during processing. This might include data from different sensors (e.g. Waske and Benediktsson 2007) or census data (e.g. Lu and Weng 2006). On the other hand, geocoding has two negative side effects. At first, not all pixels of the image with map coordinates can be directly mapped from the projected original data. In order to generate spatially continuous data sets, some way of resampling of spectral information from adjacent pixels in the original data is required. At second, the physical size of an image file might be significantly increased, especially in the case of airborne line scanner data: whenever the flight direction is not parallel to one of the axes of the map coordinate system, the image is rotated in the output grid and a high number of no data pixels exist. In addition, it is useful to increase the resolution of the output grid to preserve information during the rotation of the image (Schläpfer and Richter 2002).

Airborne hyperspectral data is characterized by high spectral information content at relatively high spatial resolution and, hence, large file sizes. Thus, the processing workflow should be optimized with respect to radiometric accuracy and processing times. In this context, Schläpfer et al. (2007) propose shifting the spatial resampling to the very end of the workflow and working in raw scan geometry. Performing the atmospheric correction before geocoding to optimize radiometric consistency has also been suggested by Hill and

Mehl (2003). Such alternative workflows appear especially useful to optimize the processing of very large hyperspectral data sets.

In Chapter III of this work a 7277 by 512 pixel image from the Hyperspectral Mapper (HyMap) acquired over Berlin, Germany, is classified using support vector machines (SVM) without previous geocoding. This way, no spectral resampling is performed before classification, but more important memory allocation problems during the classification process are avoided. Results will be used to map impervious surface coverage and therefore need to be geocoded.

In addition to the regular pixel-based approach, the SVM classification in Chapter III is applied to segmented image data. For this purpose, results from image segmentation have been stored in two separate files following the method suggested by Schiefer et al. (2005b). Overall accuracy of the segment-based classification before geocoding is generally lower than that of the pixel-based approach, e.g. 83.2% at an average segment size of 13.1 pixels compared to 88.7% at pixel level based on 1253 reference pixels (see Chapter III). However, this accuracy needs to be considered against the background of reducing the file size by a factor of 13.1 compared to the image without geocoding. Processing time of the SVM classification decreases linearly with file size. In comparison to the traditional approach, this factor of 13.1 can be multiplied by the efficiency factor achieved when performing the geocoding towards the end of the processing workflow.

Both the alternative pixel- and segment-based approach are limited to a nearest neighbor (NN) resampling during geocoding, since other interpolation methods cannot be applied to the discrete values of land cover classes or segment indices. The traditional workflow on the other hand offers a variety of interpolation methods. Some of these lead to better results in terms of geometric representation. This is especially the case for line and block-wise features, which dominate urban areas. Differences in the accuracy of maps derived from the different approaches can hardly be predicted, though. In order to assess the usefulness of the alternative workflows, the influence of the resampling methods needs to be quantified and discussed with regard to the decrease in processing times by data reduction.

In the present chapter the geocoding of the pixel-based result and one segment-based classification result from Chapter III is described (Fig. IV-1). The resulting geocoded maps from these *alternative* and *segment-compressed workflows* are then compared to maps from the *traditional workflow*, where a geocoding with bilinear interpolation is performed before the SVM classification. Differences caused by the two interpolation methods are

quantified. In addition, maps are compared to results from a field survey to assess the accuracy in map geometry. In this context the following research questions will be discussed to evaluate a possible decision for one of the approaches:

(1) Are there relevant differences in the land cover classification of interpolated pixels between the *traditional* and the *alternative workflow*?

(2) Is the lower classification accuracy of the segment-based classification further increased by geocoding in the *segment-compressed workflow*?

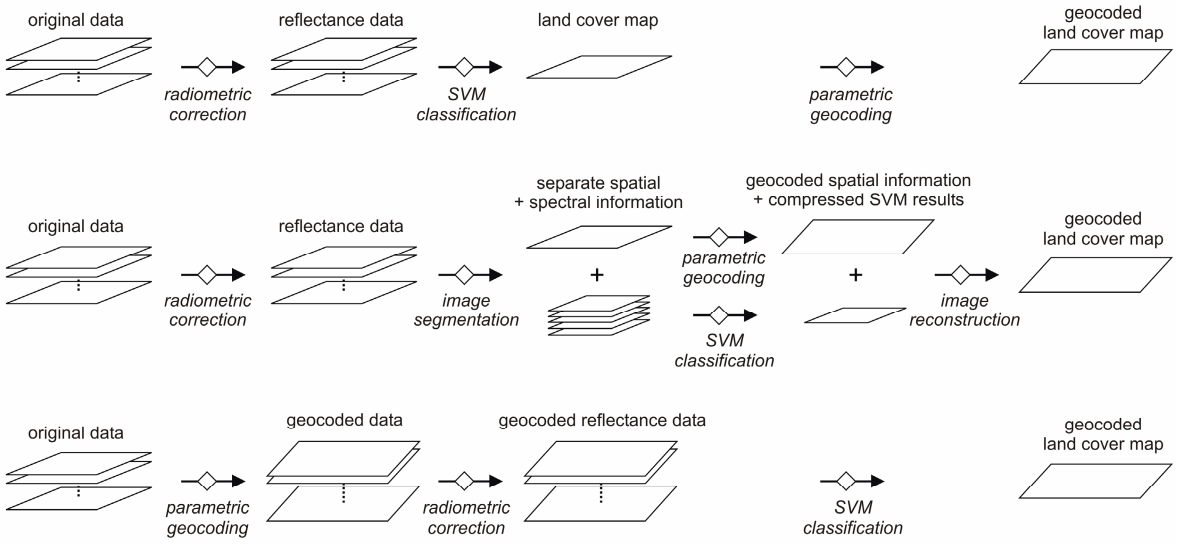

Figure IV-1: Three different workflows for mapping land cover from hyperspectral data. During the pixel-based *alternative workflow* (top) the geocoding constitutes the last processing step and the increase in physical file size is moved to the end of the workflow. In the *traditional workflow* (bottom) the SVM classification is performed on the large geocoded data set. The *segment-compressed workflow* (middle) further decreases the amount of data by separating spatial and spectral information and independently performing geocoding and SVM classification.

2 Material and methods

2.1 Image data, preprocessing and classification

To answer the research questions of this chapter, the original HyMap data and classification results from Chapter III are geocoded. The HyMap data was acquired over the city of Berlin on 20 June, 2005. The original spatial resolution of the 7277 by 512 pixel image was 3.9 by 4.5 m at nadir in across- and along-track direction, respectively. Prior to segmentation and classification the data was corrected for atmospheric effects following the approach by Richter and Schläpfer (2002) and normalized to nadir reflectance following the approach introduced in Chapter II. The proposed alternative and segment-

compressed workflow require the relief information for the atmospheric processing to be projected into raw scan geometry (Hill and Mehl 2003). The available software did not allow a processing without geocoding, however. Therefore, the image data was geocoded as described in Section 2.4 for the atmospheric correction and then re-projected into its original dimensions for the segmentation and classification. The few pixels that were not directly mapped during the first forward projection cannot be re-projected. This has no relevance, however, since pixels that were interpolated during re-projection for the image segmentation and classification will again be lost during the second forward projection.

Image segmentation was performed using the approach by Baatz and Schaepe (2000). For this work, segmented data with an average segment size of 13.1 pixels is used. Both, the image with and without segmentation were classified into the five land cover classes *vegetation*, *built-up* impervious areas, non built-up *impervious* areas, *pervious* areas, and *water* using SVM classification (see Chapter III).

2.2 Digital elevation model

A digital elevation model (DEM) that was derived from isolines in the official digital map was available. The DEM's original resolution of 25 m and 0.1 m in horizontal and vertical direction, respectively, was bilinearly resampled to 3.5 m spatial resolution in Universal Transverse Mercator Projection. A digital surface model (DSM) with information on building height was not available.

2.3 Field data

Parallel to the acquisition of the HyMap data, intensive ground mappings were performed. Using 0.25 m aerial photographs as base images, 9 rectangular plots of approximately 220 by 220 m were continuously mapped on two levels. The first level included the present land cover and surface material at ground. Altogether 21 land use related surface categories and more than 40 materials were differentiated. The second level showed the extent of tree canopy above ground. For this work the ground mapping was overlaid with the tree canopy and generalized to the five land cover classes in order to assess the difference between maps that result from the three different workflows.

2.4 Parametric geocoding

The geocoding of airborne line scanner data is different to that of image data from satellite platforms. For traditional moderate resolution satellite data, an affine transformation based

on a first degree polynomial is sufficient to correct most geometric effects, since the platform is expected to be stable during the acquisition of one scene (Goshtasby 1988). Information from a DEM might be included to correct elevation induced shifts on rough terrain (Itten et al. 1992; Toutin 2004). In the case of airborne line scanner data, the platform is usually operated at altitudes below 4000 m above ground and thus exposed to turbulence in the lower troposphere. The outer orientation of the platform is not stable and the acquired image does not represent a regular equidistant grid of pixels in across- and along-track direction. Geometric correction based on a polynomial transformation of the entire image would require an enormous number of ground control points (GCP) and is not feasible (McGwire 1996).

Therefore, a parametric approach is needed to solve the high frequency distortions in images from airborne line scanners. During acquisition, physical measurements from a differential global positioning system (DGPS) and an inertial navigation system (INS) are recorded. Based on this information and the sensor model, the six classical orientation parameters roll, pitch, yaw, easting, northing, and height for attitude and position of the platform are reconstructed for each scan line. Based on this information and a terrain model the recorded pixels are then individually projected onto a grid with the desired map projection and resolution, the so-called mapping array. The approach bears the potential of complete automation and sub-pixel accuracy when the auxiliary data can be provided with high precision and absolutely calibrated in space. (Schläpfer and Richter 2002)

According to Schläpfer (2005), critical parameters in the process are:

(1) the synchronization uncertainty: the orientation parameters are independently measured, matched with the oscillation frequency of the line scanner by interpolation and used for all pixels of the corresponding scan line;

(2) offsets in the orientation/position measurements caused by misalignments between the sensor model and the INS or inaccuracies in the DGPS estimates of altitude and true heading of the airplane; and

(3) the quality of the DEM.

The parametric geocoding in this work was performed using the software package for Parametric Geocoding (PARGE), version 2.2 (Schläpfer 2005). PARGE uses a statistical approach based on a number of GCPs to correct possible misalignment of sensor geometry and the INS. For every GCP, the difference between the real and the estimated GCP position is calculated and iteratively minimized by determining individual offsets for roll,

pitch, heading, or the aircraft position. 35 GCPs were identified in the HyMap image and referenced using 0.25 m color aerial photographs. An additional number of 15 reference GCPs was selected in the same manner for an accuracy assessment of the geocoding.

In the PARGE approach, the grid coordinates and spatial resolution of the output image are defined by the incorporated DEM, i.e. 3.5 m in this work. By choosing an output resolution 10-20% higher than that of the raw image data, a higher portion of spectral information is preserved (Schläpfer 2005). When the original pixels are mapped onto the grid with map coordinates at the original resolution 20-30% of all image information would get lost due to double mapping. Nevertheless, some image data will still be lost due to aircraft motion.

At the same time, gaps in the higher resolved mapping array need to be filled by interpolation based on surrounding pixels. Various methods for the interpolation exist, which are always a trade-off between spectral and spatial quality of the output. NN interpolation, for example, will lead to an output image which contains only original spectral information while showing unnatural block-wise spatial structures. Such spatial structures appear smoother and hence more real, when gaps in the output grid are filled by bilinear interpolation. In this case, however, interpolation causes artificial spectral mixtures. The decision between different interpolation methods should be based on the objectives of subsequent data processing. (Schläpfer and Richter 2002; Schläpfer 2005)

The mapping array was derived by first geocoding the original HyMap data. This mapping array is then used for the geocoding of data in the *alternative* and *segment-compressed workflow* with NN resampling of gaps based on the triangulation of surrounding directly mapped pixels. For the *traditional workflow*, the same mapping array was used, but gaps were filled by bilinear interpolation. Bilinear interpolated gaps can be considered a "good compromise" between spatial and spectral quality (Schläpfer 2005). The classification in the *traditional workflow* was performed using the SVM classifier trained for the pixel-based classification in the *alternative workflow*. Thus, pixels that are directly mapped during geocoding will be identical for the *traditional* and pixel-based *alternative workflow*. However, the classification of interpolated gaps will differ whenever NN and bilinear resampling lead to significant differences in the spectral values of interpolated pixels.

3 Results and discussion

3.1 Accuracy assessment of the mapping array

The position of 15 reference GCPs after geocoding was used to assess the quality of the parametric geocoding alone. The accuracy of this measure yields a root mean squared error of 2.9 m and 3.1 m for Easting and Northing respectively. Hence, sub-pixel accuracy is achieved. However, GCPs on bridges or areas that have recently undergone construction show offsets of up to 5.5 m. The quality of the DEM needs to be questioned for such areas. More important, GCPs were not selected from areas covered by buildings. Without the vertical information on buildings from a DSM, displaced roof tops cannot be corrected. To reconstruct surfaces occluded by displaced buildings, information from at least one additional image is needed in addition to the DSM (Zhou et al. 2005). The impact of this phenomenon is directly driven by building height and view-angle. A building of 20 m height, for example, exhibits about 3.5 m offset at 10° off-nadir and 11.5 m offset at 30° (Schläpfer 2005). Thus the final map accuracy of built-up areas will decrease with nadir distance. For quantification of the impact of displaced buildings accurate and reliable information on buildings in the image area is required, e.g. from a cadastre.

3.2 Geocoding of HyMap images

The number of pixels of the HyMap image is increased by a factor of 5.4 during geocoding (Table IV-1). This increase is caused by the flight direction of 256° and the higher spatial resolution (Fig. IV-2). When the flight line is displayed in a rectangular grid, 70.6% of all pixels are no-data pixels outside the covered area. Regardless of their missing information content, the no-data pixels increase the physical file size. Processes like principal component transformation are critical on this physically large data set; the image segmentation algorithm applied in Chapter III is not feasible.

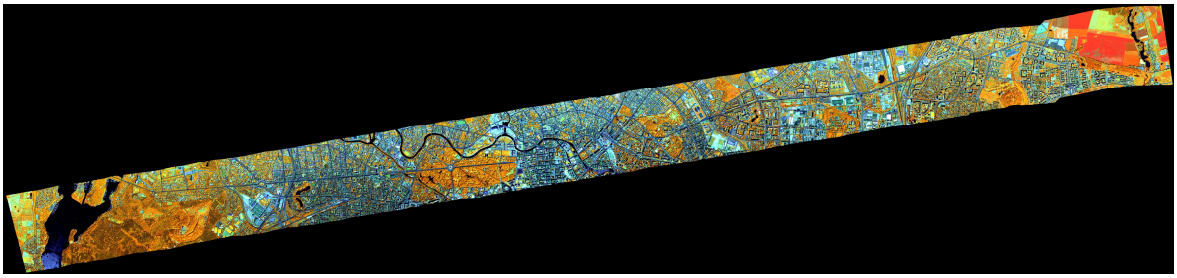

Figure IV-2: HyMap image from Berlin after geocoding (R = 829 nm; G = 1648 nm; B = 662 nm). Flight direction was 256° from East to West. Black pixels indicate no-data values outside the flight line

Table IV-1: Comparison of spatial properties and physical file size of HyMap image before and after geocoding. The physical file size relates to 114 spectral bands in 16 bit.

	Raw image	Geocoded image
No. of samples/lines	512/7,277	9,346/2,152
Overall no. of pixels	3,725,824	20,112,592
No. of pixels in flight line	3,725,824	5,904,774
No. of directly mapped pixels	3,725,824	3,711,235
No. of resampled pixels	0	2,193,539
Pixel area [m]	3.9 x 4.6	3.5 x 3.5
Physical file size [megabyte]	829,578	4,478,195

An analysis of the mapping array shows that only 0.4% of the original pixels are lost during geocoding and almost all information is preserved by the higher spatial resolution. As a consequence, however, 37.1% of all pixels in the flight line are gaps in the mapping array and need to be resampled. This way, the tradeoff between preserving information and creating additional sources of inaccuracy during the geocoding process is shown. The analysis of the influence of different resampling methods thus appears important.

Typical differences between interpolated pixels from the two approaches can be identified in the image data (Fig. IV-3). Along the edges of objects like buildings or streets, the images with bilinear interpolated gaps appear smoother than those, where gaps were filled by nearest neighbor resampling. With regard to the high number of resampled pixels the differences appear marginal, however. The actual impact of the spectral differences is best investigated based on results from the land cover classification.

3.3 Accuracy of geocoded land cover maps

As expected, the pixel-based map with NN resampling differs from that derived on the image data after bilinear interpolation. 5.2% of all pixels in the flight line are not assigned to the same land cover class in the two pixel-based workflows. All directly mapped pixels are spectrally identical and assigned to the same class. Thus, all ambiguously classified pixels are resampled pixels. They account for 14.1% of all resampled pixels and further assessment of the influence of the different workflows is required.

A statistical evaluation of the accumulated distribution of interpolated pixels by classes does not suggest class specific trends (Fig. IV-4). A comparison of subsets from the geocoded land cover maps reveals some differences between the two pixel-based approaches, although most of the results are very similar (Fig. IV-5). Straight edges appear more fringed in the NN resampled map. Especially interesting is the misclassification of pixels from the roof of a shopping center (Fig. IV-5, third column). The bilinear

interpolation of two different roofing materials (compare Fig. IV-3) leads to a line of pixels with mixed spectral information. The mixture of the two materials is assigned to the class *pervious* in either approach. Thus, a high number of erroneously classified pixels exist along the edge between the two materials.

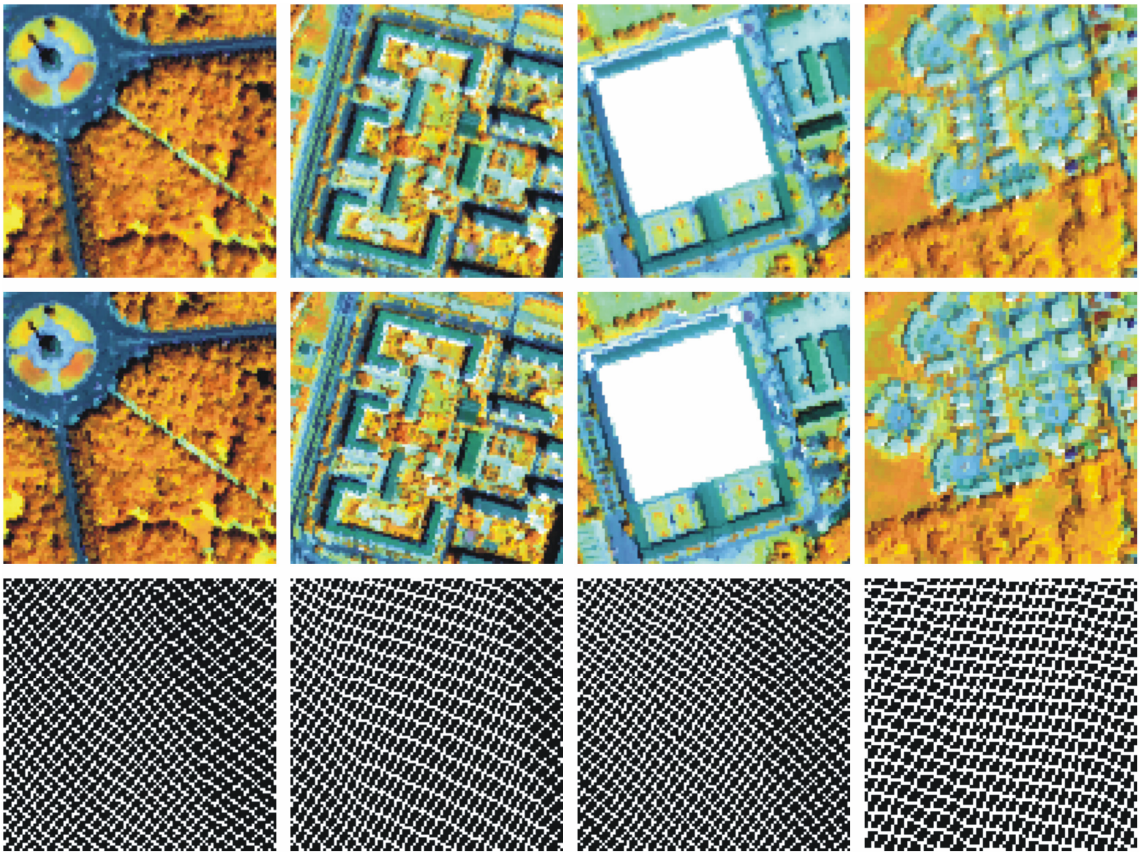

Figure IV-3: Subsets from HyMap data after geocoding with bilinear (top) and NN interpolation (middle) (R = 829 nm; G = 1648 nm; B = 662 nm). The mapping array (bottom) is shown for comparison. White pixels were resampled; black areas indicate directly mapped pixels.

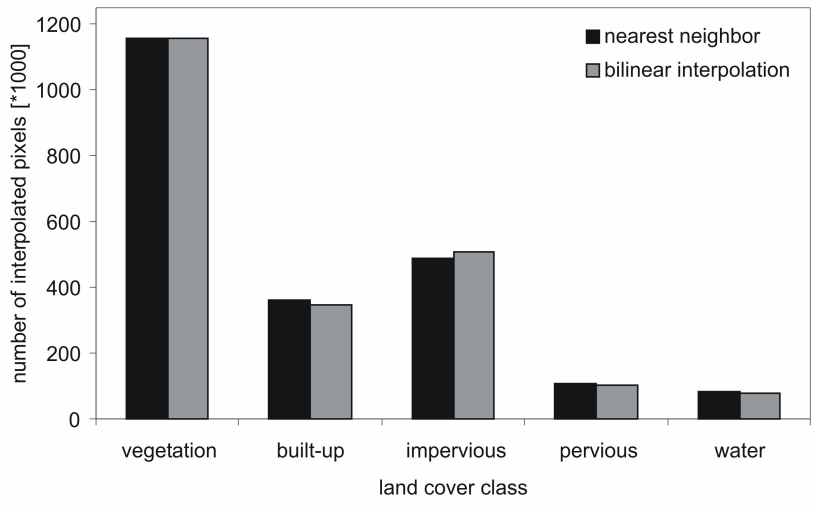

Figure IV-4: Number of interpolated pixels per land cover class for workflows with nearest neighbor resampling and bilinear interpolation of gaps in the mapping array.

To quantify the differences between the two pixel-based maps, they are compared to results from the field survey. The land cover polygons of the field survey are overlaid with the maps in raster format. The overall accuracy and producer's accuracy, i.e. percentage of area that was correctly classified within the polygons of each class, are evaluated (Fig. IV-6). Reference pixels used for the accuracy assessment before geocoding in Chapter III cannot be used in this context, since they relate to pixels in raw scan geometry which are directly mapped and not interpolated.

The overall accuracies of the maps derived by the three different workflows yield values of 68.5%, 69.5%, and 70.2% for the *alternative*, *segment-compressed* and *traditional workflow*, respectively. For different reasons, these accuracies are below those documented in Chapter III. The intersection of 4 m pixels with polygons in vector format will always cause inaccuracies along the edges of the polygons. Given the high frequent patterns and small object sizes of urban areas, this influence is relatively high and it is further increased

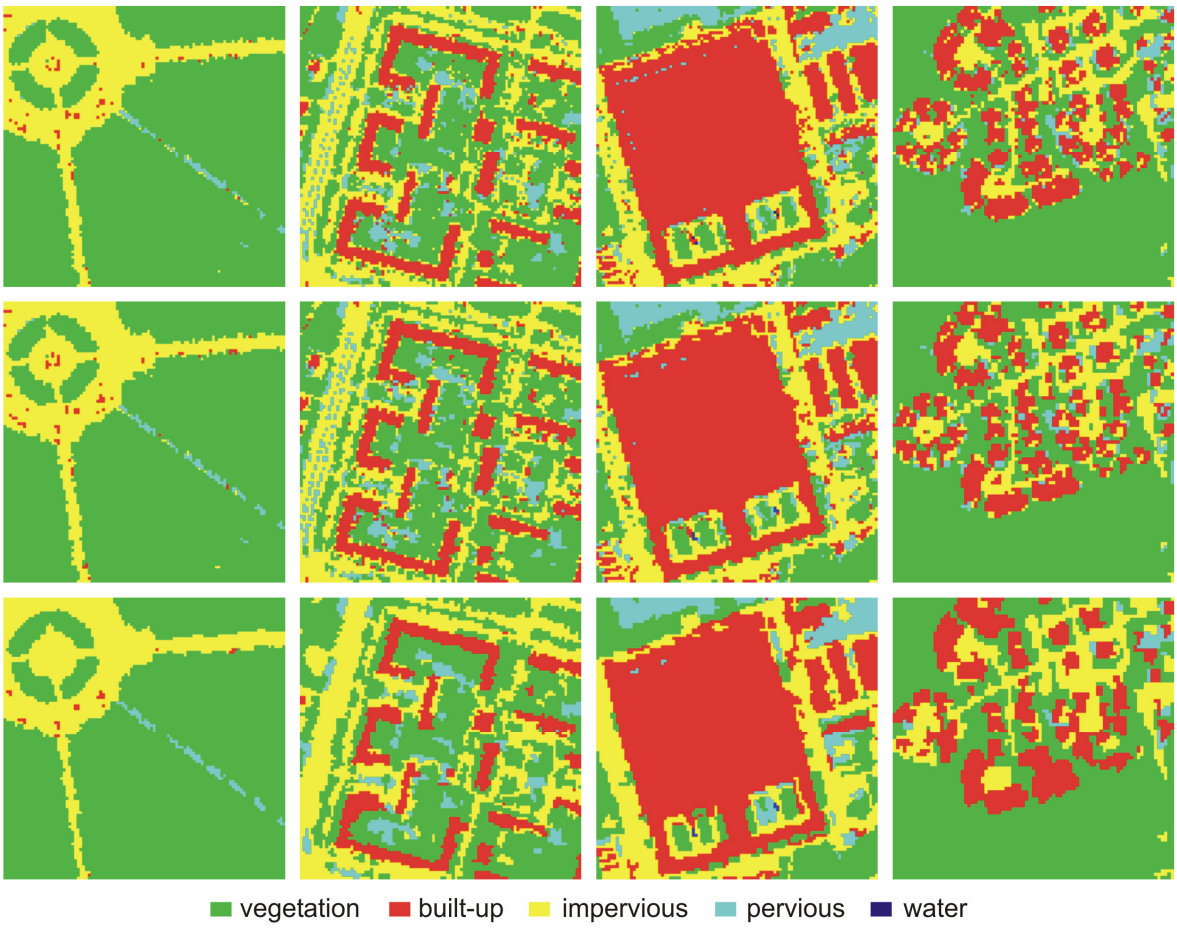

Figure IV-5: Subsets from the geocoded land cover maps from the traditional workflow (top), the alternative workflow (middle) and the segment-compressed workflow (bottom). The impact of image segmentation on land cover classification at different levels of aggregation before geocoding is discussed in Chapter III.

by the general inaccuracy of the geocoding (see Section 3.1). The missing correction of displaced buildings has already been mentioned (see Section 3.1) and is expected to contribute heavily to low map accuracies. In addition, the land use related surface categories of the field survey sometimes do not correspond to the reference pixels used in Chapter III. During the field survey, information was generalized by mapped parcels, whereas the labeling of the reference pixels relates only to the pixel and its direct neighborhood. In the case of derelict sites or of industrial grounds with heaps of sand, for example, this might cause differences. More important, the areas from the field survey are not representative for the entire image. The proportions of the classes *impervious* and *pervious* are overrepresented. They account for 50% of the mapped areas instead of a value of below 30% expected for the entire image area. Since these are two of the spectrally most critical classes, a negative bias is introduced.

The accuracies of the two pixel-based approaches show that the map that results from the *traditional workflow* is always 1% to 2% better. This workflow appears more accurate than the *alternative workflow*. Apparently, the spectral resampling during geocoding with bilinear interpolation has no negative influence on the results. This can be explained by the high number of spectrally mixed pixels in the training data from the image with 4 m spatial resolution before geocoding. The supervised SVM classifier is thus well suited for mixed signatures. The less accurate representation of lines and block-wise objects, on the other hand, appears to have negative impact on map accuracies which are based on polygons from the field survey. The first research question addressed the relevance of differences between the *traditional* and the *alternative workflow*. With regard to this question it needs

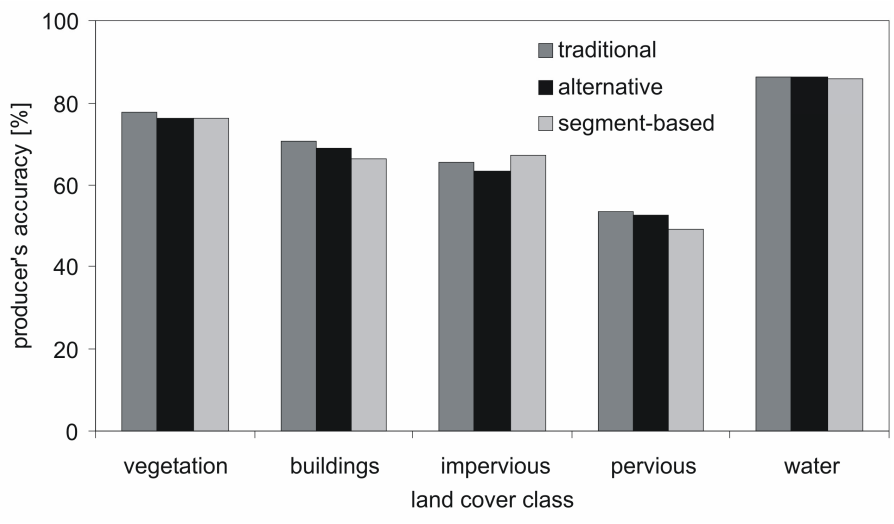

Figure IV-6 Producer's accuracies for five land cover classes based on reference data from field survey for classification results from three different processing workflows.

to be stated that 14.1% of all interpolated pixels being ambiguous is not much. However, the lower accuracies for all classes but *water* do not favor the *alternative approach*. Unfortunately, the general value and the significance of this difference cannot be evaluated based on the selection of surveyed areas. Even if the slightly lower accuracy of the *alternative workflow* was proved by additional reference data, results would need to be considered in the context of an optimized workflow and of the data reduction by a factor of 5.4. The SVM classification in the *traditional workflow* requires several hours on a very powerful computer. Processes like image segmentation are not feasible on such a data set of ~6 gigabyte.

The issue of workflow optimization is even more important when discussing results from the *segment-compressed workflow*, wherein the data size during SVM classification is decreased by a factor of ~70. Here, mapping results differ for both directly mapped and resampled pixels. Before geocoding a 4.5% difference in overall accuracy between pixel- and segment-based results at this aggregation level has been reported (see Chapter III). The accuracy assessment based on the field survey yields an overall accuracy that is in between those of the *alternative* and *traditional workflows*. Thus no relevant difference to pixel-based approaches can be reported. However, an assessment of producer's accuracies for the five classes (Fig. IV-6) shows that results from the *segment-compressed workflow* are always lowest except for the overrepresented class impervious. In addition, all surveyed areas include many wide open spaces and easily accessible grounds. Such large structures lead to the *H*-resolution case according to Strahler et al. (1986) for all classes. This is favorable for the spatially generalized segment-based analysis. The second research question asks whether the lower accuracy of the segment-based results achieved in Chapter III are further increased by geocoding in the *segment-compressed workflow*. Due to the non-representative selection of survey areas, this question cannot be finally answered. However, there are no indications for a further decrease in mapping accuracy.

In addition to the two original research questions, the general accuracy after geocoding has to be discussed at this point. The 18-20% decrease in overall accuracy of the pixel-based results during geocoding is by far more striking than the 1-2% difference between the two pixel-based workflows. Despite the mentioned non-representative selection of survey areas, it must be assumed that the various factors that have a negative influence on the final mapping accuracy after geocoding add-up to a relevant value of decrease. At a mere 70% overall accuracy, results from the land cover mapping with airborne hyperspectral data are not satisfying. Thus an additional study has to be performed, that thoroughly investigates

the potential error sources within a single processing workflow and links individual error sources to data characteristics such as spectral detail, spatial resolution or sensor geometry. For a study of this kind, a variety of different reference data sets that cover the entire flight line is needed.

4 Conclusions

Two alternative workflows for the processing of hyperspectral data are presented. Both aim at optimizing processing times while making good use of the high spectral information content of the airborne hyperspectral data. Moving the geocoding of the image data to the end of the processing reduces the amount of data for image classification by a factor of 5.4 for the pixel-based *alternative workflow*. The mandatory NN resampling during geocoding influences the accuracy of the final map. Despite a slightly lower overall accuracy compared to the *traditional workflow*, this approach is favorable for studies with very large data sets, since advanced image processing steps are either critical or not feasible in terms of processing times and memory allocation. For studies outside urban areas, i.e. areas with less frequent changes of spectrally varying materials, differences between the *traditional* and the *alternative workflow* are expected to be lower.

In the same way, the slightly lower accuracy of the *segment-compressed workflow* compared to the *traditional workflow* appears not relevant given the accumulated decrease in data size by a factor of ~70, i.e. 5.4 by geocoding and 13.1 by image segmentation. The issue of data compression will become more important with regard to increasing amounts of hyperspectral data to be processed in the future. With the increasing availability of airborne hyperspectral data products like the Airborne Reflective Emissive Spectrometer (ARES) (Müller et al. 2005) and the Airborne Prism Experiment (APEX) (Nieke et al. 2006), but also spaceborne missions like the Environmental Mapping and Analysis Project (EnMAP) (Kaufmann et al. 2005) the optimization of workflows for hyperspectral data will play an increasing role.

Against the background of the slight differences in map accuracies observed in this study, the decision on an optimal workflow should be based on processing capacities. If these are not the limiting factor, highest accuracies will be achieved with the traditional workflow. If processing times and memory allocation do not allow the traditional approach, the alternative workflow will be a reliable solution. Depending on the heterogeneity of the

observed environment and with regard to findings from Chapter III, the segment-compressed workflow appears to be a very time efficient approach.

In this work, the presumably great influence of building displacement was not considered. The occlusion of surfaces behind displaced buildings negatively impacts subsequent urban environmental analyses. Similar to the phenomenon of tree crowns obscuring the surface underneath, this effect can not be corrected, regardless whether a DSM is available or not. Thus, a detailed assessment and quantification of the influence of these phenomena at different stages within the workflow is required to evaluate the final map accuracy of classification results form airborne hyperspectral data. Such an assessment will help better understanding the decrease of overall accuracy during geocoding and evaluating the reliability of results achieved with airborne hyperspectral data.

Chapter V:
Mapping urban areas using airborne hyperspectral remote sensing data

submitted manuscript

Abstract

Urbanization significantly influences ecosystem goods and services in various ways. Accordingly, reliable and spatially explicit information on urban land cover is required for analysis of ecological conditions and urban environmental modeling, e.g. in order to correlate patterns of impervious surfaces with information on urban climate or habitats. The quality of maps from recently available, high spatial resolution remote sensing data, however, often suffers from spectral ambiguity and inaccurate representation of the complex geometric composition of urban surfaces. This study uses hyperspectral airborne line scanner data from the city of Berlin, Germany, to map a heterogeneous urban environment. The data is characterized by high spatial and spectral resolution. Diverse accuracy assessments are performed to identify sources of inaccuracy, to quantify them and to investigate to what extent remote sensing data can function as a basis for detailed urban environmental analyses. Results show that inaccuracies of the final land cover and impervious surface maps can mainly be attributed to the influence of displaced buildings occluding surfaces as a function of view-angle and to tree crowns obscuring impervious areas underneath. Despite a possible improvement of results by precise digital surface models or cadastral information, some inaccuracies will remain. The described problems occur in data from all high resolution sensors, especially at large view-angles. Possible consequences depend on the scale of subsequent analysis or on a possible combination with additional data sources.

1 Introduction

Local, regional, and global ecosystems and the goods and services they provide are significantly influenced by urbanization (Alberti et al. 2003). Urban development and the inherent change in land use negatively impact natural habitats and taxonomic richness (e.g. Blair 1996; Morse et al. 2003). They influence the microclimate as well as energy fluxes and air-flow, which again lead to phenomena like the urban heat island (UHI) and increased convective rainfall (e.g. Carlson and Arthur 2000; Collier 2006). Their positive correlation to changes in the hydrological system and pollution load in run-off or in rivers has been reported (Booth et al. 2004; Hatt et al. 2004).

Impervious surface coverage was identified as a key indicator in this context (Schueler 1994; Arnold and Gibbons 1996). Thresholds for total impervious area (TIA) in a watershed can be related to different health states of the receiving stream (Arnold and Gibbons 1996). However, such aggregated measures are not sufficient to describe biological conditions in a watershed or to function as input for environmental models; instead, detailed information on the type, density, configuration and connectivity of impervious surfaces is needed (Brabec et al. 2002; Booth et al. 2004; Carle et al. 2005; Alberti et al. 2007). For example, a strong relationship between UHI intensity and patterns of impervious areas (Bottyan et al. 2005) or between the benthic index of biological integrity and landscape variables such as mean patch size and number of road crossings (Alberti et al. 2007) have been documented. Spatially explicit land cover information has been used for describing urban environmental quality (Nichol and Wong 2005) or modeling such environmental indicators as surface temperature, run-off or biodiversity measures (e.g. Pauleit et al. 2005).

Besides information on spatial patterns of impervious land cover, it is relevant for urban planning to delineate, for example, built-up areas and open spaces (Pauleit and Duhme 2000; Nichol and Wong 2005). The density of built-up areas influences people's health and comfort (Svensson and Eliasson 2002); such information is usually not included in standard cadastre data. Detailed information on the geometry and distribution of buildings is needed in urban climatology since UHI and convective rainfall can be connected to urban morphology (Collier 2006).

In general, information on land cover can serve as an independent variable for the derivation of land use or other functional variables for ecological applications (Cadenasso et al. 2007b). Remote sensing has proved useful to provide spatially explicit information for urban land cover analyses. Aerial photography, both analog and digital, has been successfully used in this context (Pauleit et al. 2005; Cadenasso et al. 2007b). At a spatial resolution of about 0.25 m and below, it allows for a detailed mapping of urban land cover and use. It is limited, however, by its little spectral information content and a high degree of user interaction required for surface delineation. Recently, multispectral airborne line scanners like HRSC-AX or ADS40 have been introduced (Ehlers et al. 2006). Images from such instruments yield very high spatial resolutions below 0.2 m and allow fully digital semi-automated processing. Spaceborne multispectral data at a spatial resolution of 4 m and below has become available with the launch of Ikonos and Quickbird-2 in 1999 and 2001 respectively. Ever since, the number of more detailed urban remote sensing analyses has increased (e.g. Small 2003; Nichol and Wong 2005; Thanapura et al. 2007) and detailed assessments like private garden mapping (Mathieu et al. 2007) are now feasible. Beforehand, multispectral moderate resolution satellite imagery was instead used to describe urbanization processes at larger scales and aggregated densities of impervious surface coverage (Ward et al. 2000; Lu and Weng 2006). The spatial resolution of data from airborne hyperspectral scanners is similar to that of satellites like Quickbird. Its very high spectral resolution recommends hyperspectral imagery for urban analysis because the spectral similarity of anthropogenic surface materials in urban environments does not allow to directly map land cover from multispectral data (Herold et al. 2003).

Regardless of spectral characteristics, high and very high spatial resolution imagery reveals general drawbacks of remote sensing based urban analyses that are caused by the exhibited central perspective *sensor view*:

(1) 3-D-objects will be displaced at large sensor view-angles. This phenomenon can be observed in large field-of-view (FOV) airborne line scanner data and in aerial photographs, but similarly in data from high resolution spaceborne instruments like Quickbird or Ikonos that are often acquired with off-nadir view to allow more frequent acquisition. With increasing distance from nadir, roof-tops of buildings are displaced and façades will appear at the position of the buildings' ground plots. The area behind the 3-D-objects is occluded. This slant projection of buildings can lead to significant misestimates of impervious land cover during image analysis (Pauleit and Duhme 2000).

(2) urban streets might be covered by the crowns of trees on sidewalks. This effect generally applies to remote sensing based approaches. In the case of impervious surface mapping, the *sensor view* will heavily overestimate vegetated surfaces.

Regardless of the final scale of analysis and focus of an application, a detailed description of three major elements of urban heterogeneity – vegetation, built structures and surface materials – is required to facilitate understanding relationships in the coupled human-natural urban system (Cadenasso et al. 2007b). This study explores the potential of airborne hyperspectral remote sensing data to provide reliable information on urban land cover and impervious surface coverage for a spatially explicit analysis of the urban environment. Given the high spectral resolution of the data most inaccuracies during the mapping are expected to relate to problems that results from the complex geometrical composition and differences between *sensor view* and *true ground cover* of urban areas. This way, we focus on phenomena that might exist in any high spatial resolution remote sensing data used for detailed urban analysis. We quantify inaccuracies based on a variety of reference data to identify potential sources of error. Finally, we discuss to what extent maps based on hyperspectral imagery can provide reliable information for ecological analyses and environmental modeling of urban areas.

2 Conceptual framework

Urban land cover classifications that delineate built-up and non built-up impervious areas are challenging. The two spectrally heterogeneous classes include surfaces with diverse spectral properties, while spectrally similar materials exist in both classes (Herold et al. 2003). In addition, inorganic soils, i.e. pervious surfaces, can appear very similar to impervious materials like concrete.

When the spectral differentiation of land cover is successful during image classification, the complicated geometrical composition of urban areas needs to be coped with to achieve an accurate map that can be linked with other information for subsequent analyses. This is ideally achieved by incorporating accurate 3-D-models in the orthorectification process. Such digital surface models (DSM) are more frequent nowadays due to the increasing availability of laser scanning systems. It will take several more years, however, until detailed and up-to-date 3-D information exists for many urban areas world-wide. When no DSM is available, displaced buildings will - as a function of their height and the sensor's view-angle - impact the accuracy of results. In our case, no DSM was available. Even with

a DSM, occluded surfaces due to an oblique view cannot be reconstructed in single orthophotos (Zhou et al. 2005). Also, the phenomenon of trees obscuring ground cover underneath remains and its impacts can hardly be predicted. Despite the importance of information on tree cover itself, several ecological assessments require knowledge on the underlying surface, e.g. for hydrological modeling.

This study is organized around three questions for the detailed assessment of possible inaccuracies of urban land cover maps generated from airborne hyperspectral data:

(1) Does airborne hyperspectral remote sensing data provide the spectral information needed to reliably delineate urban land cover?

(2) How spatially accurate are maps from airborne line scanner data in urban areas?

(3) How great is the impact of tree crowns obscuring impervious surface underneath?

To answer these questions the following steps are performed:

(1) a heterogeneous urban environment is classified with a state-of-the-art classifier. The land cover classes vegetation, buildings, non built-up impervious area (paved), soil, and water are delineated;

(2) a map on the impervious surface coverage is derived from the orthorectified land cover map;

(3) different accuracy assessments are performed that explicitly address the individual sources of inaccuracy. The quality of the image processing as a whole is assessed and drawbacks of individual processing steps are identified.

By performing the study in a well-known urban environment with diverse reference data sets available, a thorough assessment and quantification of inaccuracies is possible. This way, important insights for similar studies in less known areas of the world can be derived.

3 Airborne hyperspectral remote sensing of urban areas

Hyperspectral remote sensing data, also referred to as “imaging spectrometry data”, is characterized by its very high spectral information content (Goetz et al. 1985). For each pixel in the image a quasi-continuous spectrum exists which represents the measured reflected sunlight in the visible (VIS), near-infrared (NIR) and short wave-infrared wavelength regions (SWIR). Whereas the bands in multispectral imagery cover rather wide wavelength regions (e.g. 60-250 nm in the case of Landsat Thematic Mapper), the bands in

hyperspectral data are narrow (e.g. 10-15 nm). The resulting spectra enable, for example, analyzing narrow absorption features (e.g. McMorrow et al. 2004) (Fig. V-1) and the quantification of ecological variables (Ustin et al. 2004).

Airborne hyperspectral remote sensing was first introduced in the mid-1980s and emerged with the availability of data from the Airborne Visible/Infrared Imaging Spectrometer (AVIRIS) (Vane et al. 1993). First used in geological applications (e.g. Kruse et al. 1993b), hyperspectral data was introduced to other environmental applications such as green and non-photosynthetic vegetation mapping (Roberts et al. 1993), biophysical modeling (Jacquemoud et al. 1995) or wildfire mapping (Dennison 2006). Nowadays, data from several airborne imaging spectrometers is used in various contexts, for example data from the Digital Airborne Imaging Spectrometer (DAIS7915) (e.g. Roessner et al. 2001), Hyperspectral Mapper (HyMap) (e.g. Schlerf et al. 2005) or the Compact Airborne Spectrographic Imager (CASI) (e.g. Wang et al. 2007). The quality of the data is determined by the sensor's spectral characteristics and its signal-to-noise ratio (SNR). The number of instruments is increasing and hence more hyperspectral data will be available for research and application.

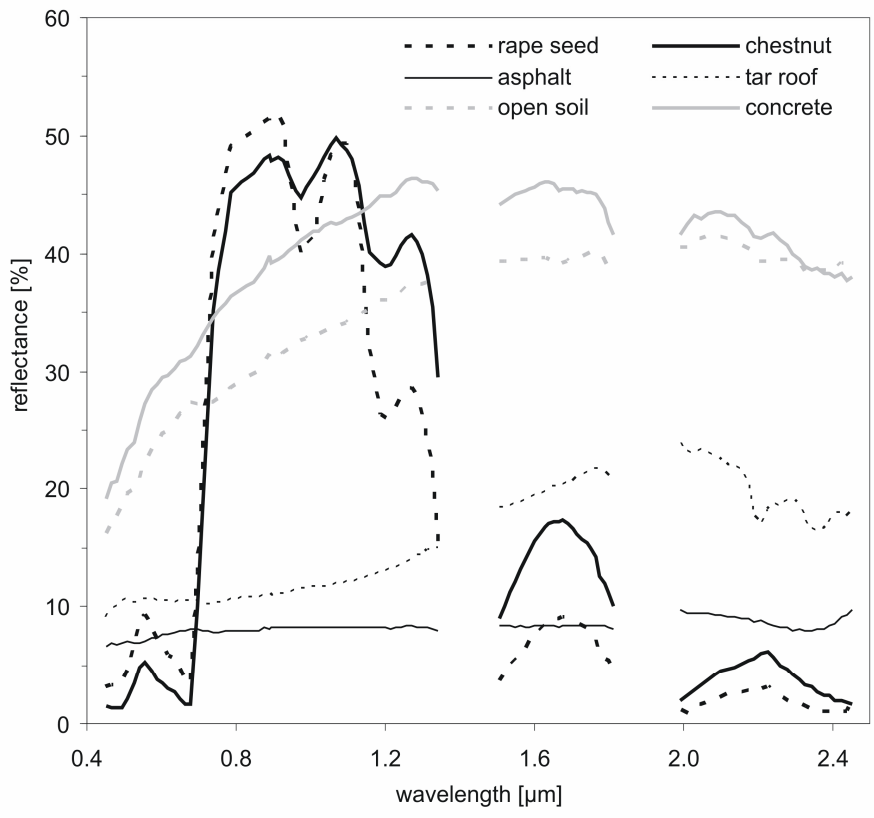

Figure V-1: Reflectance spectra from the airborne Hyperspectral Mapper (HyMap) for different surfaces. Gaps are due to atmospheric absorption.

Whereas the high spectral information content of airborne hyperspectral data is very beneficial for many applications, their pre-processing and analysis are more complicated than traditional spaceborne multispectral data. This is caused by data inherent phenomena like the presence of water vapor absorption features in the spectrum or sensor characteristics such as a wide field-of-view (FOV) (Fig. V-2). This FOV and hence large view-angles, θ_v, towards the edges of the flight line are necessary to cover large areas at low operating altitudes but they enhance the differences between *sensor view* and *true ground cover* or between sun-facing and shaded façades. The problem of correcting atmospheric effects and reflectance anisotropy is solved for the urban environment to a satisfying extent (Richter and Schläpfer 2002; Schiefer et al. 2006). The orthorectification of the data can achieve sub-pixel accuracy, but results depend heavily on the quality of the available digital elevation model (DEM) or ideally DSM (Schläpfer and Richter 2002).

4 Material and methods

4.1 Study area

We used data from the metropolitan area of Berlin, Germany, in this work. The history and structure of the city make it an ideal study area for the addressed research questions. The rise of the Prussian empire and the era of industrialization dominate the original structure of the city. After heavy destruction during World War II, a period of separation and parallel development under opposite political systems led to diverse new urban structures. Following the fall of the Berlin Wall and the closing down of industrial complexes from

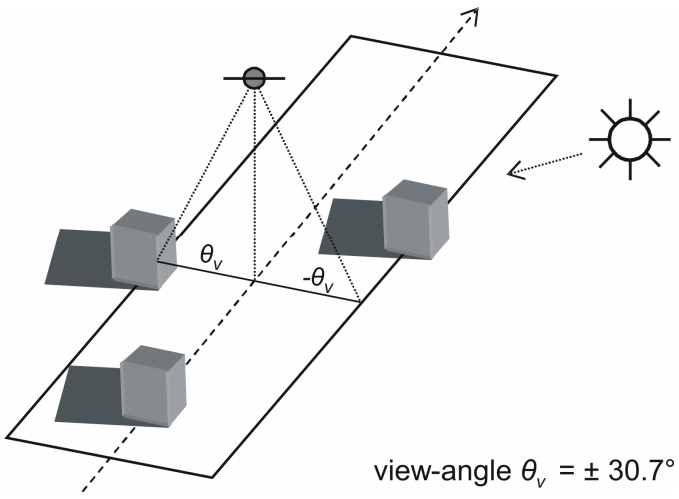

Figure V-2: Image acquisition by the large FOV airborne line scanner HyMap in urban areas. Façades appear in the image at large view-angles and are differently illuminated.

socialist times, many derelict sites exist and Berlin has recently been experiencing large scale development in very central areas (e.g. Postdamer Platz). The study area hence covers a great variety of urban structure types. This situation is unique for a metropolitan area in the western hemisphere and the three research questions can be thoroughly investigated: the spectral variety of roofing materials, for example, is high; the height and spatial composition of buildings is diverse; in the very most cases trees exist along streets. (Sukopp 1990; Balder et al. 1997; SenStadt 2007)

The 32.5 by 2.2 km study area is outlined by the extent of the available hyperspectral data set and covers a representative gradient from the western urban fringe through the city center to the eastern municipal boundary (Fig. V-3). It includes:

a) the central business and governmental district with large administrative buildings, wide open spaces, historical boulevards or newly constructed shopping and transportation areas (Fig. V-4.a,b);

b) residential areas of different densities and from different development periods (Fig. V-4.c-e);

c) pre-cast apartment complexes and wide boulevards in former East Berlin (Fig. V-4.f);

d) parks and recreational areas (Fig. V-4.g);

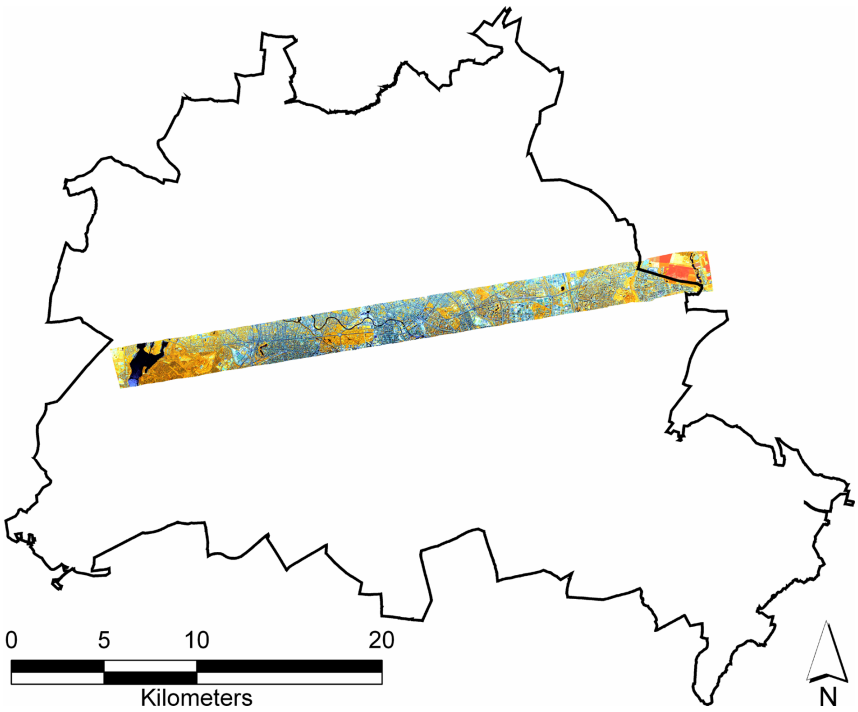

Figure V-3: Study area and municipal boundary of Berlin. The outlines of the study area are determined by the extent of the airborne image data set. Image data is shown after preprocessing in false-color composite (R = 829 nm; G = 1648 nm; B = 662 nm).

e) private garden areas (Fig. V-4.h);

f) industrial grounds (Fig. V-4.i);

g) derelict land (Fig. V-4.j);

h) suburban areas (Fig. V-4.k);

i) inner-urban forests, water bodies and rivers, and small agricultural patches towards the end of the flight line (Fig. V-4.l).

j) Image data

The airborne imaging spectrometer HyMap acquires data between 0.4 and 2.5 µm in 128 spectral bands (see eample spectra in Fig. V-1) with an average bandwidth of 10 to 15 nm. The sensor's FOV is 61.3°. The 7277 by 512 pixel raw image was originally registered at a spatial resolution of 3.9 by 4.5 m at nadir.

The hyperspectral image used in this work was acquired on 20 June, 2005 around 10.46 AM local time. The data set was corrected for atmospheric effects and converted to surface

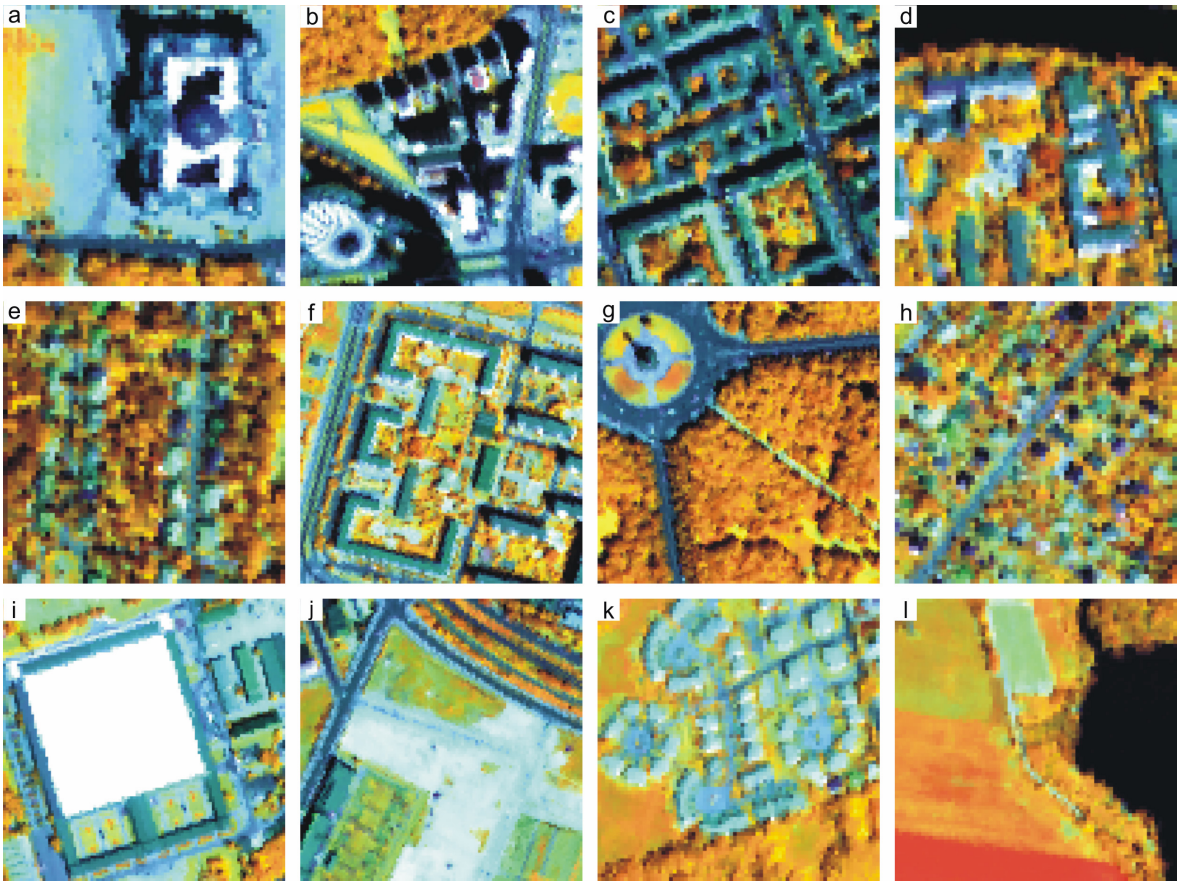

Figure V-4: Examples of different urban structure types in the hyperspectral data set (R = 829 nm; G = 1648 nm; B = 662 nm). Details see text.

reflectance (Richter and Schläpfer 2002). View-angle dependent brightness gradients were eliminated (Schiefer et al. 2006, Chapter II of this work). The number of bands was reduced to 114 based on the signal-to-noise ratio. After image classification the resulting maps were orthorectified and resampled to a pixel size of 3.5 m (Schläpfer and Richter 2002). A raster DEM derived from the contour lines of the official digital map was resampled from its original spatial and vertical resolution of 25 m and 0.1 m, respectively, to 3.5 m spatial resolution for the correction. A DSM was not available. The accuracy assessment of the orthorectification itself showed a root mean squared error (RMSE) of 2.9 and 3.1 m in easting and northing, respectively, that is explained by the missing accuracy of the DEM.

4.2 Land cover classification

The land cover classification was performed using support vector machines (SVM). SVM have recently been experiencing increased attention. They outperformed other classifiers in several studies, they require a relatively small number of training samples, and are insensitive to high dimensional data (e.g. Huang et al. 2002; Pal and Mather 2006). SVM are a supervised classification algorithm that delineates classes by fitting a separating hyperplane in the spectral feature space (Burges 1998). SVM can handle complex class distributions, including multi-modal classes, i.e. classes that contain a variety of materials with different spectral properties. Spectrally heterogeneous classes are difficult to assess with traditional parametric classifiers (Seto and Liu 2003). For our study, the software imageSVM was used (Janz and van der Linden 2007).

The training samples were acquired by a clustered sampling strategy: at first, 64 seed pixels were randomly drawn from the full image. 29 pixels around each of these seeds (a 5 x 5 window plus the four outer diagonal pixels) were then assigned to one of the five classes. A small number of additional seed pixels were interactively placed on rare but characteristic surfaces. All pixels were labeled based on very high resolution aerial photographs in Google Earth. Altogether, 2133 training samples were used for the SVM classification.

4.3 Reference data and accuracy assessment

A detailed accuracy analysis according to the research questions in this work requires reference data of different characteristics and from multiple sources. Digital aerial photographs and information from the Urban Environmental Information System (UEIS)

and cadastre were available from the municipal administration. In addition, a detailed field survey was performed synchronously to the acquisition of the image data. Based on these different sources of reference data, reference products were generated for the assessment of the individual processing steps during image analysis (Fig. V-5). The different assessments are then discussed in the context of the three research questions.

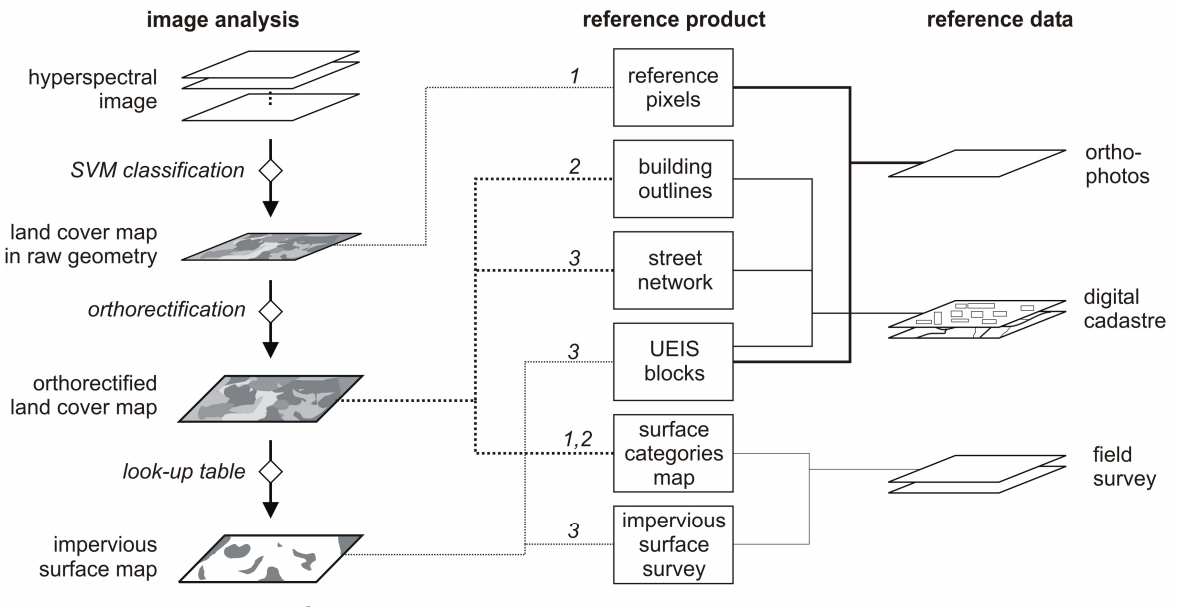

Figure V-5: Hyperspectral image analysis steps, reference products and the data sets they are based on. The different reference products were derived from orthophotos, digital cadastral information and field surveys. They are used to assess different steps of image analysis (dotted lines). Italic numbers indicate, which research question is addressed by the corresponding assessment.

Orthophotos

A set 0.25 m resolution digital color aerial photographs was available through the Berlin Department for Urban Development. The data set covers the entire area of Berlin and was taken in August 2004. In addition, Google Earth provides aerial photographs of slightly higher spatial resolution for the city.

To assess how well urban land cover classes can be mapped based on hyperspectral information, a stratified set of independent reference pixels was selected from the image before orthorectification. These were used to derive a confusion matrix for the land cover map and to calculate the overall accuracy, kappa value (κ), and producer's and user's accuracy (Congalton and Green 1999). At first, rectangular polygons of about 200 by 300 pixels were manually drawn on areas of six typical urban structure types to account for the heterogeneity of the urban environment. These included: the central business and governmental district (in the following named *center*); dense residential areas with

Table V-1: Reference pixels of five land cover classes as distributed in urban structure types.

Class	Reference pixels randomly selected from								Total
	center	dense	single	complexes	suburban	industrial	dark	rest	
vegetation	28	52	91	77	112	42	55	108	565
buildings	58	41	36	23	5	29	-	32	224
paved	57	54	18	40	2	62	42	34	309
soil	1	4	4	7	26	18	-	12	72
water	4	-	-	2	5	-	61	11	83
Total	148	151	149	149	150	151	158	197	1253

attached buildings and narrow courtyards (*dense*); open residential areas with single houses and gardens (*single*); pre-cast apartment complexes surrounded by recreational areas (*complexes*); individual houses surrounded by agricultural patches and forest along the urban-suburban fringe (*suburban*); industrial and commercial grounds (*industrial*). About 150 reference pixels were randomly drawn for each urban structure type (Table V-1). To better investigate the classification quality in dark areas (*dark*), i.e. areas with low contrast like water or shaded surfaces, 158 extra points were randomly selected using a dark area mask (reflectance at 1.650 µm < 5%). 197 pixels were randomly selected from the rest of the image (*rest*), to represent remaining areas. Altogether, 1253 reference pixels in the image were assigned to one of the five classes based on their spectral properties and contextual information from the aerial photographs.

Digital environmental and cadastral information

The Berlin Department for Urban Development provides digital information based on a digital map at the scale of 1:5000 in the UEIS (SenStadt 2007). The polygons in the UEIS represent structural units that refer to transportation areas, residential blocks or water bodies for the year 2005. In addition, the spatial extent of buildings was available through the city's digital cadastre. Altogether, 550,000 buildings exist in this second database. It is very accurate for residential buildings but misses some structures on industrial grounds and private gardening areas.

To investigate the influence of object displacement on map accuracy, all building outlines in the cadastral database that are located in the study area were extracted. Since the direction and degree of object displacement depends on the objects' position in relation to the nadir-line, i.e. increased displacement with increased oblique view, the extracted building outlines were stratified into three zones parallel to the flight direction: pixels north of the nadir line at large positive view-angles ($\theta_v > 10°$); pixels along the nadir line ($10° \geq \theta_v \geq -10°$); and pixels south of the nadir line ($\theta_v < -10°$). In a similar way, the *street*

network was extracted from the UEIS and stratified accordingly. Showing the true ground cover, this assessment was used to quantify the street area that is covered by trees. At large view-angles, high buildings might actually occlude parts of the street behind it and this assessment therefore relates indirectly to the issue of object displacement. The accuracy assessment based on building outlines and the street network also serves to indirectly investigate the quality of the spectral land cover classification.

In addition, 37 residential blocks of different size were randomly selected from the UEIS to assess the quality of the map on impervious surface coverage. For this purpose, the corresponding polygons were extracted, buildings were excluded from the polygon, and the outlines were then projected onto the aerial photographs. Based on an equidistant raster of 20 by 20 m (40 by 40 m for polygons greater 25,000 m²), a set of points within each polygon was labeled either pervious or impervious. Two different values of TIA were then assigned to the polygons: (1) a value based on the visible surface that relates to the *sensor view*; (2) a value corresponding to true ground cover, which was derived after identifying the ground cover underneath trees. The two values were used to assess the map on impervious surface coverage and the influence of tree cover.

Field survey

Parallel to the over-flight of the HyMap sensor, a detailed field survey was performed. Based on the 0.25 m aerial photographs, two different digital layers were mapped in a geographical information system (GIS). The first layer specifies 21 surface types associated to land use and more than 40 different types of dominant surface materials at ground level. In a second layer, the extent of individual trees or groups of trees is mapped on top of the ground level. Altogether, 17 survey areas of approximately 220 by 220 m were mapped this way; nine of them were located within the area covered by the hyperspectral image. The distribution of land cover in the survey areas is not representative for the whole city. To enable a continuous mapping, dense residential areas with closed courtyards or inaccessible industrial sites were avoided. Easy to map park areas with closed tree canopy were also excluded. The abundance of open space or derelict sites is above average. Displacements of buildings in the aerial photographs have been accounted for during mapping.

The information of the two GIS-layers was used in two ways. At first, it was intersected and generalized into 12 land cover related surface categories for a spatially contiguous assessment of the land cover map (Table V-2). Intersecting regions were then assigned the

Table V-2: Surface categories for detailed assessment of the land cover classification with corresponding description and area for nine field survey areas. The class to which the surfaces were assigned in the training data for classification is indicated.

Category	Description	Label in training data	Area [m²]
individual trees	single coniferous and deciduous	*vegetation*	16,224
tree groups	closed canopies of more than 1 tree	*vegetation*	30,864
Shrubs	deciduous and coniferous at different heights; partly interrupted by bark mulch and organic soil	*vegetation/soil*	6737
Lawn	irrigated; non-irrigated; sparse	*vegetation*	90,650
Soil	soil, including pervious sports areas	*soil*	10,472
derelict sites	different stages of succession; might include rubble	*soil/vegetation*	9517
construction sites	open pits; might include heaps of rubble and sand	*soil*	4558
roof tops	all types of buildings and materials	*buildings*	46,040
Tracks	tram and railroad; tracks with gravel	*paved*	4386
Courtyard	industrial grounds and courtyards of different size	*paved*	15,581
Sealed	all other non built-up impervious surfaces	*paved*	147,867
Water	Water	*water*	7441

attributes from the tree cover layer. Thus, the resulting layer rather represents the *sensor view* situation (Fig. V-6, left). The 12 surface categories help to identify potentially critical surface types within the land cover classes.

At second, the ground layer was generalized to impervious and pervious surfaces, with values of 100% and 0%, respectively, and intersected with the tree canopy layer. The resulting four categories can be used to derive the relation between TIA of the survey areas in *sensor view* situation and *true ground cover* (Fig. V-6, right). This impervious surface survey was used to assess the impervious surface map from the HyMap data with regard to tree cover.

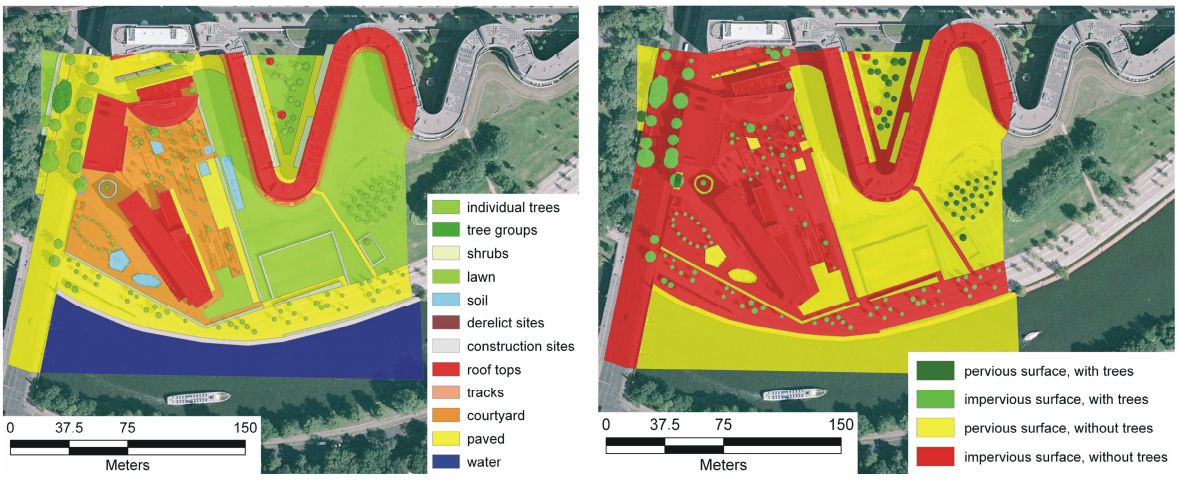

Figure V-6: Reference maps derived from ground mapping shown for one of nine subsets. The 12 land cover related surface categories were used for a spatially continuous assessment of the land cover map (left). The four categories of surface types related to imperviousness were used to assess the sensor view in comparison to the true ground cover (right).

5 Results

5.1 Land cover classification

The land cover classification without orthorectification yields an overall accuracy of 88.7% ($\kappa = 0.84$) based on the 1253 reference pixels. Confusion is low for all classes and the user's accuracy is relativels well balanced (Table V-3). The individual assessment within the urban structure types shows accuracies of 90% or better for green areas (single residential 89.3%, apartment complexes 94%, suburban 94.7%). The remaining classes exhibit accuracies above 80% (center 83.1%, dense residential 84.6%, industrial 80.8%). 52.7% of the study area are classified as *vegetation*, 16.2% as *buildings*. 22.3% of the area are identified as non built-up *paved* grounds. *Soil* and *water* constitute the smallest classes at 4.8% and 3.9% respectively. Since reference pixels were selected from the image itself and aerial photographs only used to aid during labeling, possible geometric inaccuracies between the classification output and reference products are not taken into account. Thus, overall accuracy relates to the spectral classification quality and not to final map accuracy.

The assessment of land cover derived from hyperspectral imagery within the building outlines from the cadastral data leads to an accuracy for the class *buildings* that is below the user's accuracy of the classification without orthorectification. The accuracy differs clearly according to the distance to the nadir line (Table V-4). Whereas 65.5% of all pixels in the building polygons are classified correctly near nadir, values decrease to 52.3% in the southern and 62.4% in the northern parts of the study area. The small decrease in northern parts is compensated by *vegetation*, *paved* and *soil* pixels; the greater decrease in southern parts leads to an increase of paved and vegetated areas.

The number of pixels correctly classified as *paved* surface on areas of the street network is generally lower than that of buildings within building outlines. Instead, a consistently high fraction of pixels is labeled as *vegetation*. This *vegetation* fraction is higher in the northern parts while a decrease of *paved* pixels combined with an increase in *buildings* can be observed in the southern parts (Table V-4).

The analysis based on surface categories derived from the field survey shows how the accuracy of the land cover map differs for different surface types within the land cover classes (Table V-5). For all surface categories, the correct land cover class constitutes the greatest fraction, but for some of them this fraction is only 40% to 50%. The low value for the small water area is negligible and caused by an inaccurate digitization along the shore.

Table V-3: Confusion matrix, producer's and user's accuracy for land cover classification results.

Classification	Reference pixels					Total	User's accuracy
	vegetation	built-up	impervious	pervious	water		
vegetation	541	4	5	7	2	559	96.8
built-up	0	183	24	5	0	212	86.3
impervious	20	33	270	21	3	347	77.8
pervious	4	4	6	39	0	53	73.6
water	0	0	4	0	78	82	95.1
Total	565	224	309	72	83	1253	
Producer's acc.	95.8	81.7	87.4	54.2	94.0		

Table V-4: Distribution of land cover for stratified areas of building outlines and street network.

Class	Building outline				Street network			
	> 10°	nadir	< -10°	overall	> 10°	nadir	< -10°	overall
vegetation	13.0	11.5	17.8	14.2	36.5	31.5	31.9	33.3
buildings	62.4	65.5	52.3	60.0	10.7	8.1	13.2	10.6
paved	19.5	19.0	25.1	21.2	50.2	58.2	51.7	53.4
soil	4.8	3.5	3.9	4.1	2.4	2.1	2.7	2.4
water	0.3	0.5	0.7	0.5	0.2	0.2	0.2	0.2

Table V-5: Distribution of land cover as mapped from HyMap data for different surface categories. The correct assignment is indicated in bold.

Category	*buildings*	*paved*	*vegetation*	*soil*	*water*
individual trees	6.5	25.5	**62.3**	5.6	0.0
tree groups	1.0	5.5	**91.6**	1.9	0.0
Shrubs	13.6	17.9	**60.2**	8.3	0.0
Lawn	2.8	8.8	**74.8**	13.5	0.1
Soil	3.6	8.2	26.9	**61.3**	0.0
derelict sites	3.6	29.2	18.7	**48.6**	0.0
construction sites	19.8	29.9	9.5	**40.8**	0.0
roof tops	**68.8**	21.9	6.7	1.6	1.0
Tracks	7.9	**72.8**	17.2	2.2	0.0
Courtyard	26.3	**44.5**	23.3	5.3	0.6
Sealed	15.2	**64.9**	15.1	4.2	0.6
Water	2.1	3.4	0.2	8.0	**86.3**

5.2 Impervious surface coverage

The map on impervious surface coverage is derived from the land cover classification. All pixels were assigned a value of 0% - in the case of *vegetation*, *soil*, and *water* - or 100% for *buildings* and non built-up *paved* areas. Although more differentiated approaches to assign degrees of imperviousness to surface types exist in literature (e.g. Hodgson et al. 2003), it was decided to use these values that are also used by the city's planning department. Identical values were assigned to the land cover in the reference data sets and this simple approach is not expected to have a positive bias on presented accuracies.

Collapsing classes in the original 5 class confusion matrix by impervious and pervious surfaces leads to an overall accuracy of 94.3% based on the 1253 reference pixels. For an areal assessment of impervious surfaces, the HyMap based map is first compared to results from the field survey. The RMSE based on the nine survey areas within the HyMap data frame is 8.8 and 10.4 for the situation with trees and based on the true ground cover underneath the trees, respectively. The higher value in the case of true ground cover shows how TIA is underestimated by the HyMap data.

Similar results are achieved by the comparison of the HyMap based map to estimates for the 37 UEIS polygons. These polygons cover a wider range of surface compositions than the survey areas. RMSEs of 14.3 and 20.7 are calculated with and without tree cover respectively. Again, an offset results from comparing HyMap based results and true ground cover, while almost a 1:1 relationship is achieved including the tree cover that shows the *sensor view* situation (Fig. V-7).

6 Discussion

In the following, results from the land cover classification of *vegetation*, *buildings*, *paved* surfaces, *soils* and *water* and the impervious surface map are discussed. The three research questions are sequentially addressed with regard to the different accuracy assessments.

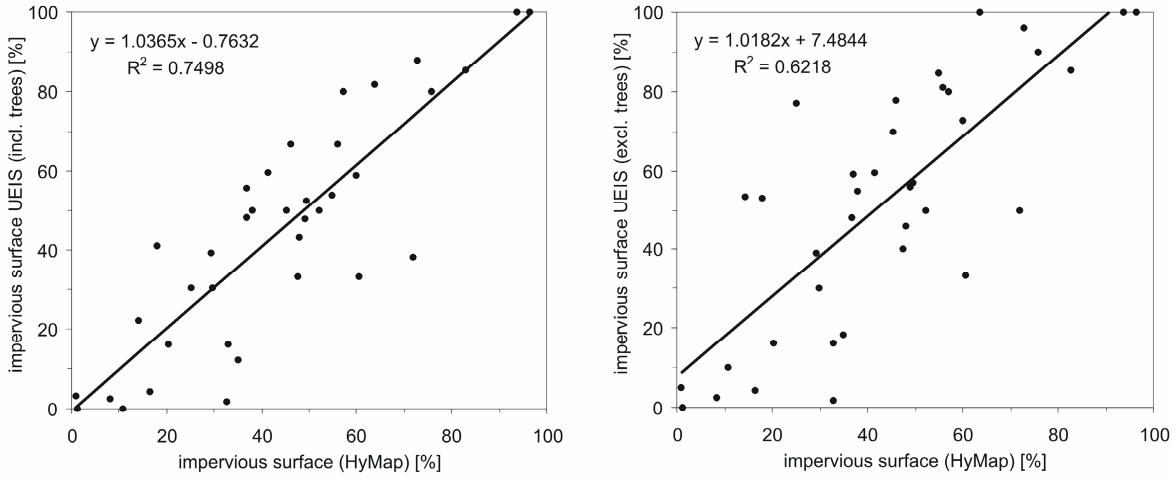

Figure V-7: Impervious surface estimates based on HyMap data compared to impervious surface fractions derived from aerial photographs for 37 UEIS polygons. Values from ground mapping relate to *sensor view* including tree cover (left) and to the *true ground cover* (right).

6.1 Accuracy of the urban land cover classification

The results clearly indicate that hyperspectral data allow the spectral differentiation of basic land cover classes in urban areas. Despite some remaining confusion between *buildings* and *paved* areas, as well as *soil* patches mistakenly labeled as *paved*, the user's accuracy of all classes is high. Even for dark areas, which are often treated as a meaningless *shadow* class (e.g. Shackelford and Davis 2003), there is 89.2% accuracy. A detailed assessment of misclassified reference pixels shows that mixed pixels and phenomena, such as cars on streets or sand heaps on industrial grounds, account for some of the confusion.

The comparison of land cover in the classified image and of the surface categories based on the field survey reveals other potential sources of error (Table V-5): the low accuracies for derelict and construction sites can be explained by the spectral similarity of sand or sandy soils in open pits and concrete surfaces on the one hand; on the other, objects like vehicles or heaps of rubble, which are spectrally more similar to competing land cover, exist on these surface categories. This underlines that land cover does not directly relate to spectral properties and that issues of land use should better be treated separately (Cadenasso et al. 2007b). The fraction of vegetation is relatively little on lawn surfaces, which may be confused with soil, due to non-irrigated lawns or sparse plant cover. This confusion of organic soil and sparse vegetation also exists the other way around and a clear distinction between the two is not possible. It is also obvious from field observations that the two classes form transitional spectral classes.

The spectral information content of airborne hyperspectral imagery is of great value in separating and describing vegetation, built structures and other surface materials. Inaccuracies that have been reported for separating buildings from non built-up impervious areas using multispectral data (e.g. Shackelford and Davis 2003) exist to a lesser extent. Remaining confusion related to spectral ambiguity has to be judged against the general advantages of remote sensing, i.e. synchronous coverage of large area at relatively low cost (Mathieu et al. 2007). Considering the number of dynamic surfaces like construction sites and derelict areas, the possibility of regular monitoring is an important asset of remote sensing approaches. These points apply especially for regions in the world with incomplete, inaccurate or missing cadastre information and a lack of detailed maps on urban environmental indicators (Miller and Small 2003).

The SVM classification in this work neither requires building spectral sub-classes nor incorporating texture measures (e.g. Benediktsson et al. 2005) or segment-based analysis

(e.g. Shackelford and Davis 2003). It only uses the full hyperspectral information of original pixels. This way, the classification approach is very simple and requires no additional and often time intensive processing steps like image segmentation or feature extraction. Taking into account the high accuracies within areas of the different urban structure types, SVM classifications of HyMap data are expected to generally perform well for urban areas.

6.2 Spatial accuracy of land cover and impervious surface maps

The difference between the high accuracy for the class *buildings* based on the set of reference pixels (Table V-3) and the small portion of overall 60% of pixels classified as *buildings* within the building polygons from the cadastral information (Table V-4) is obvious. Since reference pixels do not account for geometric inaccuracies, this discrepancy can be related to insufficient orthorectification and object displacement. The value of 65.5% buildings in polygons near nadir is explained by the 4 m resolution of the image data, the general inaccuracy of the orthorectification (compare Section 4.2) and by a slight displacement of very high buildings within this interval. Thus the buildings' positions from remote sensing based mapping and polygon outlines from cadastral data never match perfectly (Fig. V-8, upper-right). This general disparity between the orthorectified image data in raster format and the vectorized polygons can also be observed by comparing the HyMap based map to those from the field survey. Accuracy of the land cover map for surface categories that mainly exist as small patches is lower than for those categories of rather large spatial extent. The latter contain less mixed pixels and are less influenced by the mentioned inaccuracies. For example, single trees are mapped at significantly lower accuracy than tree groups or lawn surfaces. Areas with shrubs often form narrow corridors and are many times located close to high buildings.

The impact of the building displacement alone can be assessed by comparing the portion of *building* pixels within polygons of the nadir region to areas acquired at large view-angles. Off-nadir accuracies are generally lower. The decreases of 13.2% and 3.1% for southern and northern parts of the image, respectively, can be explained by the influence of shade: on the one hand, non-illuminated façades that are visible in the southward sensor view are classified as *paved* (Fig. V-8, bottom); the illuminated façades to the north, on the other, can be differentiated from *paved* surfaces and the classification within the building polygon is more accurate, although the roof pixels appear north of the buildings' actual position (Fig. V-8, upper-left). Vegetation increases at larger view-angles, due to trees in

front of the façades. The spectral signal of vegetation is very dominant on dark areas with low reflectance. Therefore non-illuminated mixed pixels are mostly labeled *vegetation*. This explains the greater increase in vegetation to the south. In general, the decrease of 13.2% rather reflects the impact of the displaced roofs than the decrease of 3.1% that is compensated by the "correctly" assigned façades. The impact of buildings occluding adjacent surfaces is also indirectly shown by the other reference products: in the maps from the field survey, 26% of the surface categorized as courtyard is classified as *buildings*. The portion of pixels classified as *building* within the street network polygon increases at larger view-angles where the buildings exhibit more displacement. In general, the displacement is a function of view-angle and building height. A building of 20 m height, for example, exhibits ~ 3.5 m or ~1 pixel offset at 10° off-nadir and 11.5 m or 3-4 pixel offset at 30°. Even when a DSM is available, occluded surfaces can only be reconstructed when at least one additional image acquired from a different position is available (Zhou et al. 2005).

The spatial accuracy of the land cover map based on airborne hyperspectral data varies significantly for different areas in the image, i.e. different view-angles (Schläpfer and Richter 2002). For most urban environmental studies, the detailed information on patterns of impervious areas and the abundance of roof-top areas is required at larger units like the

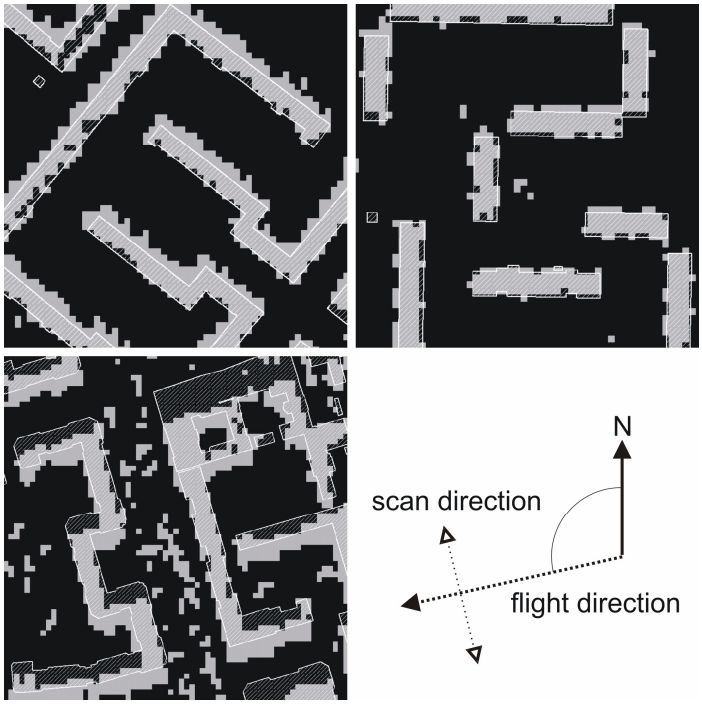

Figure V-8: Building positions from land cover mapping compared to polygons from cadastre. Roof-tops at large view-angles north of the nadir region are shifted northwards (upper-left), south of the nadir region they are shifted southwards and façades are not illuminated (bottom). Buildings near nadir exhibit no shift (upper-right).

UEIS blocks for the city of Berlin or for an entire watershed (Tong and Chen 2002). In these cases, the total area of such objects is mapped with sufficient accuracy by airborne hyperspectral data. Whenever configuration and connectivity of built-up land or land cover in general is required (e.g. Alberti et al. 2007), the object displacement is not expected to be of great negative impact due to its regular and homogeneous increase by view-angle. In such cases, it is rather the missing information on the occluded surfaces behind buildings that may hamper analyses. This is especially important when trees are underestimated in narrow street canyons due to the high relevance of trees for modeling urban environmental quality (Nichol and Wong 2005). Similarly, the overestimation of built-up areas at large view-angles to the north, which is caused by both roof-tops and façades being classified as *building*, may have negative impact.

In urban climate models, buildings are often explicitly addressed. Sometimes, this information is averaged to grid cell variables (e.g. Martilli et al. 2002), other times a level of detail is required, that would be influenced by building displacement (e.g. Harman and Belcher 2006). In either case, however, information on building height or roof inclination is needed. This underlines the need to combine land cover products derived by means of remote sensing, with additional digital information. In such cases, the geometric inaccuracy of the hyperspectral information at large view-angles appears most critical and the use of a precise DSM during geometric processing is required to produce spatially accurate information.

6.3 Influence of tree cover on impervious surface estimates

The delineation of impervious areas by spectral information works well. Most of the remaining misclassification relates to confusion of soil and the two impervious classes. By aggregating buildings and non built-up impervious areas, some of the described inaccuracies become obsolete. For example, the misclassification of dark façades as *paved* at large view-angles does not change results when buildings and paved areas are treated as one. However, the phenomenon of buildings occluding non impervious areas at large view-angles remains.

The phenomenon of trees obscuring impervious areas, on the other hand, is shown to be of great relevance in all accuracy assessments. More than 30% of the pixels within the area of the street network of the UEIS are classified as vegetation. Given the distinct spectral properties of vegetation, this error can not be explained by spectral classification errors. Differences between the nadir region and large view-angles are generally low due to the

little height of trees. The increase in the northern parts is explained by the dominance of the very brightly illuminated portions of trees in mixed pixels.

The fact that image data represents the sensor view situation with tree cover and the general underestimation of impervious area are also shown by the comparison of imperviousness values based on HyMap and values derived for subsets from the field survey and for the UEIS polygons (Fig. V-7). In both cases, the analysis underlines that the sensor view situation correlates well, whereas true ground cover is generally underestimated by analysis from remote sensing image data.

The rate of error can also be shown in the reference data itself: Comparing the estimates of impervious surface coverage for the 37 UEIS polygons with and without trees obscuring paved areas shows an average difference of 7.5%. For three polygons, estimates differ by 30% and offsets exist at all degrees of imperviousness (Fig. V-9). The same assessment based on all 17 field survey areas leads to an underestimation of only 3.8% in average.

The influence of trees obscuring impervious surface is very critical and, more importantly, hard to predict. The discrepancy between 33.3% vegetation obscuring the area of the street network, 7.5% offset on residential UEIS blocks (where streets and building objects have been excluded), and 3.8% for survey areas, which contain a great portion of open spaces, is great. Given the high variation of values, it appears impossible to apply a standard correction to underestimated impervious surface coverage. We could not discover a direct relation between TIA and the amount of impervious surface covered by trees based on the available reference data.

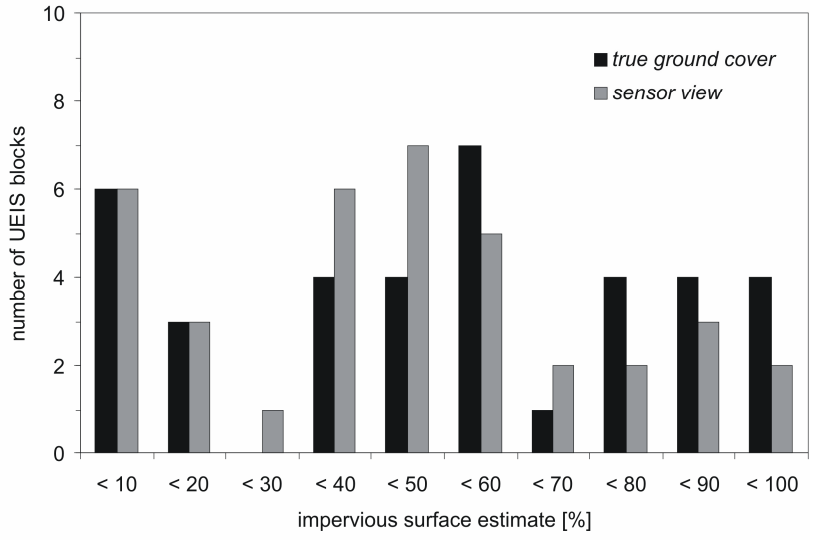

Figure V-9: Distribution of impervious surface estimates for 37 UEIS polygons. Values relate to *sensor view* including tree cover and to the *true ground cover*.

Detailed spatial information on streets, the geometry of the street canyon, and the distribution of trees is needed in many boundary layer climate models, for example to model airflow and pollutant distribution (Tsai and Chen 2004), the surface-atmosphere energy exchanges (Pearlmutter et al. 2007), or in UHI simulations (Hirano et al. 2004). For cities comparable to Berlin, a semi-automated mapping of streets from remote sensing data appears infeasible considering error rates of about 30%. In such cases, additional digital information on the street network is crucial. Whenever digital information on streets exists, remote sensing can provide important additional information on the distribution of trees above the digitized surface.

7 Conclusion

The quality of urban surface mapping based on airborne hyperspectral remote sensing data was investigated in this work. The high spatial and spectral resolution of the image data and the diverse reference information allowed for the performance of intensive accuracy assessments and the identification of sources of inaccuracy. The precision of the land cover classification, the influence of geometric inaccuracy caused by the complex urban geometry and the remote sensing perspective, and the impact of trees obscuring surface underneath were addressed.

By classifying the hyperspectral data with an SVM classifier, high classification accuracy was achieved for five land cover classes including the spectrally critical classes *buildings* and *paved*. The spectral information of multispectral sensors like Ikonos does not allow the differentiation of such surfaces (Small 2003). Classification accuracy is high for all urban structure types and the setup of the classification approach is simple. We assume that the combination of HyMap data and SVM can be successfully used in other urban environments. More instruments with similar characteristics, for example the Airborne Reflective Emissive Spectrometer (ARES) (Müller et al. 2005), will be available in near future and the number of applications in this field is expected to increase. This way, similar data will be more and more available for urban regions with less additional information.

The orthorectification of airborne hyperspectral data will often include the use of a DEM similar to the one used in this work. The detailed analysis of map accuracy revealed the negative impact of a missing DSM. The decision, of whether the work with commonly available DEMs is sufficient, must be based on the scope and scale of analysis. In the environmental context, the missing information on occluded surfaces behind high

buildings at large view-angles appears more critical than the homogeneous and linear displacement of objects. Information on patterns of impervious surface, including a differentiated treatment of built-up and non built-up areas, is possible at relatively fine scales. The combination of image information and additional digital data is probably limited to regions near nadir or to sensors with generally small swath widths. This issue is of high relevance for remote sensing based analysis because spaceborne instruments with high spatial resolution, like Quickbird or Ikonos, frequently use off-nadir acquisition at view-angles of up to 30°. The availability of an accurate DSM will further increase the value of airborne hyperspectral data for urban environmental analyses.

The impact of trees obscuring possibly impervious surfaces underneath was shown to be highly variant and of important relevance, especially in the case of the street network. This impact is a general problem in remote sensing based analyses. The continuous mapping of the street network will be influenced by trees in *sensor view* and hence information on the connectivity and configuration of impervious areas. By performing multitemporal analyses at leaf-on/leaf-off situation, the quantification of this impact in relation to different urban structure types might be possible. In this case, the information derived from airborne hyperspectral remote sensing data is expected to serve as a useful input for an increased number of urban environmental analyses.

Acknowledgements

The author is grateful to T. Scheuschner for the great help during GIS analysis and the effort he put into visualizing results from the ground mapping. B. Kleinschmit, B. Coenradie, L. Haag, A. Damm, and the Berlin City Department for Urban Development are thanked for providing the reference data based on the UEIS and the digital cadastre. The contribution of the students from Humboldt-Universität who performed the field survey is greatly appreciated. P. Griffiths helped with the GIS integration of the survey data and together with M. Langhans he performed great parts of the preprocessing of the HyMap data. S. van der Linden was funded by the scholarship programs of the German Federal Environmental Foundation (DBU) and the German Academic Exchange Service (DAAD). The cost of the HyMap data was covered by the DBU the German Research Foundation (DFG) under project number no. HO 2568/2-1, and the DFG research training group 780/2.

Chapter VI:
Synthesis

1 Summary

The global dimension of urbanization requires adequate approaches to monitor and analyze the extent of urban areas and the environmental conditions therein. This thesis investigated the potential of airborne hyperspectral data to provide information on impervious urban areas that is needed for an integrated analysis of such coupled natural and human systems. For this purpose all processing steps from raw data to the final map products were performed. Two processing steps that were lacking optimization with regard to the challenges typical for urban areas have been advanced, i.e. the normalization of brightness gradients and the land cover classification approach. Impacts of the mandatory geocoding and the frequently applied image segmentation on map accuracy were investigated and discussed against the background of workflow optimization.

The metropolitan area of Berlin proved to be a useful study site for this investigation, because of three reasons. First, a variety of urban structure types were covered. Second, a large amount of field data were collected parallel to the remote sensing data acquisition, e.g. land cover maps and spectroscopic field measurements. Third, abundant additional data were available for validation of land cover maps and impervious surface estimates. Thus, comparison of image processing products to various independent data sets was possible at each stage of the processing chain.

The four research questions that were stated in Chapter I are addressed individually before main conclusions are drawn:

(1) Can brightness gradients in airborne hyperspectral data from urban areas be eliminated using an empirical normalization approach that requires no additional field measurements?

In Chapter II, the existence of surface type specific brightness gradients was shown. The curvature of these view-angle dependent gradients was explained based on the directional properties of corresponding surfaces. The two empirical approaches that were suggested for the normalization of this phenomenon, i.e. the *class-wise* and the *weighted class-wise* method, both eliminated the brightness gradients. Based on reference surfaces from additional HyMap data the superiority of the suggested approaches to the traditional global normalization approach was demonstrated.

The class-wise normalization approach constitutes an empirical solution that is well suited for the spectral and spatial heterogeneity of urban environments. It does not require information from spectral libraries or the parameterization of complex models. Extending the approach by assigning weighted correction factors offers the possibility to handle surface types that are characterized by smooth transition. The approaches may thus also be useful in natural ecosystems where gradual changes in surface types are typical. Examples for such situations include forest type transitions along altitudinal gradients, arid- and semi-arid regions, or agricultural areas at early growth stages.

(2) Do support vector machines bear the potential to directly use the full hyperspectral information for the successful delineation of urban land cover classes such as built-up and non built-up impervious surfaces without separate feature extraction or the previous definition of spectral sub-classes?

In Chapter III, SVM were used to classify a large and heterogeneous HyMap image into five land cover classes. All classes, including those characterized by high spectral heterogeneity and multimodal distributions (compare Fig. I-2), were separated without a previous definition of spectral sub-classes. The classification was performed on the original spectral bands and yielded high overall and class-specific accuracies for all urban structure types. Results underline the high potential of SVM for complex classification problems without previous feature extraction or selection.

Thus, results from Chapter III show that a sequential processing workflow similar to the one suggested by Kuo and Landgrebe (2004) (Fig. I-3) is not necessary. This is further stressed by the results from additional tests which went beyond the scope of Chapter III:

- transforming the HyMap image into PCs did not improve classification results. Results achieved on the first 20 PCs, for example, were inferior to those achieved on 114 original spectral bands and the feature extraction decreased classification accuracy.

- a sequential classification approach with hierarchically organized SVM did not lead to higher accuracy. Such approaches that split the complex multiclass problem into more simple sub-problems proved useful for the work with artificial neural networks (Udelhoven et al. 2000). For SVM, however, such a strategy did not improve classification accuracies. These findings are accordance with those from Melgani and Bruzzone (2004) and prove that SVM classifications are very accurate without complex classification setups.

- results from the SVM classification did not decrease when applied to the image data *without* normalized brightness gradients. Therefore, similar classification results might be

achieved with a processing workflow even simpler than the one in this work. Nevertheless, the normalization of the brightness gradients is mandatory when spectral libraries or image data from different acquisition times or locations are integrated into the classification.

SVM can thus be recommended for complex problems due to their high classification accuracy *and* for their ability to achieve optimal results with a simple and intuitive setup. This way, they fulfill the requirements Richards (2005) mentions for future classification methods.

(3) How accurate can land cover and impervious surface coverage be mapped from hyperspectral images and what are the main sources of inaccuracy?

In Chapter V, the influence of different potential sources of inaccuracies on the land cover map and the derived map on impervious surface coverage were assessed. The accuracies of the two maps were evaluated prior to and after geocoding based on various reference data. This way, the decrease in accuracy could be linked either to individual processing steps or to phenomena that generally limit remotely sensed information.

Results show that hyperspectral data provides the spectral information needed to differentiate the major elements of urban heterogeneity according to Cadenasso et al. (2007b) and to estimate impervious surface coverage based on this land cover information. Problems with mixed pixels and spectrally ambiguous surfaces during SVM classification of the HyMap data were overall relatively little, but contributed to the overall error. Additional relevant error sources could be identified, though: the geocoding generally caused inaccuracies, as was seen in nadir regions; the additional impact of the missing information on building heights was shown by the increasing error of the corresponding class at larger view-angles; the view-angle independent assignment of streets to vegetation proved the influence of tree crowns obscuring surfaces underneath. This phenomenon leads to a general negative offset in the estimation of impervious surface coverage.

The consequences of individual errors and the overall error for subsequent analyses depend on the spatial scale and the scope of analysis. For example, information on the spectrally well recognized but systematically displaced buildings can be used for a block-wise analysis of the spatial patterns of building. However, severe problems will be caused by such spatial offsets when data from additional sources is combined with the remotely sensed information on individual buildings. In general, the occlusion of surfaces behind buildings and the overestimation of vegetation due to tree crowns – two problems that are not exclusive to hyperspectral data – must be considered as the most critical error source.

(4) To what extent is the efficiency of the processing workflow in terms of processing times and accuracy influenced by alternative processing sequences and the introduction of data compression by image segmentation?

The influence of image segmentation and the processing workflow were discussed at several points in this work. In terms of accuracy, image segmentation did not prove a useful processing step for the classification of the HyMap data from Berlin: the comparison of pixel- and segment-based results in Chapter III showed that no ideal single aggregation level can be identified. Segment-based processing should therefore not be generally preferred over pixel-based approaches. Moreover, concepts are required which enable a simple integration of the positive but scale-dependent influences from multiple levels for the classification of heterogeneous areas. The multi-level approach introduced in Chapter III has been extended for agricultural areas by Waske and van der Linden (2008); tests on the HyMap data from Berlin will follow.

Despite the lower accuracy of classifications of single segment levels, the issue of data size reduction in such approaches is worth keeping in mind when setting up the workflow. Processing power of modern computers increases constantly. However, so do data volumes due to simultaneously increasing resolutions. Operational processing of very large data sets is often difficult without using data compression. Spectral compression, such as feature extraction by PC transformation, was shown to decrease accuracies when using SVM (compare *research question 2*). Image segmentation on the other hand appears to be a useful alternative for spatial compression, due to the preservation of hyperspectral characteristics, its high compression factor and little decrease in classification accuracy. The discussion of Chapter IV is round-up by the multiple assessments in Chapter V which were also applied to the segmented data at average segment size 13.1 pixels. The error sources identified on pixel-based data in Chapter V affected the segment-compressed data to the same extent. Thus, no additional drawbacks of segment-compressed analysis can be reported and the approach appears worthwhile when data size becomes very large and processing times during classification might be reduced by a factor of 70, for example.

The position of the geocoding in the processing workflow has to be seen in a similar context. Moving this processing step to the end of the workflow can be more time effective while being only slightly less accurate. When additional data sources are required during processing, it might even be useful to convert these data into raw image geometry – if possible. The suggestion by Schläpfer et al. (2007) to customize processing workflows

according to the requirements of final end-user products is therefore supported by findings from this work.

2 Main conclusions

The operational use of remote sensing approaches for monitoring the dynamic modifications of the Earth's surface by humans requires accurate and reliable data products. In order to generate such products, raw data with a high content of useful information are needed. The methods used to process these data have to make best use of the contained information while being simple in their approach, generally applicable, and capable of dealing with large data sets. The presented work addresses these requirements in several ways and investigates the general strengths and limitations of airborne hyperspectral data for mapping impervious land cover in urban areas. In this context it appeared useful to concentrate on five basic land cover classes on a relatively large and heterogeneous data set instead of optimizing a more differentiated classification scheme on a subset of the data.

Results from this work confirm on the one hand that urban areas are challenging for remote sensing approaches and in parts require special processing steps. On the other, they show that the accuracies of land cover maps and products derived from those depend not solely on the image classification but on several processing steps and on the general limitations of remote sensing.

The spectral information of the HyMap data allowed delineating the spectrally similar built-up and non built-up impervious surfaces at high accuracy. This differentiation is essential for many urban analyses (Cadenasso et al. 2007b). Maps on impervious surface coverage can well be derived from such land cover information and inaccuracies of such maps do not relate to the spectral characteristics of the data. Thus, the additional spectral information content of hyperspectral data compared to multispectral data is valuable for urban applications and the usefulness for further development of more operational hyperspectral systems is underlined.

The high spectral classification accuracy can also be attributed to the strength of the SVM classifier. SVM have previously been compared to other classifiers by several authors (e.g. Huang et al. 2002; Pal and Mather 2006). Similar comparisons based on the HyMap data from Berlin showed that SVM outperformed the traditional maximum likelihood classifier

(Fu et al. 1969) and advanced decision tree classifications such as Random Forests (Breiman 2001). All supervised classifiers depend to a great extent on the selection of training data. However, the good results in this work were achieved with a simple and time-saving training data collection scheme and SVM were shown to make best use of all provided data. Due to their good performance in the complex urban environment, SVM can be expected to be well suited for most other applications in a variety of environments. In the same way SVM allowed for a simple classification setup in this work, they can be expected to simplify other challenging classification problems, such as change detections where complex classes are frequent and training data for traditional classifiers is notoriously difficult to collect (e.g. Kuemmerle et al. 2008).

The limitations of the work with airborne hyperspectral data in urban areas are not mainly caused by the spectral characteristics but rather by the wide FOV or general problems of remote sensing: displaced buildings and occluded surfaces always exist when data is acquired at large view-angles; the surface underneath tree crowns is invisible for any optical sensor. This causes in parts the drawbacks of remote sensing data compared to data from field surveys (Miller and Small 2003), especially for estimating absolute values of impervious surface coverage. However, the areas of most rapid urbanization are often those where no additional data are available. In this case remotely sensed maps are the best solution available. Quantifying errors associated with the final mapping product, as carried out in this thesis, is therefore of great interest and an important prerequisite to help end-users and decision makers in judging the reliability of their data.

Image processing in this work was challenging, due to the focus of the application, the characteristics of airborne hyperspectral data, and the complexity introduced by the heterogeneous urban environment. Thus, the methodological insights derived via mapping impervious areas in Berlin may be of relevance for many more – equally complex or more simplistic – applications. This includes not only applications using hyperspectral data from urban areas but also urban applications with data from other optical sensors or hyperspectral applications of non urban areas. This thesis is therefore an important step towards the broader application of remote sensing in urban areas. More studies of this kind will have to follow which deal with the research questions arising from the conclusions drawn above, studies that for example perform the step from land cover to land use or urban biotopes (Bochow et al. 2007) or that integrate SVM classification into the monitoring of the spatiotemporal growth of megacities.

3 Prospects of urban remote sensing

"Urbanization brings with it both opportunities and challenges" (UN 2006). The concentration of people is a response to the most dynamic economic activities in urban centers, which leads to various social and economic benefits. Concurrently, urban dwellers enjoy higher quality and more accessible health services. Cities are also at the forefront of political and cultural change. They are places where new ideas and products emerge and from which they spread. Thus, urbanization in less developed countries can be viewed as an indicator of development rather than a phenomenon with mainly negative consequences. It is a measure of globalization. (Sánchez-Rodríguez et al. 2005; UN 2006)

Against this background, urbanization will continue and so will its major role in altering the ecosystems in cities and their surroundings (Kareiva et al. 2007). A better understanding of urbanization will help to understand its influence on local, regional and global ecosystem. Remote sensing and EO in general are of crucial importance in this context, particularly since urbanization is most dynamic in regions with little spatial information. Thus, in the immediate future the potential role for the application of remote sensing data alone is likely to be greater in cities in less developed regions than in cities in developed countries. Here the integration of remote sensing with other data types is likely to be most fruitful (Miller and Small 2003).

From a technical perspective, new developments that appear interesting for urban applications can be reported in almost any acquisition domain. Various new sensors have recently become available or will become available in the near future: multispectral very high spatial resolution imagery decreases the mixed pixel problem in urban environments to the greatest extent (Ehlers 2007); synthetic aperture radar (SAR) data of up to 1 m spatial resolution as acquired by TerraSAR-X (Stangl et al. 2006) will offer new opportunities for radar remote sensing in urban areas, but also lead to new, so far unknown challenges for data processing; the combination of terrain information from laserscanning or SAR with optical data can be expected to become more frequent (Gamba and Houshmand 2002); and the extension of airborne hyperspectral sensors towards the thermal wavelengths regions will further improve the understanding of urban environments by means of remote sensing (Richter et al. 2005). The combined use of image data from such new sources will help to further improve the challenging applications addressed in this work. Especially the introduction of detailed information on surface elevation will help to delineate buildings, to improve the geocoding and to identify trees. This way the analysis of urban imperviousness can be expected to become more accurate. However, the

results from the present work underpin that a detailed assessment of potential errors is essential when new data sources are used or data from different sources are combined.

Richards (2005) discusses the increasing abundance of data from different sources and mentions new approaches for the processing of multisource data as one of the greatest challenges in remote sensing. SVM can be expected to be of great importance for future urban applications. Their algorithmic development is still ongoing (e.g. Bazi and Melgani 2006; Bruzzone et al. 2006) and they have already proved successfull in combining hyperspectral data and laserscanning information (Koetz et al. 2008) or data from SAR and optical sensors (Waske and van der Linden 2008) in non-urban environments. Although results achieved by SVM are convincing, traditional classifiers are still widely used and users hesitate to integrate rather recent machine learning developments into their analysis. To broaden the community of users of such more effective approaches, user-oriented implementations are needed that are optimized for the requirements remote sensing applications and minimize the number of parameters to be set (e.g. Janz et al. 2007).

Despite the constant improvement in data quality and new methodological developments, urban remote sensing alone can not advance the knowledge on the impacts of urbanization. It will, however, play an important role in many future approaches that further integrate ecological and social sciences. It is this integration of different disciplines that it is critical to move beyond the existing approaches for studying coupled systems, to develop more comprehensive portfolios, and to build an international research network spanning local, regional, national, and global levels (Liu et al. 2007). Studying the complex process of urbanization requires such integrated approaches.

References

Alberti, M. (2005). The effects of urban patterns on ecosystem function. *International Regional Science Review, 28*, 168-192.

Alberti, M., Booth, D., Hill, K., Coburn, B., Avolio, C., Coe, S., & Spirandelli, D. (2007). The impact of urban patterns on aquatic ecosystems: An empirical analysis in Puget lowland sub-basins. *Landscape and Urban Planning, 80*, 345-361.

Alberti, M., Marzluff, J.M., Shulenberger, E., Bradley, G., Ryan, C., & Zumbrunnen, C. (2003). Integrating humans into ecology: Opportunities and challenges for studying urban ecosystems. *Bioscience, 53*, 1169-1179.

Alder, G. (1995). Tackling Poverty in Nairobis Informal Settlements - Developing an Institutional Strategy. *Environment and Urbanization, 7*, 85-107.

Arnold, C.L., & Gibbons, C.J. (1996). Impervious surface coverage - The emergence of a key environmental indicator. *Journal of the American Planning Association, 62*, 243-258.

Baatz, M., & Schaepe, A. (2000). Multiresolution Segmentation: an optimization approach for high quality multi-scale image segmentation. In Strobl, J., Blaschke, T. & Griesebner, G. (Eds.), *Angewandte Geographische Informationsverarbeitung XII. Beiträge zum AGIT-Symposium 1999* (pp. 12-23). Heidelberg: Herbert Wichmann Verlag.

Balder, H., Ehlebracht, K., & Mahler, E. (1997). *Straßenbäume: Planen, Pflanzen, Pflegen am Beispiel Berlin* [Street trees: Planning, planting, cultivating in the case of Berlin]. Berlin-Hannover: Patzer Verlag.

Baraldi, A., & Parmiggiani, F. (1995). An investigation of the textural characteristics associated with gray level cooccurrence matrix statistical parameters. *IEEE Transactions on Geoscience and Remote Sensing, 33*, 293-304.

Bazi, Y., & Melgani, F. (2006). Toward an optimal SVM classification system for hyperspectral remote sensing images. *IEEE Transactions on Geoscience and Remote Sensing, 44*, 3374-3385.

Beisl, U. (2001). *Correction of bidirectional effects in imaging spectrometer data*, Remote Sensing Series, 37. Zurich: University of Zurich.

Beisl, U., & Woodhouse, N. (2004). Correction of atmospheric and bidirectional effects in multispectral ADS40 images for mapping purposes. *Proceedings of the 20th ISPRS Congress*, 12-23 July, 2004, Istanbul, Turkey.

Ben-Dor, E., Levin, N., & Saaroni, H. (2001). A spectral based recognition of the urban environment using the visible and near-infrared spectral region (0.4-1.1 μm). A case study over Tel-Aviv, Israel. *International Journal of Remote Sensing, 22*, 2193-2218.

Benediktsson, J.A., Palmason, J.A., & Sveinsson, J.R. (2005). Classification of hyperspectral data from urban areas based on extended morphological profiles. *IEEE Transactions on Geoscience and Remote Sensing, 43*, 480-491.

Benediktsson, J.A., Swain, P.H., & Ersoy, O.K. (1990). Neural Network Approaches Versus Statistical-Methods in Classification of Multisource Remote-Sensing Data. *IEEE Transactions on Geoscience and Remote Sensing, 28*, 540-552.

Blair, R.B. (1996). Land use and avian species diversity along an urban gradient. *Ecological Applications, 6*, 506-519.

Boardman, J.W. (1998). Post-ATREM polishing of AVIRIS apparent reflectance data using EFFORT: A lesson in accuracy versus precision. *Summaries of the 7th JPL Airborne Earth Science Workshop*, Pasadena, USA.

Bochow, M., Segl, K., & Kaufmann, H. (2007). Automating the Build-Up Process of Feature-Based Fuzzy Logic Models for the Identification of Urban Biotopes from Hyperspectral Remote Sensing Data. *Proceedings URBAN/URS 2007 Joint Event*, 11-13 April, 2007, Paris, France, CD-ROM.

Booth, D.B., Karr, J.R., Schauman, S., Konrad, C.P., Morley, S.A., Larson, M.G., & Burger, S.J. (2004). Reviving urban streams: Land use, hydrology, biology, and human behavior. *Journal of the American Water Resources Association, 40*, 1351-1364.

Bottyan, Z., Kircsi, A., Szegedi, S., & Unger, J. (2005). The relationship between built-up areas and the spatial development of the mean maximum urban heat island in Debrecen, Hungary. *International Journal of Climatology, 25*, 405-418.

Brabec, E., Schulte, S., & Richards, P.L. (2002). Impervious surfaces and water quality: A review of current literature and its implications for watershed planning. *Journal of Planning Literature, 16*, 499-514.

Breiman, L. (2001). Random forests. *Machine Learning, 45*, 5-32.

Bruzzone, L., & Carlin, L. (2006). A multilevel context-based system for classification of very high spatial resolution images. *IEEE Transactions on Geoscience and Remote Sensing, 44*, 2587-2600.

Bruzzone, L., Chi, M.M., & Marconcini, M. (2006). A novel transductive SVM for semisupervised classification of remote-sensing images. *IEEE Transactions on Geoscience and Remote Sensing, 44*, 3363-3373.

Burges, C.J.C. (1998). A tutorial on Support Vector Machines for pattern recognition. *Data Mining and Knowledge Discovery, 2*, 121-167.

Cadenasso, M.L., Pickett, S.T.A., Burch, W.A., & Machlis, G.E. (2007a). *Human Ecosystems in the First Urban Century: Patch Dynamics Integrating Ecology and Social Science*. New Haven: Yale University Press.

Cadenasso, M.L., Pickett, S.T.A., & Schwarz, K. (2007b). Spatial heterogeneity in urban ecosystems: reconceptualizing land cover and a framework for classification. *Frontiers in Ecology and the Environment, 5*, 80-88.

Carle, M.V., Halpin, P.N., & Stow, C.A. (2005). Patterns of watershed urbanization and impacts on water quality. *Journal of the American Water Resources Association, 41*, 693-708.

Carlson, T.N., & Arthur, S.T. (2000). The impact of land use - land cover changes due to urbanization on surface microclimate and hydrology: a satellite perspective. *Global and Planetary Change, 25*, 49-65.

Carpenter, S.R., Caraco, N.F., Correll, D.L., Howarth, R.W., Sharpley, A.N., & Smith, V.H. (1998). Nonpoint pollution of surface waters with phosphorus and nitrogen. *Ecological Applications, 8*, 559-568.

Chen, C.C., & Lin, C.J. (2001). LIBSVM: a library for support vector machines [online]. Available from: http://www.csie.ntu.edu.tw/~cjlin/libsvm [accessed September 2007].

Chopping, M.J. (2000). Testing a LiSK BRDF Model with in Situ Bidirectional Reflectance Factor Measurements over Semiarid Grasslands. *Remote Sensing of Environment, 74*, 287-312.

Chopping, M.J., Rango, A., & Ritchie, J.C. (2002). Improved semi-arid community type differentiation with the NOAA AVHRR via exploitation of the directional signal. *IEEE Transactions on Geoscience and Remote Sensing, 40*, 1132-1149.

Cocks, T., Jenssen, R., Stewart, I., Willson, I., & Shields, T. (1998). The HyMap(TM) airborne hyperspectral sensor: The system, calibration and preformance. In Schaepman, M., Schlapfer, D. & Itten, K. (Eds.) (1998), *Proceedings 1st EARSeL workshop on imaging spectroscopy*, 6-8 October, 1998, Zürich, Switzerland (pp. 37-42).

Collier, C.G. (2006). The impact of urban areas on weather. *Quarterly Journal of the Royal Meteorological Society, 132*, 1-25.

Congalton, R., & Green, K. (1999). *Assessing the Accuracy of Remotely Sensed Data: Principles and Practices*. Boca Raton: Lewis.

Damm, A., Hostert, P., & Schiefer, S. (2005). Investigating urban railway corridors with geometric high resolution satellite data. In Moeller, M. & Wentz, E. (Eds.) (2005), *Proceedings 5th International Symposium Remote Sensing of Urban Areas (URS 2005)*, 14-16 March, 2005, Tempe, USA.

Deering, D.W. (1989). Field measurements of bidirectional reflectance. In Asrar, G. (Ed.) *Theory and applications of optical remote sensing* (pp. 14-65). New York: Wiley.

DeFries, R.S., Bounoua, L., & Collatz, G.J. (2002). Human modification of the landscape and surface climate in the next fifty years. *Global Change Biology, 8*, 438-458.

Dembrowski, H. (2004). The urban century. Editorial. *Magazine for Development and Cooperation, 2004*, 1.

Dennison, P.E. (2006). Fire detection in imaging spectrometer data using atmospheric carbon dioxide absorption. *International Journal of Remote Sensing, 27*, 3049-3055.

Diermayer, E., Hostert, P., Schiefer, S., & Damm, A. (2006). Comparing pixel- and object-based classification of imperviousness with HRSC-AX data. In Hostert, P., Schiefer, S. & Damm, A. (Eds.) (2006), *Proceedings 1st Workshop of the EARSeL Special*

Intrest Group Urban Remote Sensing - "Challenges and Solutions", 2-3 March, 2006 Berlin, Germany, CD-ROM.

Ehlers, M. (2007). New Developments and trends for Urban Remote Sensing. In Weng, Q. & Quattrochi, D. (Eds.), *Urban Remote Sensing* (pp. 357-376). Boca Raton: CRC Press.

Ehlers, M., Geehler, M., & Janowsky, R. (2006). Automated techniques for environmental monitoring and change analyses for ultra high resolution remote sensing data. *Photogrammetric Engineering and Remote Sensing, 72*, 835-844.

EPA [United States Environmental Protection Agency] (2001). *Our built and natural environments, a technical review of the interaction between land use, transportation and environmental quality*. Washington, DC: EPA.

Evans, C., Jones, R., Svalbe, I., & Berman, M. (2002). Segmenting multispectral landsat TM images into field units. *IEEE Transactions on Geoscience and Remote Sensing, 40*, 1054-1064.

Feingersh, T., Dorigo, W., Richter, R., & Ben-Dor, E. (2005). A new model-driven correction factor for BRDF effects in HRS data. In Zagajewski, B. & Sobczak, M. (Eds.) (2006), *Proceedings 4th EARSeL workshop on Imaging Spectroscopy - "New Qualities in Environmental Studies"*, 27-29 April, 2005, Warsaw, Poland (pp. 565-576).

Foley, J.A., DeFries, R., Asner, G.P., Barford, C., Bonan, G., Carpenter, S.R., Chapin, F.S., Coe, M.T., Daily, G.C., Gibbs, H.K., Helkowski, J.H., Holloway, T., Howard, E.A., Kucharik, C.J., Monfreda, C., Patz, J.A., Prentice, I.C., Ramankutty, N., & Snyder, P.K. (2005). Global consequences of land use. *Science, 309*, 570-574.

Foody, G.M. (2004). Thematic map comparison: Evaluating the statistical significance of differences in classification accuracy. *Photogrammetric Engineering and Remote Sensing, 70*, 627-633.

Foody, G.M., & Mathur, A. (2004). A relative evaluation of multiclass image classification by support vector machines. *IEEE Transactions on Geoscience and Remote Sensing, 42*, 1335-1343.

Foody, G.M., & Mathur, A. (2006). The use of small training sets containing mixed pixels for accurate hard image classification: Training on mixed spectral responses for classification by a SVM. *Remote Sensing of Environment, 103*, 179-189.

Friedl, M.A., & Brodley, C.E. (1997). Decision tree classification of land cover from remotely sensed data. *Remote Sensing of Environment, 61*, 399-409.

Fu, K.S., Landgrebe, D.A., & Phillips, T.L. (1969). Information processing of remotely sensed agricultural data. *Proceedings IEEE, 57*, 639-653.

Gamba, P., & Dell'Acqua, F. (2007). Spectral resolution in the context of very high resolution urban remote sensing. In Weng, Q. & Quattrochi, D. (Eds.), *Urban Remote Sensing* (pp. 377-391). Boca Raton: CRC Press.

Gamba, P., & Houshmand, B. (2002). Joint analysis of SAR, LIDAR and aerial imagery for simultaneous extraction of land cover, DTM and 3D shape of buildings. *International Journal of Remote Sensing, 23*, 4439-4450.

Goel, N.S. (1988). Models of vegetation canopy reflectance and their use in estimation of biophysical parameters from reflectance data. *Remote Sensing Reviews, 41*, 553-564.

Goetz, A.F.H., Vane, G., Solomon, J.E., & Rock, B.N. (1985). Imaging Spectrometry for Earth Remote-Sensing. *Science, 228*, 1147-1153.

Goshtasby, A. (1988). Registration of Images with Geometric Distortions. *IEEE Transactions on Geoscience and Remote Sensing, 26*, 60-64.

Green, R.O., Eastwood, M.L., Sarture, C.M., Chrien, T.G., Aronsson, M., Chippendale, B.J., Faust, J.A., Pavri, B.E., Chovit, C.J., Solis, M.S., Olah, M.R., & Williams, O. (1998). Imaging spectroscopy and the Airborne Visible Infrared Imaging Spectrometer (AVIRIS). *Remote Sensing of Environment, 65*, 227-248.

Gualtieri, J.A., & Cromp, R.F. (1998). Support vector machines for hyperspectral remote sensing classification. In Merisko, R.J. (Ed.) (1998), *Proceedings SPIE-27th AIPRWorkshop Advances in Computer Assisted Recognition*, vol. 3584 (pp. 221-232).

Guanter, L., Alonso, L., & Moreno, J. (2005). First results from the PROBA/CHRIS hyperspectral/multiangular satellite system over land and water targets. *IEEE Geoscience and Remote Sensing Letters, 2*, 250-254.

Harman, I.N., & Belcher, S.E. (2006). The surface energy balance and boundary layer over urban street canyons. *Quarterly Journal of the Royal Meteorological Society, 132*, 2749-2768.

Hatt, B.E., Fletcher, T.D., Walsh, C.J., & Taylor, S.L. (2004). The influence of urban density and drainage infrastructure on the concentrations and loads of pollutants in small streams. *Environmental Management, 34*, 112-124.

Heiden, U., Segl, K., Roessner, S., & Kaufmann, H. (2007). Determination of robust spectral features for identification of urban surface materials in hyperspectral remote sensing data. *Remote Sensing of Environment, 111*, 537-552.

Herold, M., Gardner, M.E., & Roberts, D.A. (2003). Spectral resolution requirements for mapping urban areas. *IEEE Transactions on Geoscience and Remote Sensing, 41*, 1907-1919.

Herold, M., Roberts, D.A., Gardner, M.E., & Dennison, P.E. (2004). Spectrometry for urban area remote sensing - Development and analysis of a spectral library from 350 to 2400 nm. *Remote Sensing of Environment, 91*, 304-319.

Herold, M., Schiefer, S., Hostert, P., & Roberts, D.A. (2006). Applying Imaging Spectrometry in Urban Areas. In Quattrochi, D.A. & Weng, Q.H. (Eds.), *Urban Remote Sensing* (pp. 137-161). Boca Raton: CRC Press Inc.

Hill, J., & Mehl, W. (2003). Geo- und radiometrische Aufbereitung multi- und hyperspektraler Daten zur Erzeugung langjähriger kalibrierter Zeitreihen. *Photogrammetrie, Fernerkundung, Geoinformation, 2003*, 7-14.

Hirano, Y., Yasuoka, Y., & Ichinose, T. (2004). Urban climate simulation by incorporating satellite-derived vegetation cover distribution into a mesoscale meteorological model. *Theoretical and Applied Climatology, 79*, 175-184.

Hodgson, M.E., Jensen, J.R., Tullis, J.A., Riordan, K.D., & Archer, C.M. (2003). Synergistic use of lidar and color aerial photography for mapping urban parcel imperviousness. *Photogrammetric Engineering and Remote Sensing, 69*, 973-980.

Hsu, C.W., & Lin, C.J. (2002). A comparison of methods for multiclass support vector machines. *IEEE Transactions on Neural Networks, 13*, 415-425.

Hu, B.X., Lucht, W., Li, X.W., & Strahler, A.H. (1997). Validation of kernel-drives semiempirical models for the surface bidirectional reflectance distribution function of land surfaces. *Remote Sensing of Environment, 62*, 201-214.

Huang, C., Davis, L.S., & Townshend, J.R.G. (2002). An assessment of support vector machines for land cover classification. *International Journal of Remote Sensing, 23*, 725-749.

Hughes, G.F. (1968). On the mean accuracy of statistical pattern recognizers. *IEEE Transactions on Information Theory, 14*, 55-63.

Imhoff, M.L., Bounoua, L., Ricketts, T., Loucks, C., Harriss, R., & Lawrence, W.T. (2004). Global patterns in human consumption of net primary production. *Nature, 429*, 870-873.

Itten, K., Meyer, P., Kellenberger, T., Leu, R., Sandmeier, S., Bitter, P., & Seidel, K. (1992). *Correction of the Impact of Topography and Atmosphere on Landsat-TM Forest Mapping of Alpine Regions*, Remote Sensing Series, 18. Zurich: University of Zurich.

Jacquemoud, S., Bacour, C., Poilve, H., & Frangi, J.P. (2000). Comparison of four radiative transfer models to simulate plant canopies reflectance: Direct and inverse mode. *Remote Sensing of Environment, 74*, 471-481.

Jacquemoud, S., Baret, F., Andrieu, B., Danson, F.M., & Jaggard, K. (1995). Extraction of Vegetation Biophysical Parameters by Inversion of the Prospect Plus Sail Models on Sugar-Beet Canopy Reflectance Data - Application to TM and AVIRIS Sensors. *Remote Sensing of Environment, 52*, 163-172.

Janz, A., & van der Linden, S. (2007). imageSVM - Support Vector Machine Classification for Remote Sensing Image Data [online]. Available from: http://www.hu-geomatics.de [accessed September 2007].

Janz, A., van der Linden, S., Waske, B., & Hostert, P. (2007). imageSVM - a user-oriented tool for advanced classification of hyperspectral data using support vector machines. In Reusen, I. & Cools, J. (Eds.) (2007), *Proceedings 5th EARSeL Workshop on Imaging Spectroscopy - "Imaging Spectroscopy: Innovation in environmental research"*, 23-25 April, 2007, Bruges, Belgium, CD-ROM.

Jensen, J.R., & Cowen, D.C. (1999). Remote sensing of urban suburban infrastructure and socio-economic attributes. *Photogrammetric Engineering and Remote Sensing, 65*, 611-622.

Johnson, L.F., Hlavka, C.A., & Peterson, D.L. (1994). Multivariate-Analysis of Aviris Data for Canopy Biochemical Estimation Along the Oregon Transect. *Remote Sensing of Environment, 47*, 216-230.

Kareiva, P., Watts, S., McDonald, R., & Boucher, T. (2007). Domesticated nature: Shaping landscapes and ecosystems for human welfare. *Science, 316*, 1866-1869.

Kaufmann, H., Segl, K., Chabrillat, S., Müller, A., Richter, R., Schreier, G., Hofer, S., Stuffler, T., Haydn, R., Bach, H., & Benz, U. (2005). ENMAP - an advanced hyperspectral mission. In Zagajewski, B. & Sobczak, M. (Eds.) (2006), *Proceedings 4th EARSeL workshop on Imaging Spectroscopy - "New Qualities in Environmental Studies"*, 27-29 April, 2005, Warsaw, Poland (pp. 55-59).

Kennedy, R.E., Cohen, W.B., & Takao, G. (1997). Empirical methods to compensate for a view-angle-dependent brightness gradient in AVIRIS imagery. *Remote Sensing of Environment, 62*, 277-291.

Kimes, D.S. (1983). Dynamics of Directional Reflectance Factor Distributions for Vegetation Canopies. *Applied Optics, 22*, 1364-1372.

Kimes, D.S., Knyazikhin, Y., Privette, J.L., Abuelgasim, A.A., & Gao, F. (2000). Inversion methods for physically-based models. *Remote Sensing Reviews, 18*, 381-439.

Kittler, J. (1998). Combining classifiers: A theoretical framework. *Pattern Analysis and Applications, 1*, 18-27.

Koetz, B., Morsdorf, F., van der Linden, S., Curt, T., & Allgöwer, B. (2008). Multi-source land cover classification for forest fire management based on imaging spectrometry and LiDAR data. *Forest Ecology and Management, in press*.

Kötz, B., Schaepman, M., Morsdorf, F., Bowyer, P., Itten, K., & Allgower, B. (2004). Radiative transfer modeling within a heterogeneous canopy for estimation of forest fire fuel properties. *Remote Sensing of Environment, 92*, 332-344.

Kruse, F.A., Lefkoff, A.B., Boardman, J.W., Heidebrecht, K.B., Shapiro, A.T., Barloon, P.J., & Goetz, A.F.H. (1993a). The Spectral Image-Processing System (Sips) - Interactive Visualization and Analysis of Imaging Spectrometer Data. *Remote Sensing of Environment, 44*, 145-163.

Kruse, F.A., Lefkoff, A.B., & Dietz, J.B. (1993b). Expert System-Based Mineral Mapping in Northern Death-Valley, California Nevada, Using the Airborne Visible Infrared Imaging Spectrometer (AVIRIS). *Remote Sensing of Environment, 44*, 309-336.

Kuemmerle, T., Hostert, P., Radeloff, V., van der Linden, S., Perzanowski, K., & Kruhlov, I. (2008). Cross-border comparison of post-socialist farmland abandonment. *Ecosystems, in press*.

Kuo, B.-C., & Landgrebe, D.A. (2004). Nonparametric weighted feature extraction for classification. *IEEE Transactions on Geoscience and Remote Sensing, 42*, 1096-1105.

Lacherade, S., Miesch, C., Briottet, X., & Le Men, H. (2005). Spectral variability and bidirectional reflectance behaviour of urban materials at a 20 cm spatial resolution in the visible and near-infrared wavelengths. A case study over Toulouse (France). *International Journal of Remote Sensing (Letter), 26*, 3859-3866.

Langhans, M., van der Linden, S., Damm, A., & Hostert, P. (2007). The influence of bidirectional reflectance in airborne hyperspectral data on spectral angle mapping and linear spectral mixture analysis. In Reusen, I. & Cools, J. (Eds.) (2007), *Proceedings 5th EARSeL Workshop on Imaging Spectroscopy - "Imaging Spectroscopy: Innovation in environmental research"*, April 23-25, 2007, Bruges, Belgium, CD-ROM.

Leroy, M., & Roujean, J.L. (1994). Sun and View Angle Corrections on Reflectances Derived from Noaa Avhrr Data. *IEEE Transactions on Geoscience and Remote Sensing, 32*, 684-697.

Li, X.W., & Strahler, A.H. (1986). Geometric-Optical Bidirectional Reflectance Modeling of a Conifer Forest Canopy. *IEEE Transactions on Geoscience and Remote Sensing, 24*, 906-919.

Liu, J.G., Dietz, T., Carpenter, S.R., Alberti, M., Folke, C., Moran, E., Pell, A.N., Deadman, P., Kratz, T., Lubchenco, J., Ostrom, E., Ouyang, Z., Provencher, W., Redman, C.L., Schneider, S.H., & Taylor, W.W. (2007). Complexity of coupled human and natural systems. *Science, 317*, 1513-1516.

Lu, D.S., & Weng, Q.H. (2006). Use of impervious surface in urban land-use classification. *Remote Sensing of Environment, 102*, 146-160.

Lu, D.S., Weng, Q.H., & Li, G.Y. (2006). Residential population estimation using a remote sensing derived impervious surface approach. *International Journal of Remote Sensing, 27*, 3553-3570.

Lucht, W., Schaaf, C.B., & Strahler, A.H. (2000). An algorithm for the retrieval of albedo from space using semiempirical BRDF models. *IEEE Transactions on Geoscience and Remote Sensing, 38*, 977-998.

Marcotullio, P.J., & Boyle, G. (2003). *Defining an Ecosystem Approach to Urban Management and Policy Development*, UNU/IAS Report. Tokyo: United Nations University Institute of Advanced Studies.

Martilli, A., Clappier, A., & Rotach, M.W. (2002). An urban surface exchange parameterisation for mesoscale models. *Boundary-Layer Meteorology, 104*, 261-304.

Mathieu, R., Freeman, C., & Aryal, J. (2007). Mapping private gardens in urban areas using object-oriented techniques and very high-resolution satellite imagery. *Landscape and Urban Planning, 81*, 179-192.

Matthew, M.W., Adler-Golden, S.M., Berk, A., Richtsmeier, S.C., Levine, R., & Bernstein, L.S. (2000). Status of atmospheric correction using a MODTRAN4-based algorithm.

In, *Proceedings SPIE, Algorithms for Multispectral, Hyperspectral, and Ultraspectral Imagery VI* (pp. 199-207)

McGwire, K.C. (1996). Cross-validated assessment of geometric accuracy. *Photogrammetric Engineering and Remote Sensing, 62*, 1179-1187.

McMorrow, J.M., Cutler, M.E.J., Evans, M.G., & Al-Roichdi, A. (2004). Hyperspectral indices for characterizing upland peat composition. *International Journal of Remote Sensing, 25*, 313-325.

MEA [Millenium Ecosystem Assessment] (2005). *Ecosystems and Human Well-being: Synthesis*. Washington, DC: Island Press.

Meister, G., Rothkirch, A., Spitzer, H., & Bienlein, J. (2000). BRDF field studies for remote sensing of urban areas. *Remote Sensing Reviews, 19*, 37-57.

Melgani, F., & Bruzzone, L. (2004). Classification of hyperspectral remote sensing images with support vector machines. *IEEE Transactions on Geoscience and Remote Sensing, 42*, 1778-1790.

Mesev, V. (1998). The use of census data in urban image classification. *Photogrammetric Engineering and Remote Sensing, 64*, 431-438.

Meyerson, F.A.B., Merino, L., & Durand, J. (2007). Migration and environment in the context of globalization. *Frontiers in Ecology and the Environment, 5*, 182-190.

Miller, H.J., & Han, J. (Eds.) (2001). *Geographic data mining and knowledge discovery*. London: Taylor and Francis.

Miller, R.B., & Small, C. (2003). Cities from space: potential applications of remote sensing in urban environmental research and policy. *Environmental Science & Policy, 6*, 129-137.

Morawitz, D.F., Blewett, T.M., Cohen, A., & Alberti, M. (2006). Using NDVI to assess vegetative land cover change in central Puget Sound. *Environmental Monitoring and Assessment, 114*, 85-106.

Morse, C.C., Huryn, A.D., & Cronan, C. (2003). Impervious surface area as a predictor of the effects of urbanization on stream insect communities in Maine, USA. *Environmental Monitoring and Assessment, 89*, 95-127.

Müller, A., Richter, R., Habermeyer, M., Dech, S., Segl, K., & Kaufmann, H. (2005). Spectroradiometric requirements for the reflective module of the airborne spectrometer ARES. *IEEE Geoscience and Remote Sensing Letters, 2*, 329-332.

Nichol, J., & Wong, M.S. (2005). Modeling urban environmental quality in a tropical city. *Landscape and Urban Planning, 73*, 49-58.

Nicodemus, F.E., Richmond, J.C., Hsia, J.J., Ginsberg, I.W., & Limperis, T. (1977). *Geometrical considerations and nomenclature for reflectance.* Washington D.C.: US Department of Commerce, National Bureau of Standards.

Nieke, J., Itten, K., Debruyn, W., & APEX-Team (2006). The airborne imaging spectrometer APEX: from concept to realisation. In Zagajewski, B. & sobczak, M. (Eds.) (2006), *Proceedings 4th EARSeL workshop on Imaging Spectroscopy - "New Qualities in Environmental Studies"*, 27-29 April, 2005, Warschau, Poland (pp. 73-80).

North, P.R.J. (1996). Three-dimensional forest light interaction model using a Monte Carlo method. *IEEE Transactions on Geoscience and Remote Sensing, 34*, 946-956.

NRC [National Research Council, Space Studies Board] (2007). *Earth Science and Applications from Space: Natoinal Imperatives for the Next Decade and Beyond (Prepublication copy)*. Washington DC: National Academy of Science.

Pal, M., & Mather, P.M. (2006). Some issues in the classification of DAIS hyperspectral data. *International Journal of Remote Sensing, 27*, 2895-2916.

Park, J. (1997). Globalization and the Urban Century: Refashioning a Post-Habitat II Reseach Agenda. *Proceedings Post-Habitat II Action on International Co-operation and Partnership in the Asia-Pacific Region*, 20-21 February, 1997, Fukuoka, Japan.

Patz, J.A., Daszak, P., Tabor, G.M., Aguirre, A.A., Pearl, M., Epstein, J., Wolfe, N.D., Kilpatrick, A.M., Foufopoulos, J., Molyneux, D., & Bradley, D.J. (2004). Unhealthy landscapes: Policy recommendations on land use change and infectious disease emergence. *Environmental Health Perspectives, 112*, 1092-1098.

Pauleit, S., & Duhme, F. (2000). Assessing the environmental performance of land cover types for urban planning. *Landscape and Urban Planning, 52*, 1-20.

Pauleit, S., Ennos, R., & Golding, Y. (2005). Modeling the environmental impacts of urban land use and land cover change - a study in Merseyside, UK. *Landscape and Urban Planning, 71*, 295-310.

Pearlmutter, D., Berliner, P., & Shaviv, E. (2007). Integrated modeling of pedestrian energy exchange and thermal comfort in urban street canyons. *Building and Environment, 42*, 2396-2409.

Pinty, B., Widlowski, J.L., Gobron, N., Verstraete, M.M., & Diner, D.J. (2002). Uniqueness of multiangular measurements - Part I: An indicator of subpixel surface heterogeneity from MISR. *IEEE Transactions on Geoscience and Remote Sensing, 40*, 1560-1573.

Richards, J.A. (2005). Analysis of remotely sensed data: The formative decades and the future. *IEEE Transactions on Geoscience and Remote Sensing, 43*, 422-432.

Richter, R., Müller, A., Habermeyer, M., Dech, S., Segl, K., & Kaufmann, H. (2005). Spectral and radiometric requirements for the airborne thermal imaging spectrometer ARES. *International Journal of Remote Sensing, 26*, 3149-3162.

Richter, R., & Schläpfer, D. (2002). Geo-atmospheric processing of airborne imaging spectrometry data. Part 2: atmospheric/topographic correction. *International Journal of Remote Sensing, 23*, 2631-2649.

Ridd, M.K. (1995). Exploring a V-I-S (Vegetation-Impervious Surface-Soil) Model for Urban Ecosystem Analysis through Remote-Sensing - Comparative Anatomy for Cities. *International Journal of Remote Sensing, 16*, 2165-2185.

Roberts, D.A., Smith, M.O., & Adams, J.B. (1993). Green Vegetation, Nonphotosynthetic Vegetation, and Soils in AVIRIS Data. *Remote Sensing of Environment, 44*, 255-269.

Roessner, S., Segl, K., Heiden, U., & Kaufmann, H. (2001). Automated differentiation of urban surfaces based on airborne hyperspectral imagery. *IEEE Transactions on Geoscience and Remote Sensing, 39*, 1525-1532.

Ross, J.K. (1981). *The radiation regime and architecture of plant stands*. The Hague: Dr. W. Junk Publishers.

Royer, A., Vincent, P., & Bonn, F. (1985). Evaluation and Correction of Viewing Angle Effects on Satellite Measurements of Bidirectional Reflectance. *Photogrammetric Engineering and Remote Sensing, 51*, 1899-1914.

RSI [Research Systems, Inc.] (2004). *ENVI - Environment for Visualizing Images, Version 4.0*.

Rydberg, A., & Borgefors, G. (2001). Integrated method for boundary delineation of agricultural fields in multispectral satellite images. *IEEE Transactions on Geoscience and Remote Sensing, 39*, 2514-2520.

Sala, O.E., Chapin, F.S., Armesto, J.J., Berlow, E., Bloomfield, J., Dirzo, R., Huber-Sanwald, E., Huenneke, L.F., Jackson, R.B., Kinzig, A., Leemans, R., Lodge, D.M., Mooney, H.A., Oesterheld, M., Poff, N.L., Sykes, M.T., Walker, B.H., Walker, M., & Wall, D.H. (2000). Biodiversity - Global biodiversity scenarios for the year 2100. *Science, 287*, 1770-1774.

Sánchez-Rodríguez, R., Seto, K.C., Simon, D., Solecki, W.D., Kraas, F., & Laumann, G. (2005). *Science Plan. Urbanization and Global Environmental Change*, IHDP Report Series. Bonn: International Human Dimensions Programm on Global Environmental Change.

Sandmeier, S., Muller, C., Hosgood, B., & Andreoli, G. (1998). Physical mechanisms in hyperspectral BRDF data of grass and watercress. *Remote Sensing of Environment, 66*, 222-233.

Schiefer, S., Hostert, P., & Damm, A. (2005a). An analysis of view-angle effects in hyperspectral data of urban areas. In Moeller, M. & Wentz, E. (Eds.) (2005), *Proceedings 3rd Int. Symp. Remote Sensing and Data Fusion Over Urban Areas (URBAN 2005)*, 14-16 March, 2005, Tempe, USA.

Schiefer, S., Hostert, P., & Damm, A. (2006). Correcting brightness gradients in hyperspectral data from urban areas. *Remote Sensing of Environment, 101*, 25-37.

Schiefer, S., Hostert, P., Diermayer, E., & Damm, A. (2005b). Compression and object-oriented processing of segmented hyperspectral images in ENVI. In Zagajewski, B. & Sobczak, M. (Eds.) (2006), *Proceedings 4th EARSeL workshop on Imaging Spectroscopy - "New Qualities in Environmental Studies"*, 27-29 April, 2005, Warsaw, Poland (pp. 609-616).

Schläpfer, D. (2005). *PARametric GEocoding, User Guide, Version 2.2*, ReSe Applications Schläpfer/Remote Sensing Laboratories of the University of Zurich.

Schläpfer, D., Nieke, J., Dell'Endice, F., Hüni, A., Biesemans, J., Meuleman, K., & Itten, K. (2007). Optimized workflow for APEX level 2/3 processing. In Reusen, I. & Cools, J. (Eds.) (2007), *Proceedings 5th EARSeL Workshop on Imaging Spectroscopy - "Imaging Spectroscopy: Innovation in environmental research"*, 23-25 April, 2007, Bruges, Belgium.

Schläpfer, D., & Richter, R. (2002). Geo-atmospheric processing of airborne imaging spectrometry data. Part 1: parametric orthorectification. *International Journal of Remote Sensing, 23*, 2609-2630.

Schlerf, M., Atzberger, C., & Hill, J. (2005). Remote sensing of forest biophysical variables using HyMap imaging spectrometer data. *Remote Sensing of Environment, 95*, 177-194.

Schöpfer, E., & Moeller, M. (2006). Comparing Metropolitan Areas - A Transferable Object-Based Image Analysis Approach. *Photogrammetrie-Fernerkundung-Geoinformation (PFG), 2006*, 277-286.

Schueler, T. (1994). The importance of imperviousness. *Watershed Protection Techniques, 1*, 100-111.

Segl, K., Roessner, S., Heiden, U., & Kaufmann, H. (2003). Fusion of spectral and shape features for identification of urban surface cover types using reflective and thermal hyperspectral data. *ISPRS Journal of Photogrammetry and Remote Sensing, 58*, 99-112.

SenStadt [Senatsverwaltung für Stadtentwicklung/Senate Department for Urban Develpment] (2007). Berlin Digital Environmental Atlas [online]. Available from: http://www.stadtentwicklung.berlin.de/umwelt/umweltatlas/edua_index.shtml [accessed September 2007].

Seto, K.C., & Fragkias, M. (2005). Quantifying spatiotemporal patterns of urban land-use change in four cities of China with time series landscape metrics. *Landscape Ecology, 20*, 871-888.

Seto, K.C., & Liu, W.G. (2003). Comparing ARTMAP neural network with the maximum-likelihood classifier for detecting urban change. *Photogrammetric Engineering and Remote Sensing, 69*, 981-990.

Shackelford, A.K., & Davis, C.H. (2003). A combined fuzzy pixel-based and object-based approach for classification of high-resolution multispectral data over urban areas. *IEEE Transactions on Geoscience and Remote Sensing, 41*, 2354-2363.

Small, C. (2001). Estimation of urban vegetation abundance by spectral mixture analysis. *International Journal of Remote Sensing, 22*, 1305-1334.

Small, C. (2003). High spatial resolution spectral mixture analysis of urban reflectance. *Remote Sensing of Environment, 88*, 170-186.

Small, C. (2004). The Landsat ETM plus spectral mixing space. *Remote Sensing of Environment, 93*, 1-17.

Small, C., & Lu, J.W.T. (2006). Estimation and vicarious validation of urban vegetation abundance by spectral mixture analysis. *Remote Sensing of Environment, 100*, 441-456.

Small, C., Pozzi, F., & Elvidge, C.D. (2005). Spatial analysis of global urban extent from DMSP-OLS night lights. *Remote Sensing of Environment, 96*, 277-291.

Smith, M.O., Ustin, S.L., Adams, J.B., & Gillespie, A.R. (1990). Vegetation in deserts: I. A regional measure of abundance from multispectral images. *Remote Sensing of Environment, 31*, 1-26.

Soegaard, H., & Moller-Jensen, L. (2003). Towards a spatial CO2 budget of a metropolitan region based on textural image classification and flux measurements. *Remote Sensing of Environment, 87*, 283-294.

Song, M., Civco, D.L., & Hurd, J.D. (2005). A competitive pixel-object approach for land cover classification. *International Journal of Remote Sensing, 26*, 4981-4997.

Stangl, M., Werninghaus, R., Schweizer, B., Fischer, C., Brandfass, M., Mittermayer, J., & Breit, H. (2006). TerraSAR-X technologies and first results. *IEE Proceedings-Radar Sonar and Navigation, 153*, 86-95.

Stefanov, W.L., Ramsey, M.S., & Christensen, P.R. (2001). Monitoring urban land cover change: An expert system approach to land cover classification of semiarid to arid urban centers. *Remote Sensing of Environment, 77*, 173-185.

Strahler, A.H., Woodcock, C.E., & Smith, J.A. (1986). On the Nature of Models in Remote-Sensing. *Remote Sensing of Environment, 20*, 121-139.

Sukopp, H. (Ed.) (1990). *Stadtoekologie. Das Beispiel Berlin* [Urban Ecology. The Berlin Case]. Berlin: Dietrich Reimer Verlag.

Svensson, M.K., & Eliasson, I. (2002). Diurnal air temperatures in built-up areas in relation to urban planning. *Landscape and Urban Planning, 61*, 37-54.

Svirejeva-Hopkins, A., Schellnhuber, H.J., & Pomaz, V.L. (2004). Urbanised territories as a specific component of the Global Carbon Cycle. *Ecological Modelling, 173*, 295-312.

Thanapura, P., Helder, D.L., Burckhard, S., Warmath, E., O'Neill, M., & Galster, D. (2007). Mapping urban land cover using QuickBird NDVI and GIS spatial modeling for runoff coefficient determination. *Photogrammetric Engineering and Remote Sensing, 73*, 57-65.

Tong, S.T.Y., & Chen, W.L. (2002). Modeling the relationship between land use and surface water quality. *Journal of Environmental Management, 66*, 377-393.

Toutin, T. (2004). Review article: Geometric processing of remote sensing images: models, algorithms and methods. *International Journal of Remote Sensing, 25*, 1893-1924.

Tsai, M.Y., & Chen, K.S. (2004). Measurements and three-dimensional modeling of air pollutant dispersion in an Urban Street Canyon. *Atmospheric Environment, 38*, 5911-5924.

Udelhoven, T., Naumann, D., & Schmitt, J. (2000). Development of a hierarchical classification system with artificial neural networks and FT-IR spectra for the identification of bacteria. *Applied Spectroscopy, 54*, 1471-1479.

UN [United Nations] (2006). *World Urbanization Prospects - The 2005 Revision. Executive Summary*. New York: United Nations Population Division.

Ustin, S.L., Roberts, D.A., Gamon, J.A., Asner, G.P., & Green, R.O. (2004). Using imaging spectroscopy to study ecosystem processes and properties. *Bioscience, 54*, 523-534.

Vane, G., Green, R.O., Chrien, T.G., Enmark, H.T., Hansen, E.G., & Porter, W.M. (1993). The Airborne Visible Infrared Imaging Spectrometer (AVIRIS). *Remote Sensing of Environment, 44*, 127-143.

Vapnik, V.N. (1998). *Statistical Learning Theory*. New York: Wiley.

Verhoef, W. (1984). Light-Scattering by Leaf Layers with Application to Canopy Reflectance Modeling - the Sail Model. *Remote Sensing of Environment, 16*, 125-141.

Vitousek, P.M. (1997). Human domination of Earth's ecosystems. *Science, 278*, 21-21.

Wackernagel, M., & Rees, W.E. (1997). Perceptual and structural barriers to investing in natural capital: Economics from an ecological footprint perspective. *Ecological Economics, 20*, 3-24.

Walthall, C.L., Norman, J.M., Welles, J.M., Campbell, G., & Blad, B.L. (1985). Simple Equation to Approximate the Bidirectional Reflectance from Vegetative Canopies and Bare Soil Surfaces. *Applied Optics, 24*, 383-387.

Wang, C., Menenti, M., Stoll, M.P., Belluco, E., & Marani, M. (2007). Mapping mixed vegetation communities in salt marshes using airborne spectral data. *Remote Sensing of Environment, 107*, 559-570.

Wang, L., Sousa, W.P., & Gong, P. (2004). Integration of object-based and pixel-based classification for mapping mangroves with IKONOS imagery. *International Journal of Remote Sensing, 25*, 5655-5668.

Wanner, W., Li, X., & Strahler, A.H. (1995). On the Derivation of Kernels for Kernel-Driven Models of Bidirectional Reflectance. *Journal of Geophysical Research-Atmospheres, 100*, 21077-21089.

Ward, D., Phinn, S.R., & Murray, A.T. (2000). Monitoring growth in rapidly urbanizing areas using remotely sensed data. *Professional Geographer, 52*, 371-386.

Waske, B., & Benediktsson, J.A. (2007). Fusion of support vector machines for classification of multisensor data. *IEEE Transactions on Geoscience and Remote Sensing, 45*, 3858-3866.

Waske, B., & van der Linden, S. (2008). Classifying multilevel imagery from SAR and optical sensors by decision fusion. *IEEE Transactions on Geoscience and Remote Sensing, 46*, 1457-1466.

Weber, C., & Puissant, A. (2003). Urbanization pressure and modeling of urban growth: example of the Tunis Metropolitan Area. *Remote Sensing of Environment, 86*, 341-352.

Welch, R. (1982). Spatial resolution requirements for urban studies. *International Journal of Remote Sensing, 3*, 139-146.

White, H.P., Miller, J.R., & Chen, J.M. (2002). Four-Scale Linear Model for Anisotropic Reflectance (FLAIR) for plant canopies - Part II: Validation and inversion with CASI, POLDER, and PARABOLA data at BOREAS. *IEEE Transactions on Geoscience and Remote Sensing, 40*, 1038-1046.

Whitford, V., Ennos, A.R., & Handley, J.F. (2001). "City form and natural process" - indicators for the ecological performance of urban areas and their application to Merseyside, UK. *Landscape and Urban Planning, 57*, 91-103.

Wilson, E.H., Hurd, J.D., Civco, D.L., Prisloe, M.P., & Arnold, C. (2003). Development of a geospatial model to quantify, describe and map urban growth. *Remote Sensing of Environment, 86*, 275-285.

Woodcock, C.E., & Strahler, A.H. (1987). The Factor of Scale in Remote-Sensing. *Remote Sensing of Environment, 21*, 311-332.

Wu, C.S. (2004). Normalized spectral mixture analysis for monitoring urban composition using ETM plus imagery. *Remote Sensing of Environment, 93*, 480-492.

Wu, C.S., & Murray, A.T. (2003). Estimating impervious surface distribution by spectral mixture analysis. *Remote Sensing of Environment, 84*, 493-505.

York, R., Rosa, E.A., & Dietz, T. (2003). Footprints on the earth: The environmental consequences of modernity. *American Sociological Review, 68*, 279-300.

Yuan, F., & Bauer, M.E. (2007). Comparison of impervious surface area and normalized difference vegetation index as indicators of surface urban heat island effects in Landsat imagery. *Remote Sensing of Environment, 106*, 375-386.

Zhou, G.Q., Chen, W.R., Kelmelis, J.A., & Zhang, D.Y. (2005). A comprehensive study on urban true orthorectification. *IEEE Transactions on Geoscience and Remote Sensing, 43*, 2138-2147.